2009

Relaxation Physics of Iron and Gadolinium Contrast Agents

Aneta Chmielewski
Western University

Relaxation Physics of Iron and Gadolinium Contrast Agents

(Spine title: Relaxation Physics of Iron and Gadolinium Contrast Agents)
(Thesis format: Monograph)

by

Aneta Chmielewski

Faculty of Medicine & Dentistry
Graduate Program in Medical Biophysics

Submitted in partial fulfillment
of the requirements for the degree of
Master of Science

School of Graduate and Postdoctoral Studies
The University of Western Ontario
London, Ontario, Canada

THE UNIVERSITY OF WESTERN ONTARIO
SCHOOL OF GRADUATE AND POSTDOCTORAL STUDIES

CERTIFICATE OF EXAMINATION

Chief Advisor

Dr. Brian K. Rutt

Advisory Committee

Dr. Paula Foster

Dr. Elizabeth Gillies

Examining Board

Dr. Rob Bartha

Dr. Charles McKenzie

Dr. Rob Hudson

The thesis by

Aneta Chmielewski

entitled

Relaxation Physics of Iron and Gadolinium Contrast Agents

is accepted in partial fulfillment of the
requirements for the degree of
Master of Science

Chair of Examination Board

Dr. Paula Foster

Dated this 28th day of September, 2009.

Abstract

Gadolinium relaxation theory was investigated to correlate chemical structure with relaxivity.

Relaxation theory was used to produce theoretical Nuclear Magnetic Resonance Dipersion profiles for Vasovist bound to Human Serum Albumin and compared to experimental results. Relaxation theory was used to calculate structural parameters for novel gadolinium MPO contrast agents.

Magnetic relaxation switch agents are nanoparticles capable of sensing molecular interactions. These nanoparticles switch between a dispersed and clustered state depending on the presence of target analytes. Relaxation ratios were derived to predict changes in relaxation times upon nanoparticle clustering and compared to experimental results.

Relaxation theory provides insights into the mechanics of and aides in the development of novel and more effective contrast agents.

Key words: Magnetic Resonance Imaging (MRI), Contrast Agnets, Gadolinium, Iron, Relaxation theory, Magnetic Relaxation Switch Agents (MRSA), NMRD (Nuclear Magnetic Resonance Dipersion), HSA (Human Serum Albumin)

For my parents and sister,

Lucjan, Urszula and Renata Chmielewski.

Acknowledgments

I wish to express my gratitude to my supervisor, Dr. Brian K. Rutt, for his guidance, scientific intuition, and expertise throughout this work. Brian has made time and effort to provide directions, professional support, and assistance with scientific presentations and this manuscript.

I would like to acknowledge Dr. John Chen, I used his NMRD fitting program for parts of this thesis, he patiently taught me and answered all of my questions about his program and NMRD fitting in general.

I am grateful to Drs. Paula Foster and Beth Gillies for their time, and helpful comments, while sitting on my advisory committee.

I would also like to acknowledge everyone in Dr. Rutt, Dr. Foster and Dr. Gillies labs for thier help through out this masters including but not limited to Soha Ramadan, Trevor Wade, Andrew Alejski, Beth Dunn, Amanda Martin, Dr. Francisco Martinez, Laura Gonzalez, Dr. John Ronald, Dr. Daniel Jirak, Klara Hofstetrova and Tracey Lui.

I would like to acknowledge the direct funding support by the Ontario Graduate Scholarship in Science and Technology.

Finally, I wish to thank my family and friends especially my parents for their encouragement and support.

Contents

List of Figures

List of Tables

List of Acronyms & Abbreviations

MRI	Magnetic resonance imaging
T_1	Longitudinal relaxation time
T_2	Transverse relaxation time
RF	Radio frequency
R_1	Longitudinal relaxation rate
R_2	Transverse relaxation rate
TTP	Tricapped trigonal prism
CSAP	Monocapped square antiprism
Gd(III)	Gadolinium ion
Gd-DTPA	Gadopentetate dimeglumine or Magnevist
Gd-DTPA-BMA	Gadodiamide or Omniscan
Gd-BOPTA	Gadobenate dimeglumine or Multihance
CNS	Central nervous system
Gd-BT-DO3A	Gadobutrol or Gadovist
Gd-DOTA	Gadoterate meglumine or Dotarem
Gd(HP-DO3A)(H_2O)	Gadoteridol or ProHance
Gd(DTPA-BMEA)(H_2O)	Gadoversetamide or OptiMARK
MS-325	Gadofosveset trisodium or Vasovist
CE-MRA	Contrast enchanced MR angiography
Gd(EOB-DTPA)	Gadoxetic acid disodium or Primovist
HSA	Human serum albumin

IS	Inner-sphere
ENDOR	Electron nuclear double resonance spectroscopy
NMRD	Nuclear magnetic resonance dispersion
EPR	Einstein, Podolsky and Rosen
ZFS	Zero-field splitting
NMR	Nuclear magnetic resonance
SBM	Solomon-Bloembergen-Morgan
GSBM	General Solomon-Bloembergen-Morgan
MPO	Myeloperoxidase
PRE	Paramagnetic relaxation enhancement
WBR	Wangsness-Bloch-Redfield
DC	Decomposition approximation
DD	Dipole-dipole interaction
para	paramagnetic
dia	diamagnetic
PBS	Phosphate buffered saline
CPMG	Carr-Purcell-Meiboom-Gill
MGDT	Mean gradient diffusion theory
OS	Outer-sphere
CE	Chemical-exchange
CLIO	Cross-linked iron oxide
Hz	Hertz
T	Tesla

List of Symbols

I	Spin quantum number
$\vec{\mu}$	Magnetic dipole moment
γ	Gyromagnetic ratio
$\hbar$	Planck's constant divided by 2π
$\vec{S}$	Spin angular momentum
$\vec{B_0}$	External magnetic field
$\vec{M}$	Magnetization vector
M_0	Magnetization at thermal equilibrium
α	Flip angle
ω_0	Larmor frequency
ΔE	Diffrence in energy between two energy levels
$\vec{B_1}$	Rotating magnetic field applied using RF coils
ω_ν	Frequency of vibrational and rotational motion
T_2^*	Transverse relaxation time including relaxation due to local field inhomogenuities
$[M]$	Concentration of contrast agent or metal ion
$[H_2O]$	Concentration of water
r_1	Longitudinal relaxivity
r_2	Transverse relaxivity
τ_c	Relaxation correlation time
T_{1e}	Electronic relaxation time

τ_R	Rotational diffusion time
τ_m	Water residency time in the first coordination sphere
τ'_m	Water residency time in the second coordination sphere
q	Hydration number
r	Metal ion water distance
$H_S(\beta, \gamma; t)$	Electronic spin Hamiltonian
H_{Zeeman}	Zeeman Hamiltonian
$H_{ZFS}(\beta, \gamma; t)$	ZFS Hamiltonian
m	Magnetic quantum number
L_z	Z component of angular momentum
S	Total angular momentum quantum number
k_{ex}	Water exchange time
T_{1M}	Relaxation time of bound water protons
P_M	Mole fraction of the metal ion
μ_0	Permeability of vacuum
g	Electronic g factor
μ_B	Bohr magneton
ω_S	Electronic frequency
ω_H	Proton Larmor frequency
γ_S	Electron gyromagnetic ratio
γ_H	Proton gyromagnetic ratio
$\frac{A}{\hbar}$	Electron-nuclear hyperfine coupling constant
τ_{s0}	Electronic relaxation time at zero-field
τ_v	Correlation time of transient ZFS fluctuations
Δ_t	Magnitude of transient ZFS fluctuations
τ_1	Correlation time of fast anisotropic motion
F^2	Order parameter representing degree of anisotropy
J	Spectral density functions

a	Distance of closest approach between water and the contrast agent ion
D	Diffusion constant
$\mathcal{L}_S$	Electron spin Liouville superoperator
$\mathcal{L}^S_{ZFS}$	Static ZFS Liouville superoperator
$\mathcal{L}_{Zeeman}$	Zeeman Liouville superoperator
$\mathcal{R}$	Electron spin relaxation superoperator
1_{op}	Unit superoperator
Q_n	Dynamic frequency shift
Δ_s	Magnitude of static ZFS fluctuations
χ^2	Quadrupolar coupling constant
η	Asymmetry parameter
ΔE_R	Change in energy with rotation of the molecule
$\Delta H^\ddagger$	Enthalpy of activation
k_B	Boltzmann's constant
ΔE_v	Change in energy with transient ZFS modulation
R^2	Pearson's coefficient squared
K_a	Anisotropy constant
E_a	Anisotropy energy
V	Crystal volume
L(x)	Langevin function
m_s	Magnetic quantum number
μ_{sp}	Magnetic moment of single nanoparticle
N_c	Number of nanoparticles in a cluster
J_F	Freed's spectral density function
J_A	Ayant's spectral density function
τ_D	Translational correlation time
f	Volume fraction
σ	Standard deviation

T	Tesla (unit of magnetic field strength)
T	Temperature (Kelvin)
N_A	Avogadro's number
τ_N	N'eel relaxation time

Chapter 1

General Introduction

1.1 Magnetic Resonance Imaging

Magnetic Resonance Imaging (MRI) is a routine diagnostic tool. MRI has many advantages including non-invasiveness, use of non-ionizing radiation and flexible contrast. Contrast in MRI images is dependent on the intrinsic properties of the tissues but can be manipulated by pulse sequences. The primary disadvantage of MRI is its relatively low sensitivity. Contrast agents are used to enhance sensitivity. Although there are some manganese and iron-based contrast agents approved for clinical use, the vast majority of clinical exams are performed using gadolinium contrast agents. There are more then 10 million MRI studies performed with gadolinium-based contrast agents each year [1]. This thesis is devoted to understanding the mechanisms underlying contrast agent relaxivity, with two chapters focused on the relaxation physics of gadolinium-based probes, and one chapter on iron-oxide-based probes.

To fully understand contrast agent relaxivity it is instructive to review the fundamentals of magnetic resonance imaging including magnetization, resonance and relaxation.

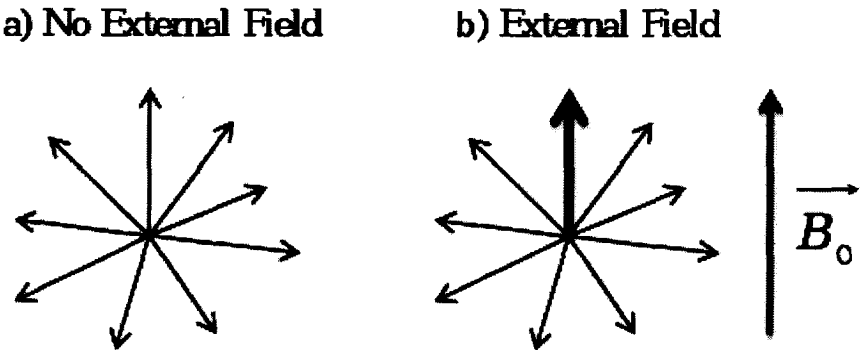

Fig. 1.1: In free space (a), the orientation of the individual magnetic moments are randomly oriented and yield no net magnetic moment. In an external magnetic field, the spins align yielding a net magnetic moment in the direction of the applied field (b).

1.1.1 Magnetization

All atomic nuclei posses an intrinsic quantity called spin angular momentum, I. Nuclei have a net non-zero spin if they have an odd number of neutrons and/or protons, in which case they behave like tiny bar magnets. Each nuclear spin has an associated magnetic moment $\overrightarrow{\mu}$, given by

$$\overrightarrow{\mu} = \gamma \overrightarrow{S} = \gamma \hbar I \tag{1.1}$$

where γ is the gyromagnetic ratio, $\overrightarrow{S}$ is the spin angular momentum, $\hbar$ is Planck's constant and I is the spin quantum number [2].

In the absence of an external magnetic field, the magnetic moments of paramagnetic material are randomly distributed and the net magnetization is zero [3]. When placed in an external magnetic field $\overrightarrow{B_0}$ the spins will align in one of two directions, with the field or against the field. Slightly more spins will align with the field, the lower energy orientation, resulting in a non-zero net magnetization, $\overrightarrow{M}$ in the direction of $\overrightarrow{B_0}$ as illustrated in Fig. 1.1. The individual spin magnetic moments do not align exactly with or against the field, but are tilted by an angle with respect to the magnetic field. The magnetic moments experience a torque that causes them to pre-

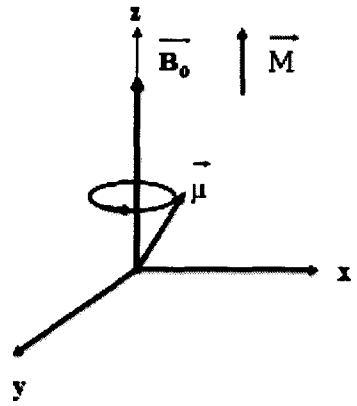

Fig. 1.2: Nuclear spins in an external field will process around the axis of the applied field at the Larmor frequency.

cess around the direction of the magnetic field at a frequency ω_0, called the Larmor frequency,

$$\omega_0 = \gamma B_0 \tag{1.2}$$

as shown in Fig. 1.2 [4].

1.1.2 Resonance

It is useful to discuss the resonance condition in terms of the net magnetization M, rather than for an individual proton. When considering a large number of protons, there is a significant amount of both absorption and emission occurring, but there will be a net absorption of energy by the tissue. If a radio frequency field B_1 perpendicular to B_0 is applied, absorption of the RF energy of frequency ω_0 will cause M to rotate away from its equilibrium orientation, perpendicular to both B_0 and B_1. For a particular combination of B_1 pulse duration and amplitude, the absorbed energy will cause M to rotate entirely into the transverse plane perpendicular to both B_0 and B_1 to produce a 90 degree rotation of M, and this is known as a 90 degree RF pulse [5]. Other excitation or "tip" angles are of course possible.

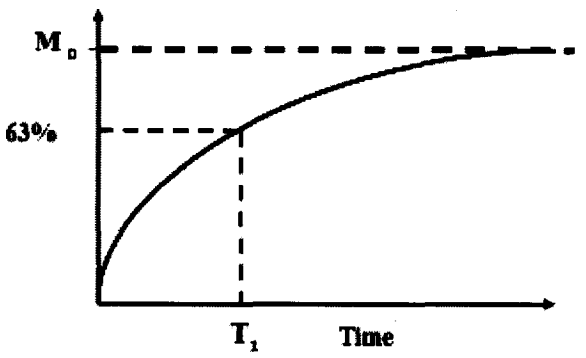

Fig. 1.3: Longitudinal relaxation curve.

1.1.3 Relaxation

Relaxation refers to the process of net magnetization returning to equilibrium, involving two mechanisms: longitudinal and transverse relaxation.

Longitudinal or T_1 relaxation describes the re-establishment of the equilibrium longitudinal magnetization M_0, along the z-axis following the application of an RF pulse. The T_1 relaxation time is defined as the time required for M to recover to 63% $(1-\frac{1}{e})$ of its equilibrium value, as shown in Fig. 1.3 and is represented by the relation $M_z(t) = M_{z,eq}(1 - e^{-t/T_1})$ [2].

The mechanism underlying T_1 relaxation is an exchange of energy between the individual spins and the surrounding lattice; hence this is commonly referred to as *spin-lattice* relaxation. This transfer of energy is facilitated by molecular motion in the vicinity of the spin; and therefore the rate of energy transfer is dependent on the frequency of this vibrational and rotational motion. When the frequency of the molecular motion is close to the precessional frequency of the spins, energy is easily transferred to the lattice. Therefore the structure and molecular composition of the molecule and its surrounding lattice influence the rate of T_1 relaxation [4].

Transverse or T_2 relaxation is the loss of phase coherence between the individual spins and therefore the decay of transverse magnetization following a 90° RF pulse

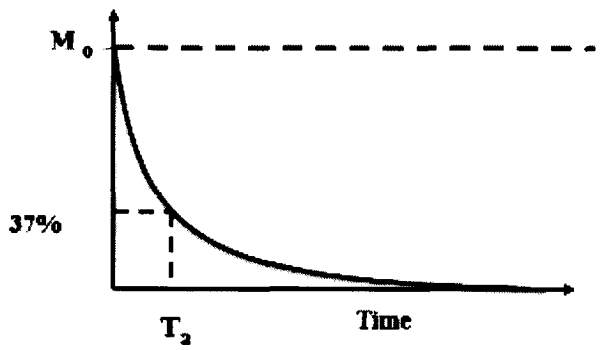

Fig. 1.4: Transverse relaxation curve.

as shown in Fig. 1.4. The T_2 relaxation time is defined as the time required for transverse magnetization to decay to 37% $(\frac{1}{e})$ of its original value and is represented by the relation $M_{xy}(t) = M_{xy}(0)e^{-t/T_2}$ [2].

T_2 relaxation is also referred to as *spin-spin* relaxation due to the energy transfer between spins. Inter and intra molecular interactions lead to subtle variations in the precession frequency, resulting in a gradual and irreversible loss of phase coherence. The individual magnetic moments begin to fan out in the transverse plane [4].

Macroscopic inhomogeneities in the static magnetic field $\overrightarrow{B_0}$ also induce dephasing of the transverse magnetization, and when these effects are included, the transverse magnetization relaxes with an overall time constant T_2^* [4].

The focus of this thesis is the relaxation physics of contrast agents; therefore, the following sections present a review of types and relaxation mechanisms of contrast agents.

1.2 Contrast Agents

An MRI contrast agent is most commonly a substance that will affect the magnetic properties of water protons to an extent that is observable in an image. There are two main classes of contrast agents: paramagnetic and superparamagnetic, both of which

shorten the relaxation times of bulk water protons. Paramagnetic contrast agents are ussually considered to be T_1-shortening, while superparamagnetic contrast agents are usually considered to be T_2-shortening. Paramagnetic contrast agents shorten both T_1 and T_2 but the T_1 effect is dominant. Superparamagnetic agents also shorten both T_1 and T_2, but depending on the size of the nanoparticulate agent, the T_2 effect is usually much larger than the T_1 effect.

1.2.1 Paramagnetic Agents

Paramagnetism is a form of magnetism that occurs only in the presence of an externally applied magnetic field. In the absence of an externally applied magnetic field, the total magnetization will drop to zero as thermal motion causes the spins to become randomly oriented. In the presence of an external field there is a small induced magnetization because a small fraction of the spins will be oriented by the field. This fraction is proportional to the field strength [6].

Paramagnetic materials which tumble at a rotational rate close to the Larmor frequency transfer energy between the paramagnetic ion and the surrounding water molecules or "lattice", thereby enhancing the longitudinal relaxation rate, or shortening the T_1 relaxation time of the water molecules. This transfer of energy occurs through dipole-dipole and scalar interactions, both requiring that the paramagnetic ion be in close contact with the water molecule. The paramagnetic species will also cause T_2 shortening due to dipole-dipole interactions as well as local field inhomogeneities. Dipole-dipole will increase both R_1 and R_2 relaxation rates (reciprocals of T_1 and T_2 relaxation times), but since in almost all tissues, the initial (pre-contrast) $R_1 \ll R_2$, the relative or fractional change in R_1 will dominate over that in R_2. Local magnetic field inhomogeneities will occur, with areas of higher contrast agent concentration experiencing a greater magnetic field than areas of lower concentration. These inhomogeneities in local magnetic field will cause a loss of phase coherence in magnetic moments, causing a shortening of T_2 [7].

1.2.2 Superparamagnetic Agents

Superparamagnetism occurs when the material is composed of very small crystallites. Superparamagnets consist of individual magnetic domains of elements, that have ferromagnetic properties in bulk. Coupling forces between these magnetic domains cause the magnetic moments of neighboring atoms to align, resulting in large internal magnetic fields [7].

At temperatures above the Curie temperature the thermal energy is sufficient to overcome coupling forces in a superparamagnetic material, causing the atomic magnetic moments to fluctuate randomly; this causes the material to behave purely paramagnetically. In the presence of an external magnetic field, the domains align and give rise to noticeable magnetization but in the absence of a magnetic field the domains rotate freely, resulting in a loss of magnetization exactly like a paramagnet [8].

At temperatures below the Curie temperature the superparamagnetic material will remain ferromagnetic. Thermal energy is not sufficient to overcome coupling forces between the magnetic moments of individual domains, therefore the magnetic moments will all align together. The excess thermal energy will change the direction of magnetization over time creating an overall magnetic field of zero. The material behaves in a manner similar to paramagnetism, except that instead of each individual spin being independently influenced by an external magnetic field, the magnetic moment of the entire crystallite tends to align with the magnetic field. In the absence of an external magnetic field the material will have an overall zero magnetization. Note that the Curie temperature for iron is 760 ^oC, so that all iron oxide nanoparticulate contrast agents exhibit superparamagnetic properties in the range of body temperatures. T_1 shortening as in paramagnetic contrast agents will be caused by dipole-dipole interactions and scalar interactions. T_2 shortening will be caused by local magnetic field inhomogeneities. Coupling forces between magnetic moments cause superparamagnets to be much stronger than paramagnets, causing much greater local

field inhomogenuites. Superparamagnets will shorten T_2 to a greater extent than T_1, and are therefore most often classified as T_2 shortening agents [8].

1.2.3 Contrast Agent Concentration

Longitudinal and transverse relaxation changes will modify MR image intensities, with the image signal modulation being dependent on contrast agent concentration: T_1 effects dominating at low doses and T_2 effects dominating at higher doses. At higher concentrations, or for stronger magnetic moments, local field inhomogeneities become more significant and cause a greater loss in phase coherence, increasing T_2 effects and overpowering T_1 effects. T_1 shortening will cause an increased signal in T_1-weighted MR images while T_2 shortening will cause a decrease in signal intensity on T_2-weighted images [7].

1.2.4 Relaxivity

Relaxivity r_i, is the change in relaxation rate after the introduction of the contrast agent (ΔR_i, i=1,2) normalized to the concentration of contrast agent or metal ion [M] [1].

$$r_i = \frac{\Delta R_i}{[M]} \qquad i = 1, 2 \tag{1.3}$$

Chapters 2 and 3 of this thesis are focused on the relaxivity physics of gadolinium-based contrast agents while chapter 4 is focused on the relaxivity physics of iron-oxide based contrast agents. The next two sections of this chapter deal with gadolinium contrast agent structure, focusing on clinically approved gadolinium contrast agents and the structural and dynamic parameters that are responsible for gadolinum relaxivity. An understanding of gadolinium relaxivity will provide a good basis for understanding iron relaxivity which will be covered in its entirety in chapter 4.

1.3 Gadolinium Contrast Agents

The majority of contrast enhanced clinical exams are performed with gadolinium complexes. The lanthanide metal, gadolinium (S= $\frac{7}{2}$), contains 7 unpaired electrons in its 4f orbital. Gadolinium is strongly paramagnetic at room temperature, and therefore forms paramagnetic complexes or T_1-shortening agents [9].

1.3.1 Requirements for Contrast Agent Stability

MRI contrast agents must be biocompatible pharmaceuticals as well as nuclear relaxation probes. Aside from standard pharmaceutical features such as water solubility and shelf stability, the requirements relevant for metal complex-based agents can be classified into three categories: relaxivity, localization in target tissue and toxicity [10].

The contrast agent must significantly increase the proton relaxation rate of the target tissue to be effective. MR imaging can detect as small as a a few percent increase in R_1, but ideally the clinical dose of contrast agent will produce many tens of percent change in relaxation rate at the target tissue. For reasons of biocompatibility, this increase in relaxivity must be achieved using non-toxic amounts of the contrast agent. For MRI contrast agents, it is sufficient only that the relaxation rates of the target tissue be enhanced in preference to other tissues [10].

For a contrast agent to be a good diagnostic tool it must be localized in the target tissue long enough to be imaged [10].

The acute and chronic toxicity of an intravenously administered metal complex is related in part to its stability in vivo and its tissue clearance behavior. Unchelated lanthanide ions are toxic at low concentrations, which means that if there is any significant ion-chelate dissociation, there is a risk of toxicity. Contrast agents should be excreted within hours of administration, and this is particularly true for chelated agents, given the fact that there is inevitably a small amount of ion-chelate dissocia-

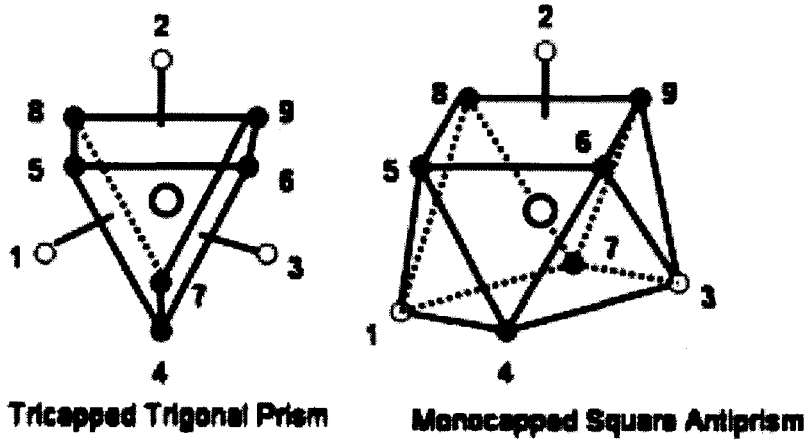

Fig. 1.5: Tricapped trigonal prism (TTP) and monocapped square antiprism (CSAP) geometries.

tion [10]. This disassociation can be caused in the body by transmetalation (exchange of the gadolinium ion with competing ions commonly found in the body like zinc and calcium). Commercially available contrast agents are very stable in both water and plasma solution, with only one molecule releasing its gadolinium ion per hundreds of millions or billions of chelate molecules. The key to stability is contrast agent structure, and as will be discussed further, some contrast agents are more stable then others. All contrast agents are released with an excess amount of chelate to increase contrast agent stability. European and USA regulation limits contrast agent use for patients with renal insufficiency [31].

1.3.2 Solid State Structure

Lanthanides tend to favor a high coordination number in aqueous media. Coordination number is the number of ligands bonded to a central ion. Chelates are complexes with two or more atoms bound to a metal ion, functioning as more than one ligand. The currently clinically approved MRI gadolinium(III)-chelates are nine-coordinate complexes (because of gadolinum's nine valance electrons), in which a ligand occupies eight binding sites at the metal center and the ninth coordination

site is occupied by a solvent water molecule. The idealized coordination geometries for a nine-coordinate complex are tricapped trigonal prism (TTP) and capped square antiprism (CSAP), as shown in Fig. 1.5 [9].

1.3.3 Clinically Approved and in Development Contrast Agents

There are currently eight gadolinium contrast agents approved for clinical use in MRI: Magnevist, Omniscan, Multihance, Gadovist, Dotarem, ProHance, Opti-MARK, Primovist and Vasovist. One gadolinium MR contrast agent, currently in development, will also be discussed, Gadofluorine. A basic overview of the chemical structure, relaxation mechanisms and applications for each of these contrast agents will be discussed.

Molecular structure of all of these contrast agents can be classified as linear (acyclic), cyclic or macrocyclic. Linear or acyclic compounds are composed of a string of atoms in a non-closed structure. Cyclic molecules are composed of atoms which form a closed ring or loop. A macrocyclic molecule is a ring of more than a dozen atoms. Macrocyclic compounds are very inert and least likely to disassociate. Linear and cyclic compounds are less stable [11]. At present, all clinically approved gadolinium contrast agent have either linear or macrocyclic structure.

Ionic contrast agents have ionic chelates and non-ionic contrast agents have non-ionic chelates. Ionic contrast agents are more stable as the gadolinium ion has a stronger bond with ionic chelates vs. non-ionic chelates [30]. Non-ionic gadolinium chelate molecules, have lower osmolality (moles of solute particles) than ionic contrast agents. Osmolality is not a major factor in terms of clinical relevance due to the small volume of contrast media used in MR examination. Theoretically high osmolality contrast agents may cause more pain or tissue necrosis than low osmolality contrast agents at higher contrast agent concentrations [32].

Magnevist

Magnevist, also known as gadopentetate dimeglumine (Gd-DTPA), was introduced in 1988 by Bayer Pharmaceuticals, making it the first clinically approved MRI contrast agent. It is the most commonly used contrast agent in MRI and most commonly used in the imaging of tumors, inflammation and vascular lesions. Gd-DTPA is a gadolinium complex of diethylenetriamine pentaacetic acid and is classed as a linear, ionic gadolinium contrast medium (Fig. 1.6) [9]. The net charge of the molecule is -2. Longitudinal relaxivity (r_1) for Magnevist is 3.3 $mM^{-1}s^{-1}$ in water at 1.5 T and temperature of 37 $°C$. Longitudinal relaxivity (r_1) for Magnevist is 4.1 $mM^{-1}s^{-1}$ in bovine plasma corresponding to an albumin concentration of 0.64 to 0.82 mmol/L at 1.5 T and temperature of 37 $°C$ [12].

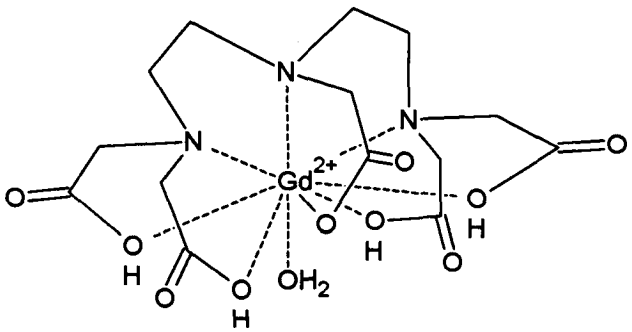

Fig. 1.6: Geometrical structure of Magnevist.

Omniscan

Omniscan, also known as gadodiamide (Gd-DTPA-BMA), was introduced in 1993 by Amersham Health. It is commonly used in imaging of blood vessels and intracranial and spinal lesions. Gd-DTPA-BMA is a gadolinium complex of diethylenetriamine pentaacetic acid-bismethylamide and is classed as a linear, non-ionic gadolinium contrast medium (Fig. 1.7) [9]. Longitudinal relaxivity (r_1) for Omniscan is 3.3 $mM^{-1}s^{-1}$ in water and 1.5 T at temperature of 37 $°C$. Longitudinal relaxivity (r_1) for Omniscan is 4.3 $mM^{-1}s^{-1}$ in bovine plasma corresponding to an albumin concentration of 0.64 to 0.82 mmol/L at 1.5 T and temperature of 37 $°C$ [12].

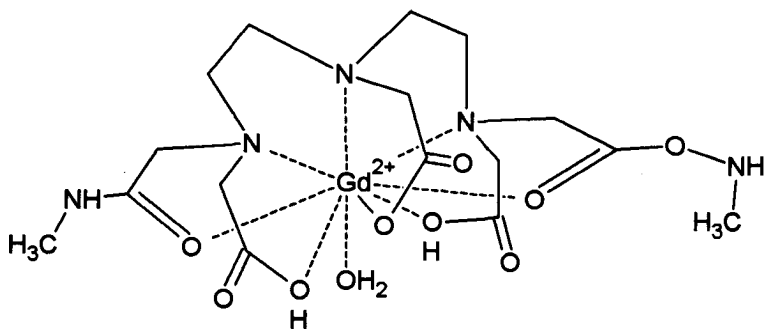

Fig. 1.7: Geometrical structure of Omniscan.

Multihance

Multihance, also known as gadobenate dimeglumine (Gd-BOPTA), was FDA approved in 2004 and is produced by Bracco Diagnostics Inc. It is commonly used in diagnosis of the liver and the central nervous system (CNS). Gd-BOPTA is classed as a linear, ionic gadolinium contrast medium (Fig. 1.8) [9]. Longitudinal relaxivity (r_1) for Multihance is 4.0 $mM^{-1}s^{-1}$ in water at field strength of 1.5 T and temperature of 37 $°C$. Longitudinal relaxivity (r_1) for Multihance is 6.3 $mM^{-1}s^{-1}$ in bovine plasma corresponding to an albumin concentration of 0.64 to 0.82 mmol/L at field strength of 1.5 T and temperature of 37 $°C$ [12].

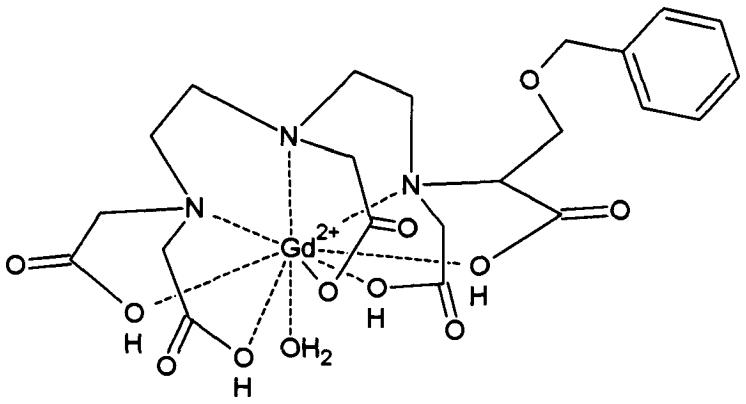

Fig. 1.8: Geometrical structure of Multihance.

Gadovist

Gadovist, also known as gadobutrol (Gd-BT-DO3A), was introduced in 1998 by Bayer Pharmaceuticals. It is commonly used in diagnosis of the central nervous system (CNS). Gd-BT-DO3A is classed as macrocyclic, non-ionic gadolinium contrast medium (Fig. 1.9) [9]. Longitudinal relaxivity (r_1) for Gadovist is 3.3 $\mathrm{mM}^{-1}s^{-1}$ in water at field strength of 1.5 T and temperature of 37 $^{\circ}C$. Longitudinal relaxivity (r_1) for Gadovist is 5.2 $\mathrm{mM}^{-1}s^{-1}$ in bovine plasma corresponding to an albumin concentration of 0.64 to 0.82 mmol/L at field strength of 1.5 T and temperature of 37 $^{\circ}C$ [12].

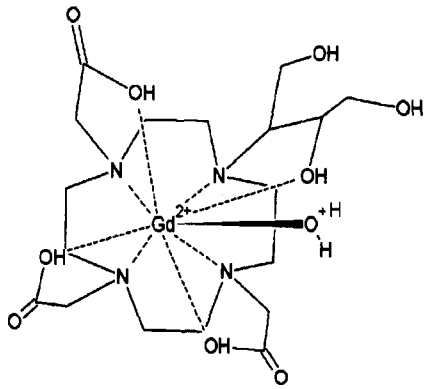

Fig. 1.9: Geometrical structure of Gadovist.

Dotarem

Dotarem, also known as gadoterate meglumine (Gd-DOTA), was introduced by Guerbet Group in 1989. It is commonly used in imaging of intracranial and spinal lesions as well as vasculature. Gd-DOTA is classed as macrocyclic, ionic gadolinium contrast medium (Fig. 1.10) [9]. Longitudinal relaxivity (r_1) for Dotarem is 2.9 $\mathrm{mM}^{-1}s^{-1}$ in water at field strength 1.5 T and temperature of 37 $^{\circ}C$. Longitudinal relaxivity (r_1) for Dotarem is 3.6 $\mathrm{mM}^{-1}s^{-1}$ in bovine plasma corresponding to an albumin concentration of 0.64 to 0.82 mmol/L at field strength 1.5 T and temperature of 37 $^{\circ}C$ [12].

ProHance

ProHance, also known as gadoteridol Gd(HP-DO3A), was FDA approved in 1992 and is produced by Bracco Diagnostics Inc. It is commonly used in imaging of the brain and spine as well as the whole body. Gd(HP-DO3A) is classed as macrocyclic, non-ionic gadolinium contrast medium (Fig. 1.11) [9]. Longitudinal relaxivity (r_1) for ProHance is 2.9 $\mathrm{mM}^{-1}s^{-1}$ in water at field strength of 1.5 T and temperature of 37 $^{\circ}C$. Longitudinal relaxivity (r_1) for ProHance is 4.1 $\mathrm{mM}^{-1}s^{-1}$ in bovine plasma corresponding to an albumin concentration of 0.64 to 0.82 mmol/L at field strength

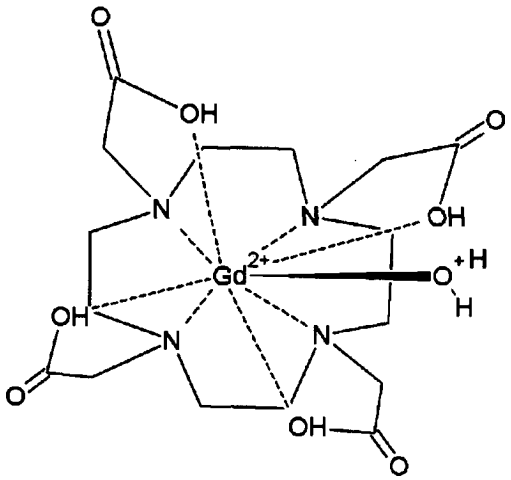

Fig. 1.10: Geometrical structure of Dotarem.

of 1.5 T and temperature of 37 $°C$ [12].

OptiMARK

OptiMARK, also known as gadoversetamide [Gd(DTPA-BMEA)(H_2O)], was FDA approved in 1999 and is produced by Covidien Ltd. It is commonly used in imaging of lesions of the brain, spine and liver as well as tumors. Gd(DTPA-BMEA)is a gadolinium chelate of diethylenetriamine pentaacetic acid bismethoxyethylamide is classed as an linear, non-ionic gadolinium contrast medium (Fig. 1.12) [9]. Longitudinal relaxivity (r_1) for OptiMARK is 3.8 $mM^{-1}s^{-1}$ in water at field strength of 1.5 T and temperature 37 $°C$. Longitudinal relaxivity (r_1) for OptiMARK is 4.7 $mM^{-1}s^{-1}$ in bovine plasma corresponding to an albumin concentration of 0.64 to 0.82 mmol/L at field strength of 1.5 T and temperature 37 $°C$ [12].

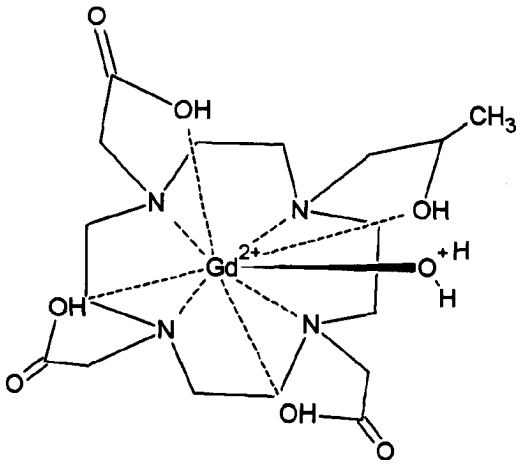

Fig. 1.11: Geometrical structure of ProHance.

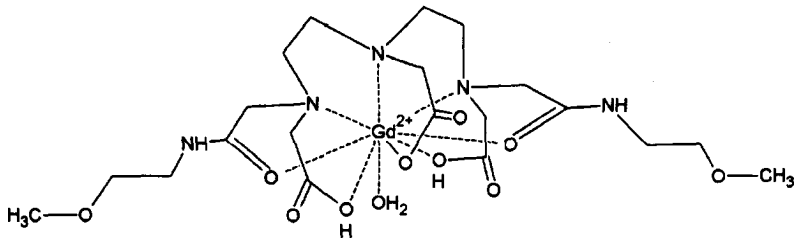

Fig. 1.12: Geometrical structure of OptiMARK.

Vasovist

Vasovist (formerly know as MS-325) is also known as gadofosveset trisodium, and is classed as an ionic and linear contrast medium. Vasovist is an albumin-targeted intravascular contrast agent. It is commonly used for contrast enhanced MR angiography (CE-MRA) for the visualization of abdominal or limb vessels in patients with suspected or known vascular disease. Vasovist binds reversibly to human albumin in plasma and results in increasing relaxivity. Vasovist is a formulation of a stable gadolinium diethylenetriaminepentaacetic acid (Gd-DTPA) chelate substituted with a diphenylcyclohexylphosphate group (gadofosveset trisodium) (Fig. 1.13) [13].

Longitudinal relaxivity (r_1) for Vasovist is 5.2 $mM^{-1}s^{-1}$ in water at field strength of 1.5 T and temperature 37 $°C$. Longitudinal relaxivity (r_1) for Vasovist is 19 $mM^{-1}s^{-1}$ in bovine plasma corresponding to an albumin concentration of 0.64 to 0.82 mmol/L at field strength of 1.5 T and temperature 37 $°C$ [12]. Longitudinal relaxivity (r_1) for Vasovist is 27.7 $mM^{-1}s^{-1}$ in human serum albumin corresponding to an albumin concentration of 0.67 mmol/L at field strength of 1.41 T and temperature 35 $°C$ [33].

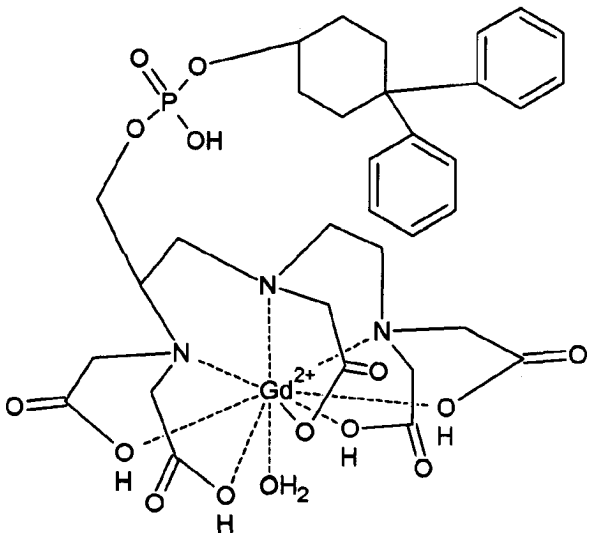

Fig. 1.13: Geometrical structure of Vasovist.

Primovist

Primovist (formerly known as Eovist) is also known as Gadoxetic acid disodium (Gd-EOB-DTPA) and is classified as a linear and non-ionic contrast agent. It is a highly specific MRI contrast agent to human serum albumin for the imaging, detection and characterization of liver conditions, including tumors and lesions. Primovist is a water-soluble ethoxybenzyl derivative of Gd-DTPA, (Fig. 1.14) [9]. Longitudinal relaxivity (r_1) for Primovist is 4.7 $mM^{-1}s^{-1}$ in water at field strength of 1.5 T and

temperature 37 $°C$. Longitudinal relaxivity (r_1) for Primovist is 6.9 $mM^{-1}s^{-1}$ in bovine plasma corresponding to an albumin concentration of 0.64 to 0.82 mmol/L at field strength of 1.5 T and temperature 37 $°C$ [12].

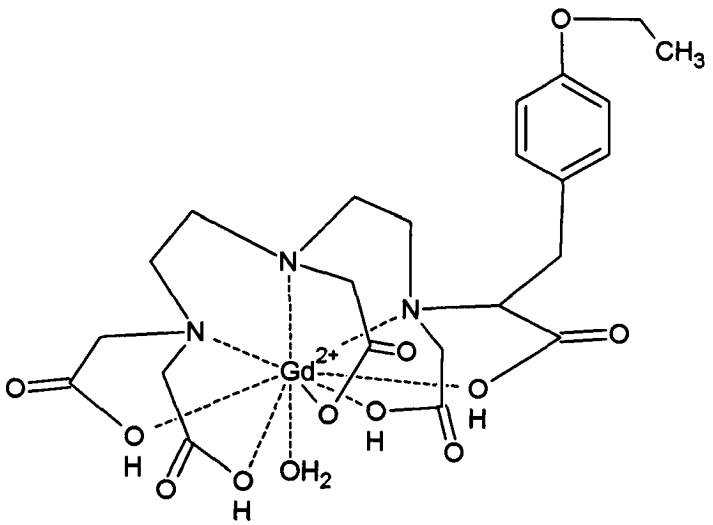

Fig. 1.14: Geometrical structure of Primovist.

Gadofluorine

Gadofluorine is not currently clinically approved. Gadofluorine is used in imaging of lymph nodes and as a blood pool agent. Gadofluorine is a macrocyclic gadolinium-based contrast agent with a hydrophobic perfluorinated side chain. The amphiphilic nature of the molecule (containing both hydrophopic and hydrophillic components) leads to non-specific bonding to a variety of proteins in tissue causing an increase in relaxivity [14]. The longitudinal relaxivity of aggregated Gadofluorine is 14.5 $mM^{-1}s^{-1}$ in water at field strength of 1.5 T and at temperature 20 $°C$. The longitudinal relaxivity of Gadofluorine is 14.1 $mM^{-1}s^{-1}$ in bovine plasma at field strength of 1.5 T and at temperature 20 $°C$, (Fig. 1.15) [12].

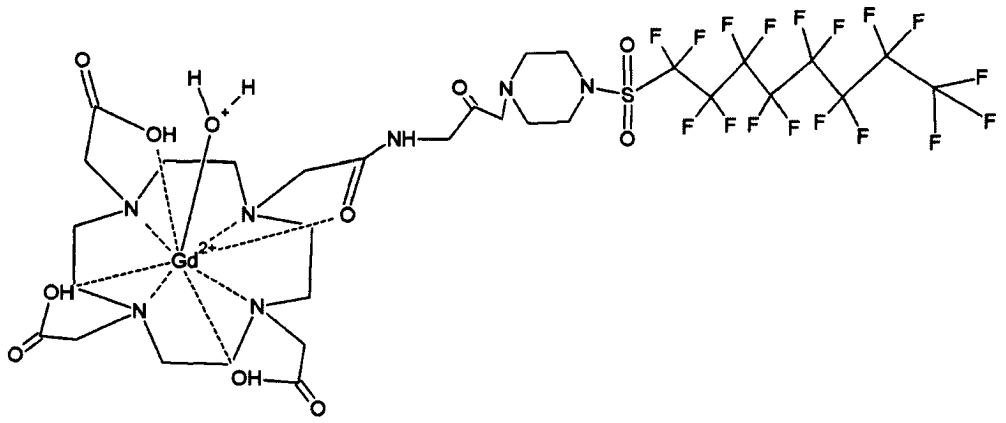

Fig. 1.15: Geometrical structure of Gadofluorine.

Table 1.1: Gadolinium contarst agent properties

Contrast Agent	Structure	Charge	r_1 $(mM^{-1}s^{-1})$ at 1.5 T, 37 ^oC in water	r_1 $(mM^{-1}s^{-1})$ at 1.5 T, 37 ^oC in bovine plasma
Magnevist	linear	ionic	3.3	4.1
Omniscan	linear	non-ionic	3.3	4.3
Multihance	linear	ionic	4.0	6.3
Gadovist	macrocyclic	non-ionic	3.3	5.2
Dotarem	macrocyclic	ionic	2.9	3.6
ProHance	macrocyclic	non-ionic	2.9	4.1
OptiMARK	linear	non-ionic	3.8	4.7
Vasovist	linear	ionic	5.2	19
Primovist	linear	non-ionic	4.7	6.9
Gadofluorine	macrocyclic	ionic	14.5	14.1

1.4 Relaxivity

Water in close proximity to the gadolinium ion is relaxed by the ion and then rapidly exchanged with the bulk water. Water that interacts with the gadolinium ion is classified into three categories: inner-sphere water, i.e. water that is directly coordinated to the gadolinium ion; second-sphere water, i.e. water molecules that hydrate the complex and have a finite residency time that is longer than the translational dif-

fusion time of pure water; outer-sphere water, i.e. water molecules whose interaction with Gd(III) is governed by translational diffusion only. T_1 relaxation of water hydrogen by Gd(III) is dominated by the dipolar mechanism. Dipolar relaxation occurs via the transfer of energy between two molecules with dipoles. Relaxation will depend on the number of water molecules, their distance from the gadolinium ion, their rate of exchange with the bulk water and the dynamics of the fluctuating magnetic dipoles [1].

Fluctuating magnetic dipoles can induce spin transitions and cause spin relaxation. Correlation time (τ_c) is defined as the time constant characterizing these fluctuations. Several factors cause fluctuating magnetic dipoles: longitudinal electronic relaxation (T_{1e}) of Gd(III), rotational diffusion (τ_R) of the complex, and water exchange in and out of the first (τ_m) and second (τ'_m) coordination spheres, as depicted in Fig. 1.16 [1].

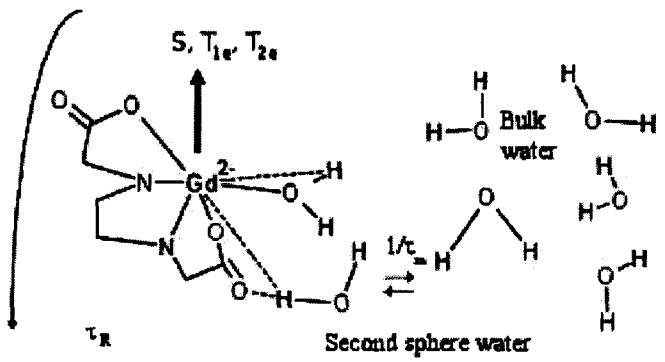

Fig. 1.16: Molecular parameters that influence inner and second-sphere relaxivity.

1.4.1 Inner-Sphere Relaxivity

Relaxivity arising from inner-sphere water is given by

$$r_1^{IS} = \frac{[M]}{[H_2O]} \frac{q}{T_{1M} + \tau_m} \tag{1.4}$$

This equation reflects a model of 2-site exchange, where q is the hydration number, [M] is the concentration of the paramagnetic contrast agent (metal ion), [H_2O] is the concentration of the water, T_{1M} is the longitudinal relaxation time of the water hydrogen in the inner-sphere and τ_m is the mean water residence time in the first coordination site [1].

Hydration Number

Hydration number, q, is the number of water molecules in the inner-coordination sphere. The contrast agent must be stable enough such that a safe amount of Gd(III) ion is released into the body. The more water molecules there are coordinated to the Gd(III) ion, the less thermodynamically stable the complex is, therefore the practicality of increasing the hydration number to increase overall relaxivity is limited. The other trade-off of increasing the hydration number is that it often allows coordination of other ligands, such as endogenous phosphate or bicarbonate, which displaces the water and decrease the overall relaxivity. There are several possible methods specific to the sample which can be used to determine hydration number, including x-ray crystallography, lifetime luminescence measurements and pulsed electron-nuclear double resonance (ENDOR) spectroscopy [1].

Gadolinium-Water Distance

Decreasing the Gd-H distance would significantly increase relaxivity in theory. Values for various Gd chelates reported in literature range between 2.7 and 3.3 Å, but these numbers are obtained from fitting Nuclear Magnetic Resonance Dispersion (NMRD) data. The Gd-H distance can also be experimentally determined using

neutron diffraction, ENDOR spectroscopy or by using isotopic exchange methods in very concentrated solution. Pulsed ENDOR studies have determined that the Gd-H distance is very close to 3.1 Å for a wide range of 8 and 9 coordinate Gd-complexes and does not depend on ligand or total charge. It therefore seems unlikely that the Gd-H distance can be significantly decreased as a means of increasing relaxivity [1].

Correlation Time

Correlation time τ_c is dominated by the shortest correlation time among rotation τ_R, electronic relaxation T_{1e}, and chemical exchange τ_m, time constants. Field strength as well as the chemical structure of the contrast agent and the molecular content and viscosity of surrounding medium determine which correlation time is dominant [1].

$$\frac{1}{\tau_c} = \frac{1}{T_{1e}} + \frac{1}{\tau_m} + \frac{1}{\tau_R} \tag{1.5}$$

Rotational Diffusion

Rotational correlation time, τ_R, can be estimated from various physical methods such as NMR relaxation, EPR, fluorescence, or can be calculated using the Stokes-Einstein equation. Rotation is often assumed to be isotropic, this is often a reasonable assumption but it may not be valid for large molecules. Internal motion within the molecule or anisotropic rotation will reduce correlation time from that predicted by an isotropic model [1].

Electronic Relaxation

Electronic relaxation T_{1e}, for Gd(III) is a complex, magnetic field dependent phenomenon. At low field (<0.1 Tesla), electronic relaxation is very fast and becomes the dominant relaxation time. However electronic relaxation rate decreases with increasing field strength, at some point becoming slower than rotational motion, and as a result correlation time changes as a function of field [1].

Electronic relaxation can be described in terms of the electronic spin Hamiltonian which is composed of Zeeman and zero field splitting terms.

$$H_S(\beta, \gamma; t) = H_{Zeeman} + H_{ZFS}(\beta, \gamma; t) \tag{1.6}$$

Zeeman interaction is the splitting observed in energy levels according to the value of the magnetic quantum number (m). The z component of angular momentum is completely described by m, $L_z = m\hbar$ [15].

Zero-field splitting is the removal of the spin microstate degeneracy (electronic energy levels are no longer equal in energy) for systems with S (spin angular momentum) $> \frac{1}{2}$ in the absence of an external applied field. Zero-field splitting causes magnetic anisotropy and has profound effects on magnetic properties [1].

Water Exchange, $k_{ex} = \frac{1}{\tau_m}$

The coordinated water must be in rapid exchange with bulk solvent in order to transmit the relaxation effect to the solvent. Water exchange is a readily measurable parameter using ^{17}O NMR transverse relaxation rate measurements at high field. Relaxivity can be limited if water exchange is too slow and the relaxation effect is poorly transmitted to the bulk. Relaxivity can also be limited if water exchange is too fast because the water isn't coordinated to the Gd(III) long enough to be relaxed [1].

1.4.2 Second-Sphere and Outer-Sphere Relaxivity

There is a contribution to relaxivity from water diffusing near the gadolinium complex. Outer-sphere relaxivity is determined by the diffusion coefficient of water and the distance of closest approach. Exchangeable hydrogens from the second coordination sphere or protonation sites on the molecule also contribute to relaxivity [1].

1.4.3 Effect of Field Strength and Temperature

Relaxivity can be strongly dependent on the applied magnetic field, with relaxivity generally, but not always, decreasing with increasing magnetic field. This would imply that contrast agents would be generally less and less effective as field strength increases, but this turns out not necessarily to be the case, since relaxation times of tissue also increase with increasing field strength, so less contrast agent at a fixed relaxivity is required to yield the same image contrast enhancement [1].

Water exchange and rotational diffusion rates are both temperature dependent, both increasing with temperature, thereby making relaxivity temperature dependent.

1.5 Thesis Objectives and Overview

Contrast agent relaxivity can be experimentally determined using magnetic resonance imaging or spectrometer derived measures of relaxation times, but is more thoroughly accomplished using nuclear magnetic resonance relaxation dispersion (NMRD) profiles. NMRD profiles are created by measuring relaxivity over a range of magnetic field strengths using a field-cycling relaxometer. A field-cycling relaxometer is an NMR apparatus capable of operating over a range of magnetic field strengths, normally exploiting pulse field electromagnets to accomplish fast field cycling.

Theories of relaxivity bridge the understanding gap between experimentally observed results and the chemical structures of the contrast agents. Studying relaxivity can provide insights into the underlying mechanisms of contrast agent relaxivity. The main objective of my thesis was to implement several of the known theories of relaxivity for both gadolinium and iron based contrast agents, and to begin to use these theoretical models to gain a better appreciation for the underlying mechanisms that govern the changes in contrast agent relaxivity that are observed to accompany protein binding, oligomerization, nanoparticle clustering, and (in future) other interesting biological activation events.

Computer programs were created to describe gadolinium relaxivity based on three theories: Solomon-Bloembergen-Morgan (SBM), Szabo-Lipari (SL) and Generalized Solomon-Bloembergen-Morgan (GSBM). These theories were then investigated to determine the dominant structural and molecular dynamic factors involved in relaxivity, to compare these three theories of relaxivity with regard to predicting NMRD profiles of clinically approved contrast agents, and finally to calculate underlying parameters using theoretical fits to experimental NMRD profiles for MS-325 bound to human serum albumin (HSA), and for a novel enzyme-activatable contrast agent: MPO(Gd).

In Chapter 2 the three theories of relaxivity are described and used to model experimental results for the contrast agent MS-325 (now known commercially as Vasovist) bound HSA.

Chapter 3 compares the factors that contribute to relaxivity for various contrast agents. The main hypothesis was that the dominant contribution to relaxivity for the known gadolinium based contrast agents is the rotational correlation time of the whole molecule (τ_R). Comparison of the contrast agent structures and their relaxivities should indicate that the biggest and therefore most slowly rotating contrast agents also have the highest relaxivity, particularly at clinical MRI field strengths. Of the three theories, the generalized Solomon-Bloembergen-Morgan (GSBM) theory was found to be most accurate over the full field strength range. Two variations of the SBM theory were used to extract structural parameters from MS-325 bound to HSA by model fitting, and these results were compared with results obtained by Caravan *et. al.* The structural parameters of a pre- and post-activated gadolinium based myeloperoxidase (MPO) sensing contrast agent were calculated from experimental NMRD profiles of these compounds.

Superparamagnetic iron oxide nanoparticle relaxivity is based on the original SBM theory developed for paramagnetic systems. There are two models describing superparamagnetic relaxivity: the high anisotropy and low anisotropy models. The main contributing factors to superparmagnetic relaxivity were investigated in Chapter 4.

A specialized subset of iron contrast agents switch from a dispersed to a clustered state when coming into contact with a target analyte. Ratios of longitudinal and transverse relaxivity before and after nanoparticle clustering were derived and compared to experimental results in Chapter 4.

Chapter 5 provides a summary of the project and future directions in relaxation theory.

Chapter 2

Theories of Gadolinium Relaxivity

Three models were used to study gadolinium relaxivity in this thesis: Solomon-Bloembergen-Morgan (SBM), Szabo and Lipari (SL) and Generalized Solomon-Bloembergen-Morgan (GSBM). SBM theory is known as the "classical theory", it assumes a dominant Zeeman interaction (high-field limit) and a negligible contribution to electronic relaxation from the static zero-field splitting (ZFS) effect [16]. The SL model is a slight modification on SBM which includes the effects of anisotropic relaxation [17]. GSBM theory applies Redfield theory on the electron spin system using Liouville formalism. GSBM includes both static and transient ZFS as well as the Zeeman interaction, and therefore it is the most accurate of all the theories over the full magnetic field range [19].

The three models were fit to experimental NMRD profiles of the gadolinium-based compound MS-325 bound to human serum albumin (HSA).

2.1 Contributions to Relaxivity

The introduction of a gadolinium contrast agent into a solvent will increase the longitudinal and transverse relaxation rates, $\frac{1}{T_1}$ and $\frac{1}{T_2}$, respectively, of solvent nuclei. The diamagnetic and paramagnetic contributions to the relaxation rates of such

solutions are additive.

$$\left(\frac{1}{T_i}\right)_{observed} = \left(\frac{1}{T_i}\right)_d + \left(\frac{1}{T_i}\right)_p \quad i = 1,2 \tag{2.1}$$

In the absence of solute-solute interaction, the solvent relaxation rates are linearly dependent on the concentration of the paramagnetic species ($[M]$); relaxivity r_i, is defined as the slope of this dependence in units of $mM^{-1}s^{-1}$ [10].

$$\left(\frac{1}{T_i}\right)_{observed} = \left(\frac{1}{T_i}\right)_d + r_i[M] \quad i = 1,2 \tag{2.2}$$

The large and fluctuating local magnetic field in the vicinity of a paramagnetic center provides this additive relaxation pathway for solvent nuclei. Specific chemical interactions are important in transmitting the paramagnetic effect. The efficacy of each type of chemical interaction is dependent on the distance and time scale of the interaction. The term "inner-sphere relaxation" (IS) pertains to water bound to the primary coordination sphere of the metal ion which exchanges with the bulk solvent. The term "outer-sphere relaxation" (OS) encompasses both hydrogen-bonded waters in the second coordination sphere and interactions due to translational diffusion of water molecules past the chelate [10].

$$\left(\frac{1}{T_i}\right)_p = \left(\frac{1}{T_i}\right)_{IS} + \left(\frac{1}{T_i}\right)_{OS} \quad i = 1,2 \tag{2.3}$$

The total relaxivity of a paramagnetic agent is therefore generally given by Eq. 2.3. The longitudinal relaxation contribution from the inner-sphere mechanism results from a chemical exchange of the water molecule between the primary coordination sphere of the paramagnetic metal ion and the bulk solvent [10].

$$\left[\frac{1}{T_1}\right]_{IS} = \frac{[M]}{[H_2O]} \frac{q}{T_{1M} + \tau_m} \tag{2.4}$$

In eq. 2.4, [M] is the concentration of the metal ion, $[H_2O]$ is the concentration of water, q is the number of water molecules bound per metal ion, T_{1M} is the relaxation time of the bound water protons, and τ_m is the residence lifetime of the bound water [10].

2.2 Solomon-Bloembergen-Morgan

In 1955, Solomon published a seminal paper on dipole-dipole (DD) relaxation. The dipole-dipole interaction is assumed to be of constant strength corresponding to a constant distance between two spins acting as magnetic dipoles. The vector connecting the two spins $\mathbf{r}_{IS}$, changes its orientation through random molecular motions. The total energy of the DD system is composed of the unperturbed system describing the Zeeman interaction and the time-dependent variation in the orientation of the $\mathbf{r}_{IS}$ vector [34].

Using a simple kinetic model, Solomon demonstrated that the spin-lattice relaxation of the two spins was described by a system of coupled differential equations, with bi-exponential functions as general solutions. A single exponential relaxation for one spin can be obtained if the other spin is different from the first and has an independent and highly efficient relaxation pathway; this condition is met if one of the spins is an electron. Spin transition probabilities are calculated using time-dependent perturbation theory with stochastic perturbation. A fundamental assumption of SBM theory is that of time-independent transition probabilities, requiring the product of the time-dependent variation in the orientation of the two spins (called the correlation time τ_c) and the strength of the perturbation be much smaller then unity ($\omega_H \tau_c << 1$). Under assumptions of rapid spin re-orientation with minimal perturbation the spectral density function can be shown to be Lorentzian [34], and this is therefore a fundamental characteristic of SBM theory.

Solomon and Bloembergen formulated a similar scalar expression for J-coupling: the coupling between two nuclear spins due to the influence of bonding electrons on the magnetic field running between the two nuclei [34].

SBM theory is known as the "classical theory"; it assumes a dominant Zeeman interaction (high-field limit) and a negligible contribution to electronic relaxation from static zero-field splitting (ZFS). For the purposes of this thesis, the low-field

regime will be defined as field strengths less than or equal to 10 MHz or 0.42 T, and the high-field regime will be defined as field strengths greater than 10 MHz or 0.42 T. SBM is inaccurate in the low-field region due to its neglect of zero field splitting, but accurate in the high field, as zero-field splitting is nonexistent for most complexes past a frequency of approximately 10 MHz [16].

SBM theory includes calculations for both inner- and outer-sphere relaxation. Metal-macromolecule complexes have very large inner-sphere contributions and outer-sphere relaxivity is often ignored. Large paramagnetic complexes exhibit long rotational tumbling times which further enhance inner-sphere relaxivity. In this thesis only inner-sphere relaxivity was calculated because of its dominant influence on total relaxivity for the contrast agents and field strengths of relevance to MRI [10].

In this work two different variations of SBM equations were implemented in MATLAB, one based on Lauffer R.B. *et. al, Chem. Rev.* **1987** and another based on Caravan P. *et. al, Inorganic Chem.* **2007**.

2.2.1 SBM Variation Based on Lauffer R.B., *Chem. Rev.* 1987, 87, 901-927.

Contrast agent relaxation time is the sum of dipolar ("through space") first term and scalar, or contact ("through-bonds") second term, contributions (2.5).

$$\frac{1}{T_{1M}} = \frac{2}{15}\left(\frac{\mu_0}{4\pi}\right)^2 \frac{\gamma_H^2 g_e^2 S(S+1)\mu_B^2}{r_{GdH}^6}\left[\frac{3\tau_c}{1+\omega_H^2\tau_c^2}+\frac{7\tau_c}{1+\omega_S^2\tau_c^2}\right] + \frac{2}{3}S(S+1)\left(\frac{A}{\hbar}\right)^2\left[\frac{\tau_e}{1+\omega_S^2\tau_c^2}\right] \tag{2.5}$$

$$\frac{1}{\tau_c} = \frac{1}{T_{1e}} + \frac{1}{\tau_m} + \frac{1}{\tau_R} \tag{2.6}$$

$$\frac{1}{\tau_e} = \frac{1}{T_{1e}} + \frac{1}{\tau_m} \tag{2.7}$$

where γ_H is the gyromagnetic ratio, g is the electronic g-factor, S is the total electron spin of the metal ion, μ_B is the Bohr magneton, μ_0 is the permeability of vacuum,

r is the proton-metal ion distance, ω_S and ω_H are the electronic and proton Larmor precessional frequencies, respectively, and $\frac{A}{\hbar}$ is the electron-nuclear hyperfine coupling constant. The correlation times that define dipole-dipole and scalar relaxation are τ_c and τ_e, respectively [10]. T_{1e} is the longitudinal electron spin relaxation time, τ_m is the water residence time, and τ_R is the rotational tumbling time of the entire metal-water unit [10].

The "3-term" in (2.5) is a function of the nuclear precession frequency while the "7-term" is a function of the electron precession frequency. Since the gyromagnetic ratio of an electron is much larger than that of a proton ($\gamma_S/\gamma_H = 658$), the magnetic field at which $\omega_S^2\tau_c^2$ equals 1, or the "7-term breakpoint" field, will be much lower than that at which $\omega_H^2\tau_c^2$ equals 1, or the "3-term breakpoint" field. At field strengths above the "7-term breakpoint", this term disperses away (approaches zero) and has a negligible contribution to the total relaxation. For this reason, the "7-term" is significant only in the low field regime.

For $S > \frac{1}{2}$ ions, collisions between the complex and solvent molecules (or "wagging" motions of the primary coordination sphere water molecules) are thought to induce distortions from octahedral symmetry that in turn lead to zero-field splitting (ZFS). Zero-field splitting is the removal of the spin microstate degeneracy for systems with $S > \frac{1}{2}$ in the absence of an external applied field. Zero-field splitting causes magnetic anisotropy and has profound effects on magnetic properties [10].

$$\frac{1}{T_{1e}} = B\left[\frac{1}{1+\omega_S^2\tau_v^2} + \frac{4}{1+4\omega_S^2\tau_v^2}\right] \tag{2.8}$$

$$B = \frac{1}{5 * \tau_{s0}} \tag{2.9}$$

Electronic relaxation occurs as a result of this ZFS modulation with T_{1e}^{-1} given by (2.8), where the constant B is related to the magnitude of the transient ZFS, τ_{s0} is the electronic relaxation time at zero field and τ_v is the correlation time characterizing the fluctuations [10].

The dipole-dipole relaxation term is dominant and the scalar relaxation term is ignored in Caravan variations of SBM theory (2.5); this is a very good approximation and a common convention.

2.2.2 Second SBM Variation, Based on Caravan P., *Inorganic Chem.* 2007, 46, 6632-6639.

Slight modifications to the SBM equations were published by Caravan in 2007, all based on simple approximations.

$$\frac{1}{T_{1M}} = \frac{2}{15}\left(\frac{\mu_0}{4\pi}\right)^2 \frac{\gamma_H^2 g_e^2 S(S+1)\mu_B^2}{r_{GdH}^6}\left[\frac{3\tau_c}{1+\omega_H^2\tau_c^2}\right] \tag{2.10}$$

$$\frac{1}{T_{1e}} = B\left[\frac{1}{1+\omega_S^2\tau_v^2} + \frac{4}{1+4\omega_S^2\tau_v^2}\right] \tag{2.11}$$

$$B = \frac{\Delta_t^2[4S(S+1)-3]\tau_v}{25} \tag{2.12}$$

$$\frac{1}{\tau_c} = \frac{1}{T_{1e}} + \frac{1}{\tau_R} \tag{2.13}$$

Equation (2.10) approximates the total inner-sphere longitudinal relaxation rate using just the dipole-dipole term. In this variation of SBM the "7-term" is also omitted based on the rationale stated above.

In this Caravan variation the constant B is calculated differently than in the Lauffer variation. In (2.12) Δ_t^2 is the magnitude of the transient zero field splitting (ZFS). The two equations for B, (2.9) and (2.12) are equivalent. With regard to the calculation of τ_c, electronic relaxation T_{1e} is dominant at low field but rotational correlation time τ_R becomes dominant at high fields. At no point is water residence time τ_m dominant in the calculation of the total correlation time, so not including τ_m in the correlation time calculation is a good approximation [17]. This approximation is valid as long as τ_R is shorter than τ_m. If τ_R becomes greater or equal to τ_m, SBM equations breakdown as a whole; therefore, this approximation is widely used in all forms of SBM theory.

2.2.3 First Szabo and Lipari Model Based on Nicolle G. M., *J. Biol. Inorganic Chem.* 2002, 7, 757-769.

The SL model includes the effect of anisotropic relaxation by modifying the spectral density term. Anisotropic relaxation is relaxation caused by anisotropic motion of the molecular side chains. The first SL variation, similar to the first SBM variation, describes dipole-dipole relaxation as a function of both nuclear and electron precession frequency.

$$\frac{1}{T_{1M}} = \frac{2}{15}\left(\frac{\mu_0}{4\pi}\right)^2 \frac{\gamma_H^2 g^2 S(S+1)\mu_B^2}{r^6}\left[3J(\omega_H;\tau_{f1}) + 7J(\omega_S;\tau_{f2})\right] \tag{2.14}$$

The longitudinal relaxation rate of the inner-sphere protons, $1/T_{1M}$ is expressed in terms of spectral density functions, $J(\omega_H;\tau_{fi})$. Molecular motion is described by a fast anisotropic local motion term with a correlation time of τ_1 and a slower isotropic global motion term with a correlation time of τ_R. F^2 is an order parameter representing the degree of anisotropy (F^2=1 is an isotropic system). The relevant spectral density functions are expressed as

$$J(\omega_H;\tau_{f1}) = \left(\frac{F^2\tau_{c1}}{1+\omega_H^2\tau_{c1}^2} + \frac{(1-F^2)\tau_{f1}}{1+\omega_H^2\tau_{f1}^2}\right), \tag{2.15}$$

$$J(\omega_S;\tau_{f2}) = \left(\frac{F^2\tau_{c2}}{1+\omega_S^2\tau_{c2}^2} + \frac{(1-F^2)\tau_{f2}}{1+\omega_S^2\tau_{f2}^2}\right), \tag{2.16}$$

$$\frac{1}{\tau_{ci}} = \frac{1}{\tau_R} + \frac{1}{\tau_m} + \frac{1}{T_{ie}} \qquad i = 1,2, \tag{2.17}$$

$$\frac{1}{\tau_{fi}} = \frac{1}{\tau_R} + \frac{1}{\tau_1} + \frac{1}{\tau_m} + \frac{1}{T_{ie}}. \tag{2.18}$$

The longitudinal and transverse electronic relaxation rates, $1/T_{1e}$ and $1/T_{2e}$ are

$$\frac{1}{T_{1e}} = \frac{1}{25}\Delta^2\tau_v[4S(S+1)-3]\left[\frac{1}{1+\omega_S^2\tau_v^2} + \frac{4}{1+4\omega_S^2\tau_v^2}\right], \tag{2.19}$$

$$\frac{1}{T_{2e}} = \Delta^2\tau_v\left[\frac{5.26}{1+0.372\omega_S^2\tau_v^2} + \frac{7.18}{1+1.24\omega_S\tau_v}\right] \tag{2.20}$$

[20]. Transverse electronic relaxation becomes a factor in contrast agent relaxation with anisotropic rotational motion of side chains. Independent rotation of the whole molecule and side chains will cause increased local magnetic field inhomogenuities and will result in an increased loss of phase coherence.

2.2.4 Second Szabo and Lipari Model Based on Caravan P., *Inorganic Chem.* 2007, 46, 6632-6639.

In the second SL variation, as in the second SBM variation, the "7-term" is omitted. It is less accurate in the low-field regime than the first SL variation but remains very accurate in the high field regime.

$$\frac{1}{T_{1M}} = \frac{2}{15}\left(\frac{\mu_0}{4\pi}\right)^2 \frac{\gamma_H^2 g^2 S(S+1)\mu_B^2}{r^6}\left[\frac{3F^2\tau_c}{1+\omega_H^2\tau_c^2} + \frac{3(1-F^2)\tau_f}{1+\omega_H^2\tau_f^2}\right] \tag{2.21}$$

$$\frac{1}{\tau_f} = \frac{1}{\tau_c} + \frac{1}{\tau_1} \tag{2.22}$$

One of the contrast agents studied in this thesis exhibits anisotropic motion due to molecular side chains, and that is MS-325 bound to HSA. MS-325 bound to human serum albumin (HSA)has been shown to exhibit a relatively small order parameter $F^2 = 0.63$ and the fast correlation time was too short to be determined $\tau_1 < 100$ ps [17].

2.3 Second-Sphere and Outer-Sphere Relaxivity

Gd(III) complexes enhance relaxivity via two additional mechanisms: second-sphere and outer-sphere relaxation. Second-sphere relaxation occurs when water molecules in the second coordination sphere bonded to the lone pairs on the carboxylate oxygen are relaxed via a dipolar mechanism. Second-sphere relaxivity is exactly described by the inner-sphere dipolar term where the relevant parameters are described with a prime, q', r' etc. in equations (2.5), (2.8), (2.6) and (2.9) [21].

Outer-sphere proton relaxation results from protons diffusing past the agent modulated by rotation and translational diffusion. Outer-sphere relaxation modulated by rotational diffusion is described as:

$$\frac{1}{T_1} = \frac{2}{15}\gamma_I^2\gamma_S^2\hbar^2\frac{q[M]S(S+1)}{[H_2O]d^6}\Big[3j(\omega_H) + j(\omega_S - \omega_H) + 6j(\omega_S + \omega_H)\Big], \tag{2.23}$$

$$j(\omega) = \frac{\tau_c}{1+\omega^2\tau_c^2}, \tag{2.24}$$

and

$$\frac{1}{\tau_c} = \frac{1}{\tau_R} + \frac{1}{T_{1e}} \tag{2.25}$$

where d is the distance between the centre ion and water molecule, [M] is the concentration of paramagnetic contrast agent and $[H_2O]$ is the concentration of water. Except for the omission of water residency time (τ_m) equation (2.23) is very similar to the dipolar part of the Solomon-Bloembergen equations (2.5) [9].

Outer-sphere proton relaxation is dominated by translational diffusion and most often described by translational diffusion theory with the omission of any rotational diffusion terms. The translationally-modulated outer-sphere diffusion contribution to T_1, based upon a rigid-sphere model is:

$$\frac{1}{T_1} = \frac{32\pi}{405}\gamma_I^2\gamma_S^2\hbar^2 S(S+1)\frac{N_A[M]}{aD}[3j(\omega_H) + 7j(\omega_S)], \tag{2.26}$$

$$j(\omega) = Re\left\{\frac{1 + \frac{1}{4}(i\omega\tau + \frac{\tau}{T_{1e}})^{\frac{1}{2}}}{1 + (i\omega\tau + \frac{\tau}{T_{1e}})^{\frac{1}{2}} + \frac{4}{9}(i\omega\tau + \frac{\tau}{T_{1e}}) + \frac{1}{9}(i\omega\tau + \frac{\tau}{T_{1e}})^{\frac{3}{2}}}\right\}, \tag{2.27}$$

$$\tau = 3\tau_D = \frac{a^2}{D}, \tag{2.28}$$

where a is the distance of closest approach between the water proton and the paramagnetic complex and D is the sum of the diffusion coefficients for the solvent protons and the contrast agent, N_A is the Avogadro's constant and [M] is the concentration of the paramagnetic contrast agent [21].

2.4 Limitations of SBM Theory

The major problem with the standard SBM approach or its modified versions is the assumption that zero-field splitting has a limited influence on electronic relaxation. Rotational modulation of the static ZFS tensor leads to more efficient electronic relaxation than in the absence of ZFS [10]. If T_{1e} and τ_R become comparable in magnitude, a basic assumption of Redfield theory is violated: that the modulation responsible for electronic (or nuclear) relaxation occurs on a much faster time scale than relaxation time itself $\tau_R << T_{1e}$ [10].

The second problem is that electronic relaxation is a function of reorientation, and therefore T_{1e} and τ_R are correlated and can not be treated as independent processes [10].

2.5 Generalized Solomon Bloembergen Morgan Theory

Generalized SBM theory, unlike simple SBM theory, includes multi-exponential electron spin relaxation as well as a dynamic frequency modification. GSBM is more complicated than SBM but can still be expressed in closed analytical form, and therefore it was included in this thesis [19].

The inner-sphere water proton relaxivity, is given by

$$r_1^{IS} = \left(\frac{2q}{[H_2O]}\right)\frac{1}{T_{1M}+\tau_m} \tag{2.29}$$

These calculations were made under fast exchange conditions $\tau_m \ll T_{1M}$ and considering only dipole-dipole relaxation. The inner-sphere spin-lattice relaxation rate is given by

$$\frac{1}{T_{1M}} = \frac{4}{3}\left(\frac{\mu_0}{4\pi}\right)^2 \hbar^2\gamma_I^2\gamma_S^2\frac{S(S+1)}{r_{IS}^6}\tau_c^{DD}. \tag{2.30}$$

where the effective electron spin-nuclear spin dipole-dipole correlation time τ_c^{DD} is defined as

$$\tau_c^{DD} = Re(0.1 \times s_1^{DD} + 0.3 \times s_0^{DD} + 0.6 \times s_{-1}^{DD}), \tag{2.31}$$

which is a weighted sum of spectral density functions s_σ^{DD}, where σ has possible values of -1, 0, and +1. The spectral density s_σ^{DD} is the Fourier-Laplace transform of the reorientation correlation function and the electron spin correlation function, $tr_S\{S_\sigma^{1\dagger} e^{i\mathcal{L}_S\tau} S_\sigma^1 \rho_S^T\}$, at the nuclear Larmor frequency ω_H.

$$\begin{aligned} s_\sigma^{DD}(\omega_H + \sigma\omega_S) &= \frac{3}{S(S+1)} \\ &\times \int_0^\infty tr_S\{S_\sigma^{1\dagger} e^{i\mathcal{L}_S\tau} S_\sigma^1 \rho_S^T\} e^{(-i\omega_H + 1/\tau_R)\tau} d\tau \\ &\equiv M_{\sigma\sigma}^{-1} \end{aligned} \tag{2.32}$$

Two assumptions are used in the derivation of (2.32). First, the complete electron spin dipole-nuclear spin dipole correlation function has been decomposed into a pure reorientational and an electron spin correlation function. This assumption is valid if the electron spin relaxation is independent of the reorientation modulated electron spin relaxation mechanism. The second assumption is that the reorientation correlation function is taken to be isotropic and characterized by one reorientation correlation time τ_R. The important quantity is the electron spin correlation function, which is given by $\langle S_\sigma^{1\dagger}(t) S_\sigma^1(0)\rangle \equiv tr_S\{S_\sigma^{1\dagger} e^{i\mathcal{L}_S\tau} S_\sigma^1 \rho_S\}$. In (2.32), the Liouville superoperator $\mathcal{L}_S$ representing the electron spin correlation function is

$$\mathcal{L}_S = \mathcal{L}_S^{Zeeman} + i\mathcal{R}_{ZFS}, \tag{2.33}$$

where $\mathcal{L}_S$ is composed of a Zeeman term and the Redfield superoperator. The latter is generated by the time-dependent ZFS interaction. S_σ^1 is the σ-component of the rank one irreducible spherical tensor operator for the electron spin and ρ_S is the electron spin density operator.

The Zeeman Hamiltonian is

$$H_S^{Zeeman} = -\hbar\gamma_S B_0 S_0^1, \tag{2.34}$$

where $\gamma_S = \frac{g_e}{2} 1.76084 \times 10^{11} rads^{-1}T^{-1}$. The spectral density s_σ^{DD} in (2.32) may be extracted as a matrix element, $M_{\sigma\sigma}^{-1}$ of the inverted full matrix $\mathcal{M}$, generated by the Liouville and Redfield superoperators (2.33) [19].

Simplified Dynamic Model of Transient ZFS-Interaction

Electron spin spectral densities assume an isotropic pseudo rotational diffusion model, described by one correlation time τ_f. The transient ZFS-interaction is described by an isotropic pseudo-rotation diffusion model which results in the following spectral densities:

$$J_n(n\omega_S) = \frac{\Delta_t^2}{5} \frac{\tau_f}{1 + (n\omega_S\tau_f)^2} + \frac{\Delta_s^2}{5} \frac{\tau_R}{1 + (n\omega_S\tau_R)^2} \tag{2.35}$$

with the dynamic frequency shift Q_n defined by

$$Q_n(n\omega_S) = -\Big(\frac{\Delta_t^2}{5} \frac{\tau_f^2 n\omega_S}{1 + (n\omega_S\tau_f)^2} + \frac{\Delta_s^2}{5} \frac{\tau_R^2 n\omega_S}{1 + (n\omega_S\tau_R)^2}\Big). \tag{2.36}$$

The spectral densities and the dynamic shift describe electron spin relaxation due to both local distortions within the first hydration shell and a reorientational modulation of a static ZFS [19].

Table 2.1: Matrix elements of $\mathbf{R}(\beta_{LM})$ for $S = 7/2$

$A = 54J_0 + 174J_1 + 66J_2 - \mathbf{i}78Q_1 + \mathbf{i}24Q_2$
$B = -24\sqrt{21}J_1$
$C = -6\sqrt{105}J_2$
$D = 24J_0 + 174J_1 + 126J_2 - \mathbf{i}18Q_1 - \mathbf{i}6Q_2$
$E = -24\sqrt{5}J_1$
$F = -60\sqrt{3}J_2$
$G = 6J_0 + 78J_1 + 186J_2 + \mathbf{i}18Q_1 - \mathbf{i}24Q_2$
$H = -120J_2$
$I = 30J_1 + 210J_2 + \mathbf{i}30Q_1 - \mathbf{i}30Q_2$

2.5.1 Analytical Solution for the Electron Spin-Spin Spectral Density s_1^{DD}

The Redfield matrix describing electron spin-spin relaxation for S=7/2 can be represented in Zeeman basis, and can be rewritten with symbols:

$$\mathbf{R} = \begin{pmatrix} A & B & C & 0 & 0 & 0 & 0 \\ B & D & E & F & 0 & 0 & 0 \\ C & E & G & 0 & H & 0 & 0 \\ 0 & F & 0 & I & 0 & F & 0 \\ 0 & 0 & H & 0 & G & E & C \\ 0 & 0 & 0 & F & E & D & B \\ 0 & 0 & 0 & 0 & C & B & A \end{pmatrix} \tag{2.37}$$

Then we add the static ZFS interaction term, defined as

$$H_0^{ZFS}(\beta_{LM}) = \sqrt{\frac{2}{3}} D_s S_{PM} d_{00}^2(\beta_{LM}) S_0^2, \tag{2.38}$$

where S_{PM} is an order parameter given by $S_{PM} = \langle d_{00}^2(\beta_{PM}) \rangle$. The resulting matrix is then transformed to an irreducible spherical electron spin tensor base with the operator basis set O_σ^Σ

$$O_\sigma^\Sigma = \sum_m \sqrt{2\Sigma + 1} \begin{pmatrix} S & S & \Sigma \\ m+\sigma & -m & -\sigma \end{pmatrix} (-1)^{S-m-\sigma} |Sm+\sigma\rangle\langle Sm| \tag{2.39}$$

Table 2.2: Matrix elements of $\mathbf{M}_{\pm 1}(\beta_{LM})$ for $S = 7/2$

$a = \frac{6}{7}(43J_0 + 51J_1 + 102J_2 - \mathbf{i}51Q_1 + \mathbf{i}8Q_2) + \mathbf{i}(\omega_H \pm \omega_S)$
$b = \frac{12\sqrt{110}}{7}(J_0 + 2J_1 - 3J_2 - \mathbf{i}2Q_1 + \mathbf{i}Q_2)$
$c = 2\sqrt{3}D_S S_{PM} d^2_{00}(\beta_{LM})$
$d = 2\sqrt{\frac{22}{7}}D_S S_{PM} d^2_{00}(\beta_{LM})$
$e = \frac{6}{77}(402J_0 + 2281J_1 + 2707J_2 - \mathbf{i}419Q_1 + \mathbf{i}17Q_2) + \mathbf{i}(\omega_H \pm \omega_S)$
$f = \frac{42\sqrt{10}}{11}(J_0 + 8J_1 - 9J_2 - \mathbf{i}2Q_1 + \mathbf{i}Q_2)$
$g = 4\sqrt{\frac{5}{7}}D_S S_{PM} d^2_{00}(\beta_{LM})$
$h = 2\sqrt{\frac{26}{11}}D_S S_{PM} d^2_{00}(\beta_{LM})$
$i = \frac{6}{11}(29J_0 + 375J_1 + 366J_2 - \mathbf{i}3Q_1 - \mathbf{i}26Q_2) + \mathbf{i}(\omega_H \pm \omega_S)$
$j = 14\sqrt{\frac{5}{143}}D_S S_{PM} d^2_{00}(\beta_{LM})$
$k = 4\sqrt{\frac{3}{13}}D_S S_{PM} d^2_{00}(\beta_{LM})$
$l = 6(3J_0 + 5J_1 + 2J_2 - \mathbf{i}Q_1 - \mathbf{i}2Q_2) + \mathbf{i}(\omega_H \pm \omega_S)$
$m = 6\sqrt{\frac{66}{7}}(J_0 - J_2 - \mathbf{i}2Q_1 - \mathbf{i}Q_2)$
$n = 2(18J_0 + 55J_1 + 77J_2 - \mathbf{i}21Q_1 + \mathbf{i}3Q_2) + \mathbf{i}(\omega_H \pm \omega_S)$
$p = 4\sqrt{\frac{130}{77}}(3J_0 + 14J_1 - 17J_2 - \mathbf{i}6Q_1 + \mathbf{i}3Q_2)$
$q = \frac{2}{13}(159J_0 + 1427J_1 + 1534J_2 - \mathbf{i}123Q_1 - \mathbf{i}36Q_2) + \mathbf{i}(\omega_H \pm \omega_S)$
$r = \frac{84}{143}\sqrt{165}(J_0 + 12J_1 - 13J_2 - \mathbf{i}2Q_1 + \mathbf{i}Q_2)$
$s = \frac{6}{13}(12J_0 + 209J_1 + 143J_2 + \mathbf{i}41Q_1 - \mathbf{i}53Q_2) + \mathbf{i}(\omega_H \pm \omega_S)$

expressed in terms of Zeeman eigenoperators $|Sm + \sigma\rangle$ and $\langle Sm|$ and where

$$\begin{pmatrix} S & S & \Sigma \\ m+\sigma & -m & -\sigma \end{pmatrix} \tag{2.40}$$

is a 3j-symbol. The resulting matrix is written with first even rank tensors and then odd rank tensors, in the order 2, 4, 6, 1, 3, 5, 7. The Zeeman matrix $\mathbf{1}i(\omega_H \pm \omega_S)$ is

added. The full matrix is

$$\mathbf{M_{\pm 1}} = \begin{pmatrix} a & b & 0 & c & d & 0 & 0 \\ b & e & f & 0 & g & h & 0 \\ 0 & f & i & 0 & 0 & j & k \\ c & 0 & 0 & l & m & 0 & 0 \\ d & g & 0 & m & n & p & 0 \\ 0 & h & j & 0 & p & q & r \\ 0 & 0 & k & 0 & 0 & r & s \end{pmatrix} \tag{2.41}$$

with the elements defined in table (2.2). The element s_1^{DD} is the (4,4) matrix element of the inverted matrix $M_{\pm 1}^{-1}$:

$$s_1^{DD} = \frac{X}{Y} \tag{2.42}$$

where

$$\begin{aligned} X = (&k^2nb^2q + eak^2p^2 - eak^2qn - asnf^2q + 2asnjfh - \\ &2aspfgj + asg^2j^2 + asf^2p^2 - 2dsgbj^2 + sb^2j^2n + 2dspfbj - \\ &2d^2sjfh + ieasnq + 2idsgbq - 2idr^2gb - iash^2n + \\ &2iasphg - 2idsphb - isb^2nq - ieasp^2 - iear^2n - ied^2sq - \\ &iasg^2q + id^2er^2 + iar^2g^2 + ir^2b^2n + id^2sh^2 - easj^2n + ed^2sj^2 + \\ &isb^2p^2 + d^2sf^2q - d^2k^2h^2 - 2kjnb^2r - 2arkjg^2 - 2ak^2phg + \\ &2d^2kjhr - 2d^2erkj - 2dk^2qgb + 2earkjn + 2arfkpg + \\ &d^2ek^2q + 4dkjgbr - 2dfkpbr - d^2r^2f^2 + 2dk^2phb + \\ &ak^2h^2n - 2akfhrn + ak^2qg^2 + ar^2f^2n - k^2p^2b^2) \end{aligned} \tag{2.43}$$

and

$$Y = (-r^2nc^2f^2 - sf^2p^2c^2 - sc^2j^2g^2 - ar^2m^2f^2 - k^2qb^2m^2 -$$
$$k^2c^2h^2n - sb^2m^2j^2 - k^2c^2qg^2 + 4derkjmc - 2desj^2mc -$$
$$2dsmcf^2q + iear^2m^2 + lk^2nb^2q + lar^2f^2n + lasg^2j^2 + ld^2sf^2q$$
$$+ier^2nc^2 + iesc^2p^2 + isb^2m^2q - 2asm^2jfh + 2k^2qmbcg -$$
$$2spbcmfj + 2akfhrm^2 - ak^2h^2m^2 + iasm^2h^2 + isc^2h^2n +$$
$$isc^2qg^2 + 2ispbcmh + 2ir^2gbmc - isc^2phg - iesc^2qn -$$
$$ieasm^2q - 2ismbcgq - 2idsh^2mc + ilsb^2p^2 + 2idesmcq -$$
$$2ider^2mc + ilr^2b^2n - ilasg^2q - ilsb^2nq + 2ilasphg -$$
$$2ildsphb - 2ildr^2gb + ilar^2g^2 - ild^2esq + 2ildsgbq +$$
$$ileasnq - ileasp^2 - ilear^2n - ilash^2n + ild^2er^2 + ild^2sh^2 +$$
$$2fkpbrmc + asm^2f^2q + 2sc^2pfgj + 2kfhrnc^2 + 2rb^2m^2kj -$$
$$4kjgbrmc + 2sgbj^2mc + 2k^2c^2phg + ek^2c^2qn + esc^2j^2n +$$
$$easm^2j^2 - 2earkjm^2 + eak^2m^2q - 2erkjnc^2 - 2k^2pbcmh +$$
$$2rkjg^2c^2 - ek^2c^2p^2 - 2sc^2jfhn - 2rfkpgc^2 + sf^2qnc^2 -$$
$$2dek^2qmc + 2dr^2f^2mc + 2dk^2h^2mc - 4dkfhrmc +$$
$$4dsmcjfh - ir^2b^2m^2 - lk^2p^2b^2 - ld^2k^2h^2 + lasf^2p^2 - leak^2qn -$$
$$2lakfhrn + 2ldk^2phb - 2ldfkpbr + 2ldspfbj +$$
$$4ldkjgbr - 2ldsgbj^2 + lak^2qg^2 + lak^2h^2n + lsb^2j^2n +$$
$$leak^2p^2 + ld^2ek^2q + ld^2esj^2 - leasj^2n + 2learkjn - ld^2r^2f^2 +$$
$$2larfkpg - 2ldk^2qgb + 2ld^2kfhr - 2ld^2erkj -$$
$$2ld^2sjfh + 2lasnjfh - lasnf^2q - 2lak^2phg - 2larkjg^2 -$$
$$2laspfgj - 2lkjnb^2r - ir^2g^2c^2). \qquad (2.44)$$

Table 2.3: Matrix elements of $\mathbf{R}(\beta_{LM})$ for $S = 7/2$

$A = 126J_1 + 42J_2$
$B = -126J_1$
$C = -42J_2$
$D = 222J_1 + 90J_2$
$E = -96J_1$
$F = -90J_2$
$G = 126J_1 + 162J_2$
$H = -30J_1$
$I = -120J_2$
$J = 30J_1 + 210J_2$

2.5.2 Analytical Expression for the Elctron Spin-Lattice Spectral Density s_0^{DD}

The Redfield matrix describes the electron spin-lattice relaxation with the Zeeman basis symbolically represented.

$$\mathbf{R} = \begin{pmatrix} A & B & C & 0 & 0 & 0 & 0 & 0 \\ B & D & E & F & 0 & 0 & 0 & 0 \\ C & E & G & H & I & 0 & 0 & 0 \\ 0 & F & H & J & 0 & I & 0 & 0 \\ 0 & 0 & I & 0 & J & H & F & 0 \\ 0 & 0 & 0 & I & H & G & E & C \\ 0 & 0 & 0 & 0 & F & E & D & B \\ 0 & 0 & 0 & 0 & 0 & C & B & A \end{pmatrix} \tag{2.45}$$

where the matrix elements are given in the table (2.3). The basis is then transformed using a similar method to the transformation of s_1^{DD}. In this case, the static ZFS

Table 2.4: Matrix elements of $\mathbf{M_1}(\beta_{LM})$ for $S = 7/2$

$a = 12(J_1 + 4J_2) - \mathbf{i}\omega_H + \frac{1}{\tau_R}$
$b = 12(12J_1 + 13J_2) - \mathbf{i}\omega_H + \frac{1}{\tau_R}$
$c = \frac{60}{13}(53J_1 + 51J_2) - \mathbf{i}\omega_H + \frac{1}{\tau_R}$
$d = \frac{168}{13}(8J_1 + 5J_2) - \mathbf{i}\omega_H + \frac{1}{\tau_R}$
$e = 24\sqrt{\frac{11}{7}}(J_1 - J_2)$
$f = 240\sqrt{\frac{13}{77}}(J_1 - J_2)$
$g = \frac{240}{13}\sqrt{\frac{343}{11}}(J_1 - J_2)$

interaction term is zero. The transformed matrix has the following form:

$$\mathbf{R} = \begin{pmatrix} 0 & 0 & 0 & 0 & 0 & 0 & 0 & 0 \\ 0 & A & 0 & H & 0 & 0 & 0 & 0 \\ 0 & 0 & B & 0 & I & 0 & 0 & 0 \\ 0 & H & 0 & C & 0 & J & 0 & 0 \\ 0 & 0 & I & 0 & D & 0 & K & 0 \\ 0 & 0 & 0 & J & 0 & E & 0 & L \\ 0 & 0 & 0 & 0 & K & 0 & F & 0 \\ 0 & 0 & 0 & 0 & 0 & L & 0 & G \end{pmatrix} \tag{2.46}$$

The above matrix can be reduced to a 4×4 matrix since only odd-rank tensor operators enter the theoretical description. The final $\mathbf{M_0}$ matrix is formed as

$$\mathbf{M_0} = \begin{pmatrix} a & e & 0 & 0 \\ e & b & f & 0 \\ 0 & f & c & g \\ 0 & 0 & g & d \end{pmatrix} \tag{2.47}$$

where the matrix elements are given in table (2.4). The inverted matrix element is given by

$$s_0^{DD} = \frac{bcd - df^2 - bg^2}{abcd - cde^2 - adf^2 - abg^2 + e^2g^2}. \tag{2.48}$$

2.6 Comparison of Theoretical Models

The contrast agent Vasovist (formerly known as MS-325) is currently of great research interest due to its high relaxivity when bound to human serum albumin (HSA). In fact MS-325 has the highest relaxivity of all clinically approved contrast agents in both its bound and unbound state. Due to the heightened interest in this contrast agent and availability of structural constants for MS-325, it was used as a primary yard stick for the evaluation of the three theoretical models for gadolinium relaxivity implemented in this thesis.

MS-325 exists as two slowly interconverting diastereoisomers A and B in a ratio of 65 to 35. Diastereoisomers are isomers which are non-superimposable mirror images of each other. Both diastereoisomers reversibly bind to HSA and at physiological conditions of $37^{o}C$, pH 7.4 in phosphate buffered saline (PBS), 4.5% HSA and 0.05 mM MS-325, there was no statistical difference in HSA affinity or relaxivity between the two isomers. The experimental NMRD profiles for MS-325 Isomers A and B were provided by Dr. Caravan, Fig. 2.1 [17].

2.6.1 Simple Solomon-Bloembergen-Morgan Based Models

Caravan *et. al.* fit theoretical models and extracted underlying parameters, using the NMRD measurements shown in Fig. 2.1 supplemented by high-field ^{17}O NMR derived relaxation measurements [17]. τ_m and τ_R were measured via ^{17}O NMR relaxation measurements. NMRD measurements were used to extract all other parameters via the anisotropic and isotropic GSBM model. The simulated NMRD profiles for the three different SBM variations shown in Fig. 2.2 were calculated using parameters of Isomer A bound to HSA, calculated by Caravan *et. al* found in Table 2.5.

SBM based theories including the Lauffer variation and the Caravan variation, and the second SL variation were plotted on top of the experimental results for isomer A of MS-325, in Fig. 2.2. All of the SBM models shown in Fig. 2.2 are accurate

Table 2.5: Parameters describing relaxivity for MS-325 complexes

Complex	temp (°C)	τ_m(ns)	τ_R(ps)	τ_v(ps)	$\Delta_t(cm^{-1})$	$\Delta_s(cm^{-1})$	$D(cm^{-1})$	F^2	r(nm)	method	ref
Isomer A +HSA	34.85	198	5000	20	0.0147		0.024	1	0.31	NMRD	[17]
Isomer B +HSA	34.85	296	4600	22	0.0135		0.024	1	0.31	NMRD	[17]
Isomer A +HSA	34.85	67	4900	16	0.0128		0.024	0.63	0.31	NMRD	[17]
Isomer B +HSA	34.85	182	4900	16	0.0122		0.024	0.67	0.31	NMRD	[17]
MS-325 A+B	36.85	72	100	18	0.04	0.011		1	0.295	NMRD	[19]
MS-325 A+B +HSA	36.85	198	10000	30	0.018	0		1	0.313	NMRD	[19]

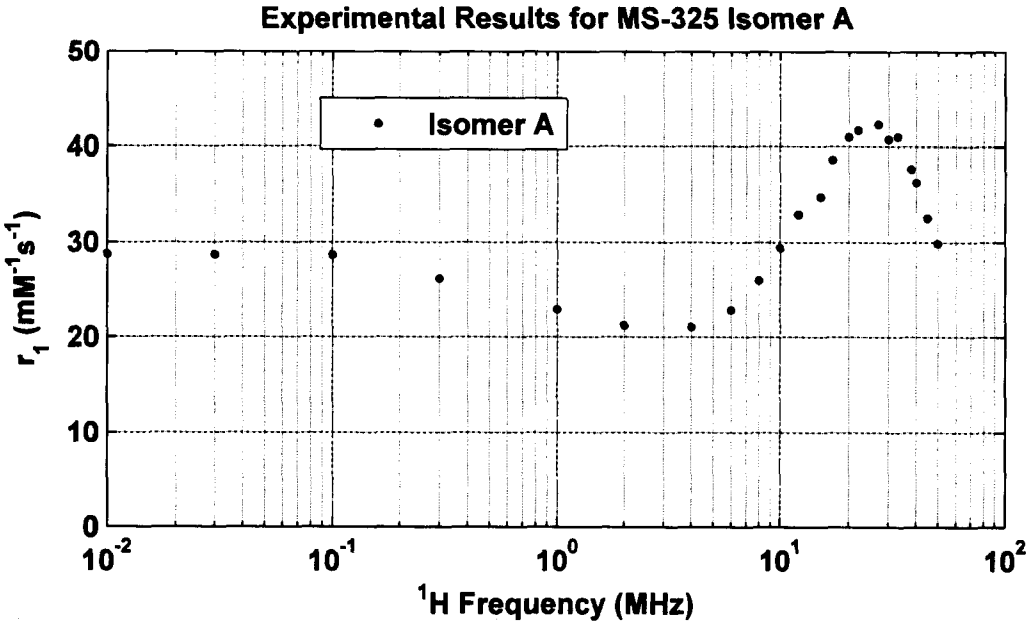

Fig. 2.1: ^1H NMRD profiles of observed relaxivity for Isomer A of MS-325 in 4.5 % HSA at 35 ^oC

in the high field limit but inaccurate in the low-field limit. As mentioned earlier this is due to the inherent neglect of static zero-field splitting (ZFS) which is dominant in the low field region. There are significant differences between the NMRD curves of the Lauffer variation and those of the Caravan and second SL variations. The Lauffer model depicts dipole-dipole relaxation as a composite of electron precession frequency ("3-term") and nuclear precession frequency ("7-term") dependence. The Caravan and second SL models both depict the dipole-dipole relaxation as dependent on nuclear precession frequency alone ("3-term"). For the Lauffer model, the nuclear precession frequency term is dominant at the high field end while the electron precession frequency term is significant at low field, but insignificant at frequencies above 2 MHz. The relatively smaller differences between the Caravan and second SL models represents the effect of anisotropic motion of the complex. Inclusion of anisotropic motion effects decreases relaxivity slightly over the clinically relevant field strength range of 5-200 MHz, and increases it outside of this range.

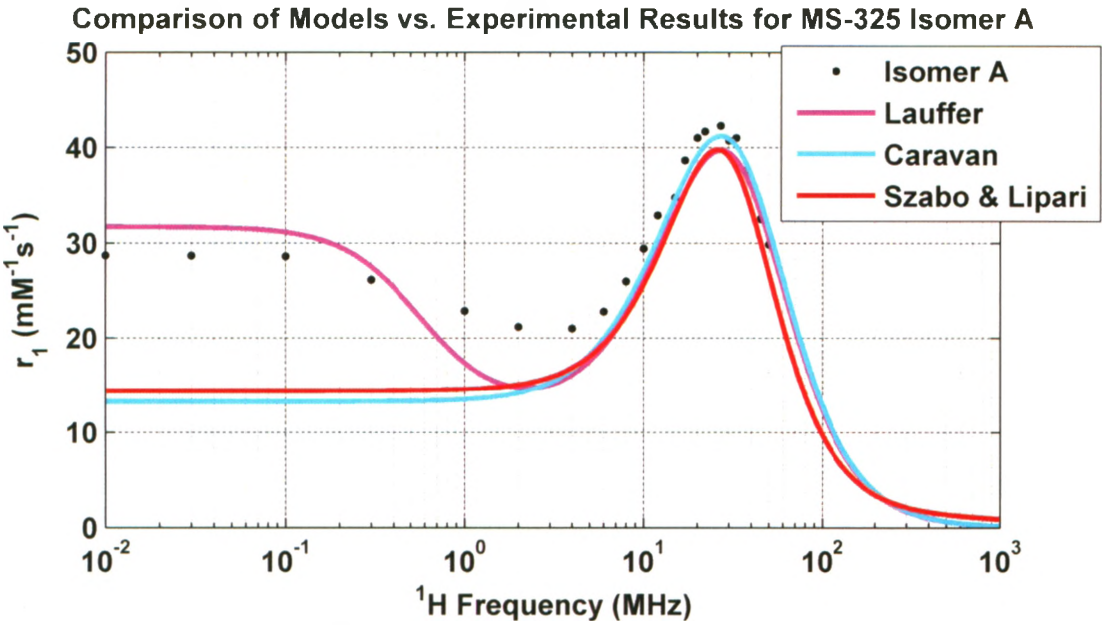

Fig. 2.2: Comparison of SBM based Lauffer variation, Caravan variation and the Szabo & Lipari model vs. experimental results of isomer A of MS-325 at 37 ^oC.

2.6.2 Generalized Solomon Bloembergen Morgan Theory

A comparison of all the theoretical models is shown if Fig. 2.3 using parameters from Caravan *et. al.* GSBM theory is clearly the most accurate of all the theories in describing high field relaxation. The remaining discrepancy between experimental results and GSBM theory in the low field region is due to the lack of inclusion of outer-sphere contributions. Outer-sphere contributions decrease in importance with increasing field strength. For these results, it is clear that GSBM theory is the most accurate model for predicting total relaxivity over the full field strength spectrum, for paramagnetic contrast agents such as MS-325.

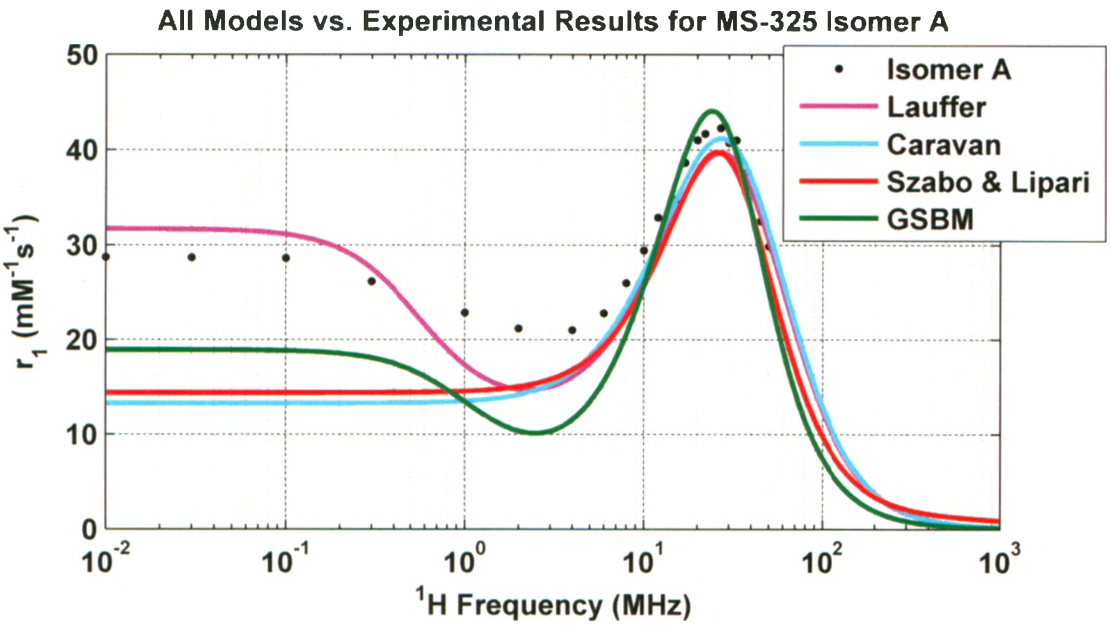

Fig. 2.3: Comparison of all models versus experimental results for isomers A of MS-325 at 37 ^{o}C.

Chapter 3

Contributions to Gadolinium Relaxivity

The three theories described in this thesis were compared on merits of accuracy, complexity and availability of input parameters. The influence of structural and molecular dynamic parameters of contrast agents was investigated; these included rotational correlation time (τ_R), water residency time (τ_m) and gadolinium-water distance (r). The influences of transient zero field splitting parameters (Δ_t,τ_v) and static zero field splitting parameters (Δ_s, τ_{s0} and D) were also studied. To further study influences of these parameters on real contrast agent relaxivity, calculated NMRD profiles were compared for Magnevist, Omniscan, Multihance, Gadovist, Dotarem, ProHance, OptiMARK, Vasovist, and Primovist, using literature values for the underlying parameters for each compound.

Two variations of the SBM theory were used to extract structural parameters from MS-325 bound to HSA, these results were compared with results obtained by Caravan *et. al.* The structural parameters of pre-activated gadolinium based agent that senses myeloperoxidase (MPO) activity, were calculated from experimental NMRD profiles of these compounds using the same fitting method.

3.1 Comparison of Relevant Parameters

One way to increase contrast agent relaxivity is to optimize the underlying parameters which govern it. These parameters are determined by the structure and dynamics of the compound and its associated water molecules, and include: rotational correlation time τ_R, water residency time τ_m and gadolinium water distance r. The influence of zero field splitting on relaxivity is described by: correlation time of transient zero field splitting distortions τ_v, magnitude of transient zero field splitting Δ_t and magnitude of static zero field splitting Δ_s. The influence of these parameters was studied by perturbing the parameters, one at a time, in the GSBM model and comparing the resultant NMRD profiles to the unperturbed NMRD profile. We used HSA-bound MS-325 as a representative compound that shows very interesting structure in its NMRD profile, but one for which the underlying parameters are well established.

3.1.1 Rotational Correlation Time τ_R

Rotational correlation time τ_R is a measure of the molecular tumbling rate. For a complex to be an effective relaxation agent, rotational rate must be slow enough such that water molecules can enter and exit the inner coordination sphere of the molecule in a time less than or equal to the rotational correlation time. For gadolinium agents, the realization that relaxivity is strongly influenced by rotational rate led to new research and development of agents that were larger and therefore tumbled more slowly, or that exhibited weak or strong binding to macromolecules which in turn led to slowing of rotational tumbling. The most common and effective solution developed to date is to have the gadolinium complex bind to the biologically abundant macromolecule human serum albumin (HSA). Binding to HSA increases relaxation and allows for selective imaging of HSA distribution within the body. HSA is the most abundant protein in the human body, and is of significance in many bodily

processes [19].

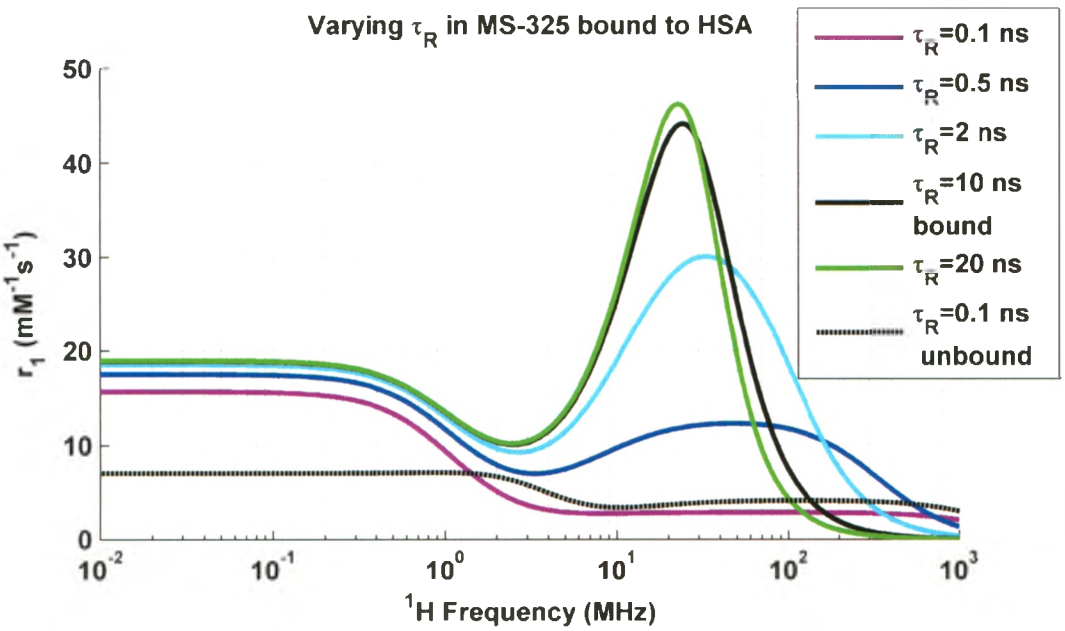

Fig. 3.1: Changing τ_R for MS-325 bound to HSA

The rotational correlation time of unbound MS-325 (combined isomers A and B) at 37 ^oC is 0.1 ns while that of HSA-bound MS-325 at 37 ^oC is 10 ns [19]. In fact, by studying the parameters in Table 2.5, it is clear that the largest parameter change going from unbound to bound states of MS-325 is that of τ_R. Therefore, to see the effect of changes in τ_R, isolated from changes in any other parameter, NMRD profiles were simulated using the GSBM model, with progressively decremented values of τ_R, starting above the HSA-bound value of 10 ns and progressing downward to the unbound value of 0.1 ns. For these simulations, the values used for all other parameters were those of isomer A and B combined MS-325 shown in Table 2.5, and all parameters were held constant except τ_R. The resulting simulated profiles are shown in Fig. 3.1; in this and all subsequent plots of this type, the GSBM-modeled profiles for HSA-bound and unbound MS-325 are shown in solid black and dotted black, respectively, for easy comparison to the parametrically perturbed profiles, which are

shown as the different solid colour profiles.

Comparing the curves in Fig. 3.1, we note several key points. First the change in τ_R over the range of 0.1 to 10 ns produces dramatic changes in relaxivity in the clinically-relevant high field regime. Second, the simple act of changing τ_R from 10 to 0.1 ns causes the NMRD profile of HSA-bound MS-325 to closely match that of unbound MS-325, at least in the high field regime, providing evidence that τ_R is the main determinant of relaxivity in this clinically relevant field strength range.

Because of the obvious importance of τ_R in the determination of relaxivity, it is considered important to directly measure this parameter by independent means. One of the more established ways to do this is through ^{17}O NMR measurements. This method works as follows: T_1 values of a dilute solution of the contrast agent in $H_2^{17}O$ water (known as acidified water) and a contrast agent free acidified $H_2^{17}O$ water reference are measured at high field. The reduced longitudinal relaxation rate ($\frac{1}{T_{1r}}$) is given by

$$\frac{1}{T_{1r}} = \frac{q[M]}{[H_2O]}\left[\frac{1}{T_1} - \frac{1}{T_{1A}}\right] = \frac{1}{T_{1M} + \tau_m} \tag{3.1}$$

where T_1 is the measured relaxation time of the solution of contrast agent concentration [M] and $H_2^{17}O$ concentration $[H_2O]$, and T_{1A} is the measured relaxation time of the reference water solution. Using these results τ_R can be easily extracted from a standard model for quadrupolar longitudinal relaxation. A quadrupolar nucleus is a nucleus with spin number $I \geq 1$ which has an associated nuclear quadrupolar moment, therefore the charge on the nucleus is not spherically symmetrical. As this molecule reorients, there is an interaction between the nuclear spin and the electric field gradient at the nucleus. This provides a mechanism for relaxation of the nucleus called the quadrupolar relaxation mechanism in addition to the dipolar relaxation due to the presence of Gd(III). This quadrupolar longitudinal relaxation is described by

$$\frac{1}{T_{1M}} = \frac{3\pi^2}{10}\frac{2I+3}{I^2(2I-1)}\chi^2(1-\eta^2/3)\left[\frac{0.2\tau_R}{1+\omega_I^2\tau_R^2} + \frac{0.8\tau_R}{1+4\omega_I^2\tau_R^2}\right] \tag{3.2}$$

In (3.2) I is the nuclear spin ($I = \frac{5}{2}$ for ^{17}O), χ^2 is the quadrupolar coupling constant, and η is an asymmetry parameter. Using the quadrupolar coupling constant for acidified water, $\chi^2(1+\eta^2/3) = 7.58$ MHz,(3.2) can be used to calculate τ_R [20], [35].

3.1.2 Water Residency Time τ_m

Water residency time within the first coordination sphere must be long enough to allow the water molecule to be relaxed but short enough such that water molecules are efficiently exchanging in and out of the first coordination sphere. The water residency time of unbound MS-325 at 37 ^oC is 72 ns while that of MS-325 at 37 ^oC is 198 ns [19].

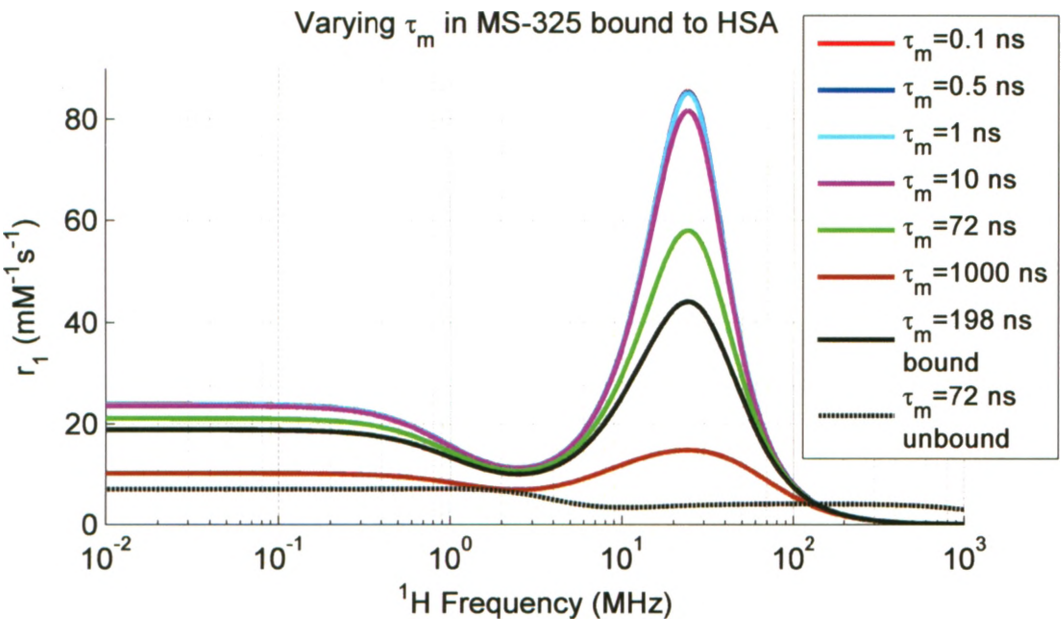

Fig. 3.2: Changing τ_m for MS-325 bound to HSA

To isolate the influence of τ_m on relaxivity, GSBM simulations were conducted starting with the parameters for HSA-bound MS-325, and then creating new profiles by varying τ_m over the range 0.1 - 1000 ns, with all other parameters held constant.

Results are shown plotted in Fig. 3.2 with the true profiles for HSA-bound and unbound MS-325 shown in solid and dashed black, respectively. From this figure, it is clear that relaxivity increases substantially with decreasing τ_m, at least over a certain range of τ_m. Over a wide range that includes the values typical of unbound and HSA-bound MS-325, τ_m seems to have a significant influence on relaxivity: decreasing τ_m from 1000 ns to 1 ns causes relaxivity to increase by 70 $mM^{-1}s^{-1}$ at a mid field strength of 25 MHz (0.6 T). On the other hand, there is no further increase in relaxivity as τ_m decreases below 1 ns. It is also worth noting that changing τ_m from 72 and 198 ns does not produce the magnitude or even direction of relaxivity change that is observed upon HSA-binding, showing that τ_m alone can not explain the observed albumin-binding relaxivity change.

The rate of water exchange between the inner-sphere water molecule and the bulk can be directly probed by measuring the transverse relaxation rates of a dilute solution of contrast agent in $H_2^{17}O$ water as a function of temperature at high field. The reduced transverse relaxation rate of $(1/T_{2r})$ of bulk $H_2^{17}O$ is given by

$$\frac{1}{T_{2r}} = \frac{q[M]}{[H_2O]}\Big[\frac{1}{T_2} - \frac{1}{T_{2A}}\Big] = \frac{1}{T_{2M} + \tau_m}. \tag{3.3}$$

The relaxation mechanism for $1/T_{2M}$ is predominantly scalar in the high field (equal or greater than 0.47 T)

$$\frac{1}{T_{2M}} = \frac{1}{3}S(S+1)\Big(\frac{A}{\hbar}\Big)^2\Big(\frac{1}{T_{1e}} + \frac{1}{\tau_m}\Big)^{-1} \tag{3.4}$$

and electronic relaxation time in the high field limit has a temperature dependence given by

$$\frac{1}{T_{1e}^{HF}} = \frac{1}{T_{1e}^{298}} exp\Big[\frac{\Delta E_{T1e}}{R}\Big(\frac{1}{T} - \frac{1}{298.15}\Big)\Big] \tag{3.5}$$

where T is temperature, R is the gas constant and $\Delta E_{T_{1e}}$ is the change in energy with change in electronic relaxation time. The high field limit is necessary in this calculation because of the direct exponential relationship between electronic relaxation time and temperature in the high field only. Using this theory, ^{17}O transverse relaxation

time measurements acquired at different temperatures permit the estimation of τ_m and ΔE_{T1e} [20].

3.1.3 Gadolinium Water Distance, r

The gadolinium water distance of unbound MS-325 at 37 ^oC is 0.295 nm while that of HSA-bound MS-325 at 37 ^oC is 0.313 nm [19]. From all of the known theories, it is expected that decreasing the gadolinium water distance will strongly increase relaxivity. To isolate and quantify the effect of changes in r on MS-325 relaxivity, GSBM simulations were conducted to observe the effect of decreasing r from 0.313 nm to 0.295 nm. Results are shown in Fig. 3.3, which shows relaxivity increasing with decreasing gadolinium water distance by an amount equal to 10 $mM^{-1}s^{-1}$ at 25 MHz as gadolinium water distance was decreased by a total of 0.018 nm. It is thought that greater changes in gadolinium water distance are unlikely due to constraints of the surrounding chelate structure. In fact measurements of gadolinium water distance for various gadolinium chelates are all in the range of 0.295 to 0.315 nm [9], [22], [23], [17]. From these results and simulations, it is clear that variations in gadolinium water distance can not explain the difference in relaxivity between HSA-bound and unbound MS-325 and in fact are not enough to cause a significant change in relaxivity or NMRD profile shape change.

There are several different methods to measure gadolinium water distance including neutron diffraction, ENDOR spectroscopy and using isotopic exchange methods in very concentrated solutions.

3.1.4 Correlation Time of Transient Zero Field Splitting Distortions, τ_v

Zero field splitting is the removal of spin microstate degeneracy for systems with S $> \frac{1}{2}$ in the absence of an external applied field. Zero field splitting effects are dictated

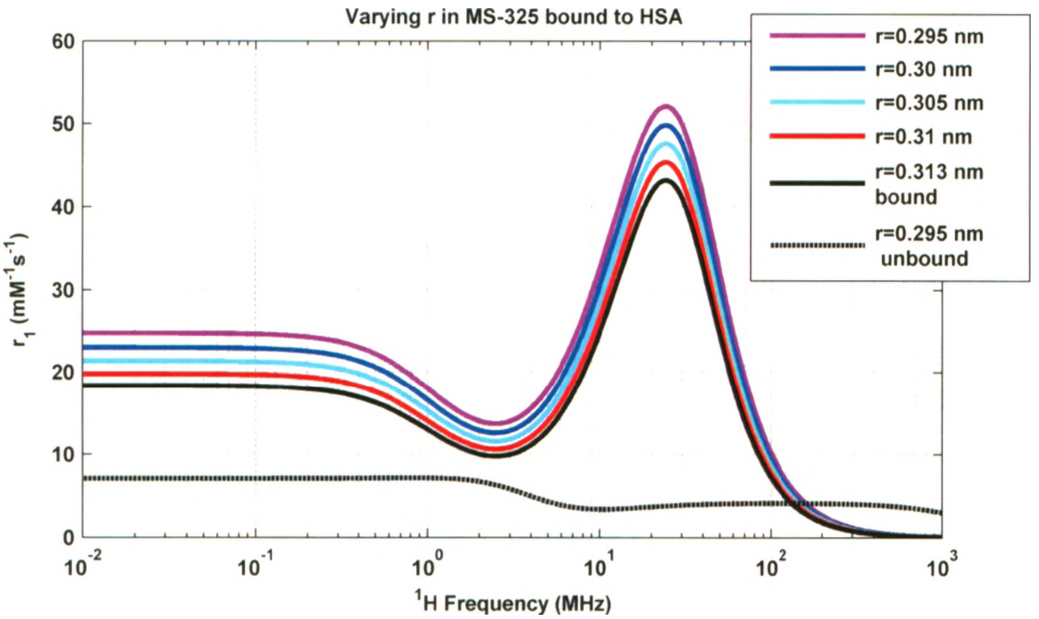

Fig. 3.3: Changing r for MS-325 bound to HSA

by group theory and crystal field theory. Zero field splitting is a composite of static ZFS and transient ZFS effects. Static ZFS effects are constant and do not change with time or rotation and vibration of the molecule. Transient ZFS effects are a result of, and are modified by, rotation and vibration of the molecule [19].

The correlation time associated with transient zero field splitting, τ_v, characterizes the changes in transient ZFS over time. The transient zero field splitting correlation time of unbound MS-325 at 37 ^oC is 18 ps while that of HSA-bound MS-325 at 37 ^oC is 30 ps [19]. To isolate the influence of τ_v on relaxivity, GSBM simulations were conducted starting with the parameters for HSA-bound MS-325, and then varying τ_v over the range 1-1000 ps, with all other parameters held constant. Results are shown plotted in Fig. 3.4 with the true profiles for HSA-bound and unbound MS-325 shown in solid and dashed black, respectively. From this figure it is clear that changes in τ_v do not substantially alter relaxivity past a proton frequency of approximately 40 MHz. In the low field region, decreasing τ_v increases relaxivity. Varying τ_v does have

a substantial influence on the shape and magnitude of the relaxivity profile in the low and mid field ranges, indicating that τ_v may have an influence in producing the characteristic mid field peak found in the HSA-bound MS-325 relaxivity profile.

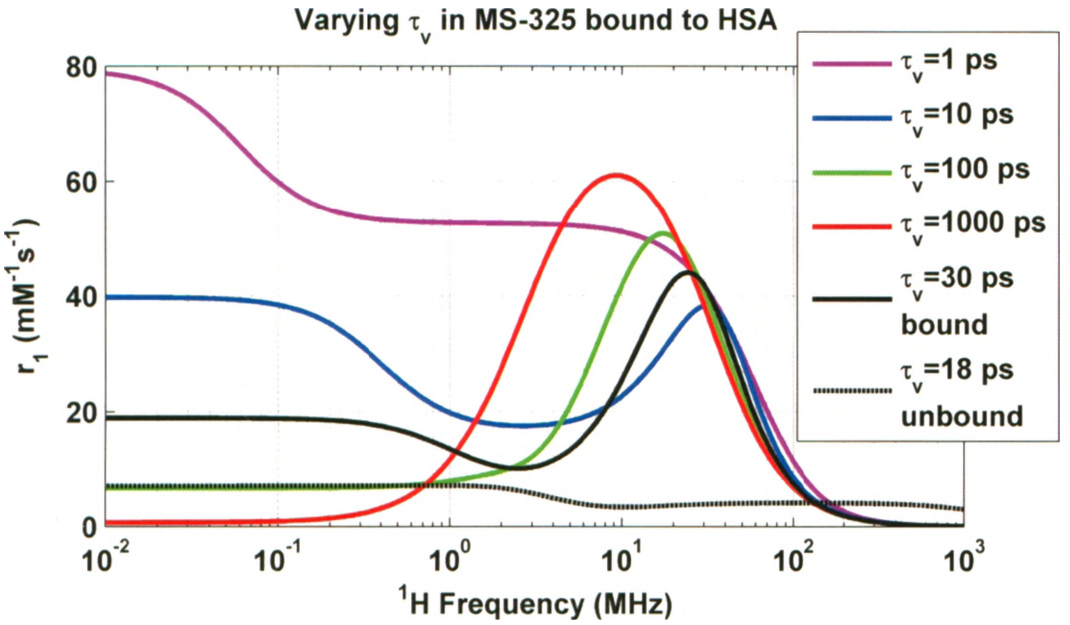

Fig. 3.4: Changing τ_v for MS-325 bound to HSA

3.1.5 Magnitude of Transient Zero Field Splitting, Δ_t

The magnitude of transient zero field splitting is symbolized as Δ_t. The magnitude of transient zero field splitting of unbound MS-325 at 37 ^oC is 0.04 cm^{-1} while that of HSA-bound MS-325 at 37 ^oC is 0.018 cm^{-1} [19]. To isolate the influence of Δ_t on relaxivity, GSBM simulations were conducted starting with the parameters for HSA-bound MS-325, and then varying Δ_t over the range 0 to 0.04 cm^{-1}, with all other parameters held constant. Results are shown plotted in Fig. 3.5 with the true profiles for HSA-bound and unbound MS-325 shown in solid and dashed black respectively. At lower field strengths, decreasing transient zero field splitting magnitude increases relaxivity. From this figure it is clear that changes in Δ_t do not substantially alter

relaxivity past a proton frequency of approximately 40 MHz. In the low field region, Δ_t has a significant impact on relaxivity: decreasing the value of Δ_t by 0.022 cm^{-1} increases relaxivity by approximately 15 $mM^{-1}s^{-1}$. The inclusion of the $\Delta_t = 0$ curve, while possibly not physical meaningful, provides good intuition into why there is a characteristic peak in the NMRD profile for HSA-bound MS-325: any appearance of ZFS effects, represented by non-zero "low field" parameters τ_v, Δ_t or Δ_s, quickly leads to strong decreases in relaxivity in the low field regime, which then disperse away well before the high field regime. As a result of this dispersion, relaxivity can quickly grow back to a high value, which is determined by the "high field" parameters τ_R and τ_m. The magnitude of Δ_t has a relatively modest effect at high field, but changes in this magnitude maybe the single most important determinant of the position of the peak relaxivity for MS-325.

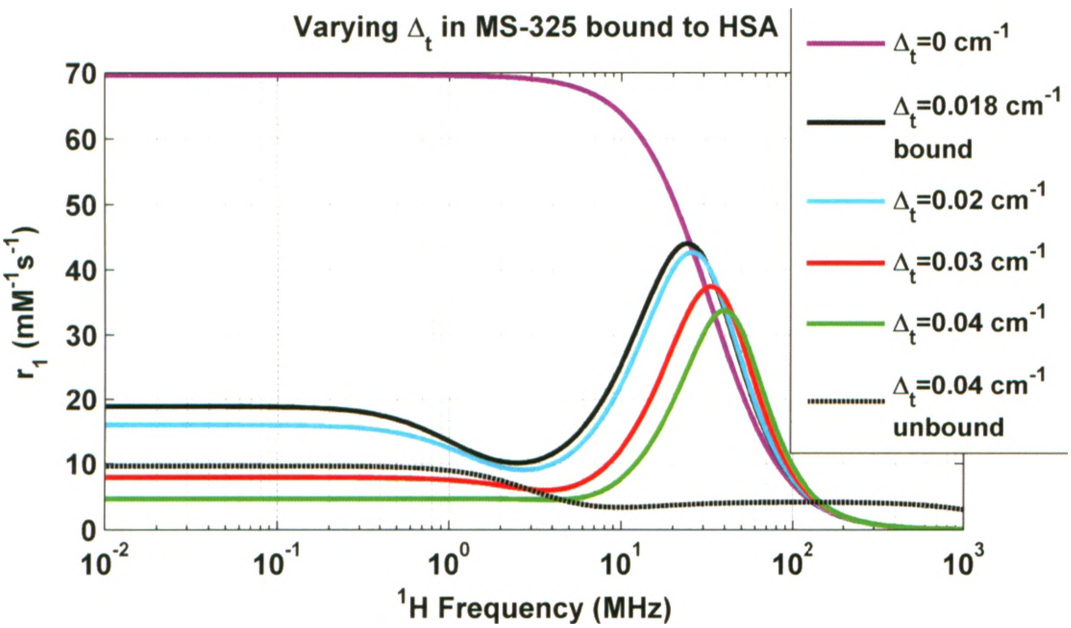

Fig. 3.5: Changing Δ_t for MS-325 bound to HSA

3.1.6 Magnitude of Static Zero Field Splitting, Δ_s

Magnitude of static zero field splitting is symbolized as Δ_s. The magnitude of static zero field splitting of unbound MS-325 at 37 ^oC is 0.011 cm^{-1} while the static zero field splitting of HSA-bound MS-325 at 37 ^oC is 0 cm^{-1} [19]. To isolate the influence of Δ_s on relaxivity, GSBM simulations were conducted starting with the parameters for HSA-bound MS-325, and then varying Δ_s over the range 0 to 0.04 cm^{-1}, with all other parameters held constant. Results are shown plotted in Fig. 3.6 with the true profiles for HSA-bound and unbound MS-325 shown in solid and dashed black respectively. From this figure it is clear that past a proton frequency of approximately 4 MHz, changes in Δ_s do not alter relaxivity. In the low field region, decreasing Δ_s only minimally increases relaxivity; there is only a substantial increase in relaxivity if $\Delta_s = 0$.

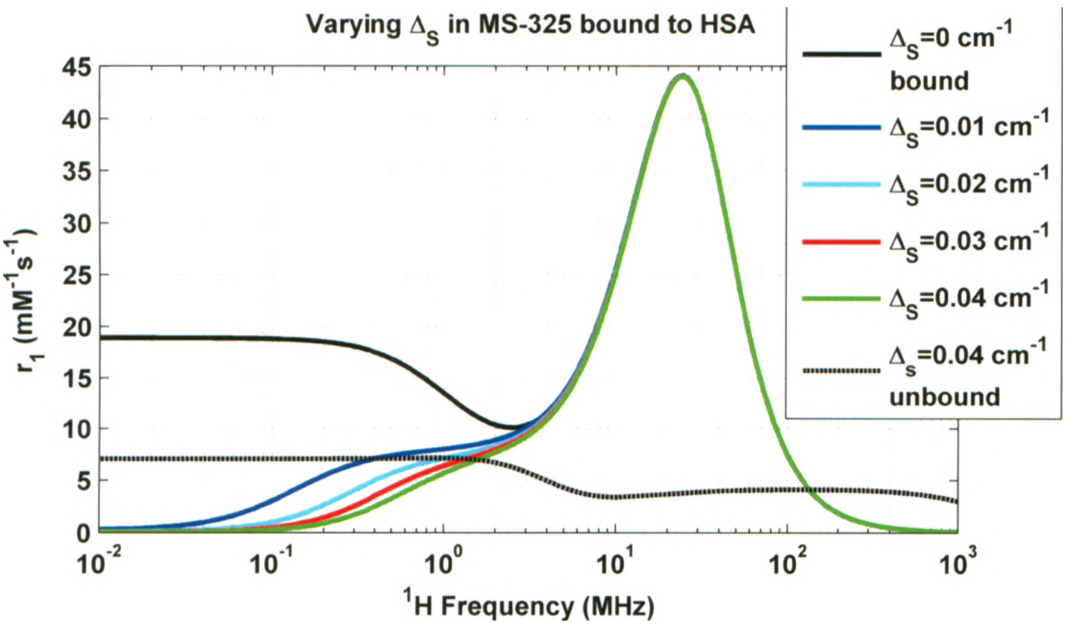

Fig. 3.6: Changing Δ_s for MS-325 bound to HSA

3.1.7 Conclusions Drawn from Parameter Comparisons

Rotational correlation time τ_R has the largest influence on relaxivity, at least for MS-325 and at least over the clinically-relevant high field regime. Water residency time τ_m has the second largest influence on relaxivity. Zero field splitting parameters are also influenced by protein binding but to a much smaller extent and even if the change upon binding was much greater, their influence would be almost entirely in the low field regime anyway. Gadolinium-water distance does not vary enough between bound and unbound states, or indeed between the different known chelates, to significantly influence relaxivity.

Electronic relaxation T_{1e}, governed largely by τ_v, Δ_t and Δ_s dominates relaxivity in the low field regime while τ_R and τ_m dominate relaxivity in the high field regime. The characteristic upswing, or peak in the NMRD profile of MS-325 bound to HSA can be explained qualitatively as a changeover from the dominant influence at low field of the electronic relaxation parameters, τ_v, Δ_t and Δ_s, to the combined influence of τ_R and τ_m at high field.

This analysis is fairly crude, due to its neglect of interactions between relaxation parameters, and the fact that multiple relaxation parameters change after an event such as HSA binding. This is the motivation for the following section, which investigates changes in longitudinal relaxivity with respect to each of the relevant parameters in a more formal mathematical way.

3.2 Sensitivity of Longitudinal Relaxivity to Three Key Parameters

From what has been learned so far, it is clear that the relaxivity of contrast agents can be a strong function of magnetic field strength, depending sensitively on certain key underlying parameters. Contrast agents MS-325 and Multihance have among the

most interesting behavior in this respect, demonstrating characteristic peaks in their NMRD profiles when bound to HSA, over a relatively narrow field strength range. For the example of MS-325 bound to HSA, the relaxivity of the compound peaks at about 25 MHz or 0.6 T. One of the objectives of this thesis was to study the structural or molecular dynamic parameters which maybe responsible for this peak amplitude and field strength and study whether this sharp relaxivity peak could be moved to a higher field strength. The most commonly used MRI field strengths are 1.5T and 3T, and therefore it is of significant interest to know whether the peak relaxivity could be shifted to one or the other of these frequencies. At 1.5T, the relaxivity of MS-325 bound to HSA is less than a quarter of the peak relaxivity that occurs at 25 Mhz. At 3T, there is basically no increase in relaxivity of HSA-bound versus unbound MS-325. It is for these practical reasons that I was motivated to analyze the sensitivity of HSA-bound MS-325 to each of the key parameters, using an analytical sensitivity analysis methodology.

The influence of each structural parameter on relaxivity was investigated by computing the relative change in longitudinal relaxivity per relative change in the underlying parameter. This analysis involved forming the partial derivatives of relaxivity with respect to each of three key underlying parameters (τ_R, τ_m and Δ_t), using the simple SBM model from Caravan P., *Inorganic Chem.* **2007**, 46, 6632-6639. The partial derivative of longitudinal relaxivity in terms of each structural parameter was normalized to provide a relative sensitivity measure of each parameter's influence on relaxivity. This quantity is unitless and allows for "apples to apples" comparisons of relative sensitivities to each of a number of parameters. The simple SBM model used does not include the static zero field splitting dependence. Since we are primarily concerned with understanding relaxivity in the clinical MRI field strength range (>0.2T), the static ZFS effects were considered to be irrelevant, allowing a simple SBM theory to be used. The gadolinium water distance r was not studied due to its limited influence on relaxivity. The effects of transient zero field splitting are repre-

sented by the correlation time τ_v and the magnitude Δ_t. The latter has a greater effect on relaxivity therefore only Δ_t was analyzed.

3.2.1 Rotational Correlation Time τ_R

Fig. 3.7 plots the relative sensitivity of longitudinal relaxivity with respect to changes in rotational correlation time, evaluated for the case of MS-325 bound to HSA. From this plot, it can be seen that there is a major transition between 30 Mhz and 200 MHz in this relative sensitivity. Rotational correlation time's influence on relaxivity is approximately 0.2 or 20% at 42.58 Mhz (1 T), 0.6 or 60 % at 63.87 MHz (1.5 T), and 0.8 or 80 % at 127.7 MHz (3 T). At very high field strengths such as 298 MHz (7 T), the influence of rotational correlation time on relaxivity is nearly equal to 100 %. This would indicate that rotational correlation time is the most significant contribution to relaxivity at clinical mid and high field strengths.

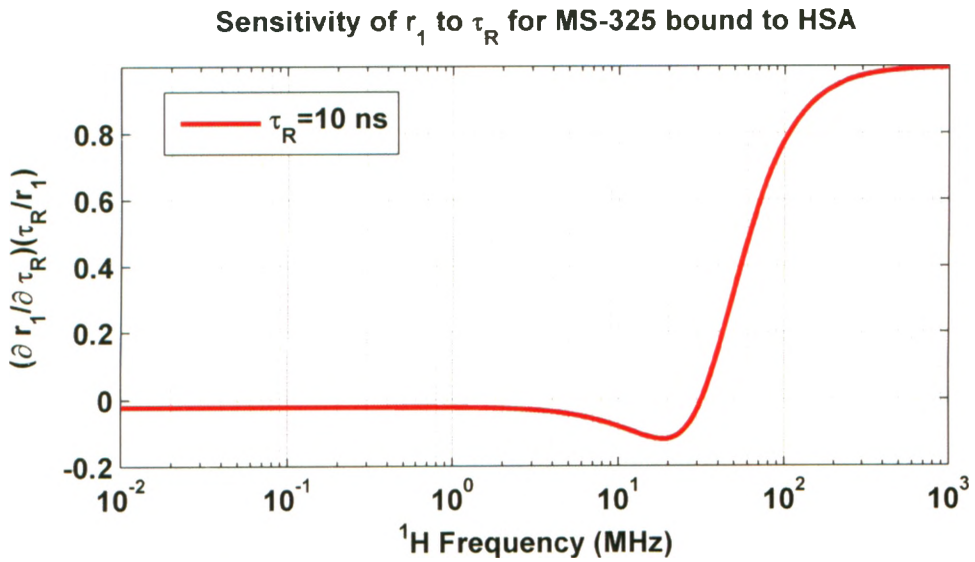

Fig. 3.7: Influence of τ_R on relaxivity for MS-325 bound to HSA

3.2.2 Water Residency Time τ_m

Fig. 3.8 plots the relative sensitivity of longitudinal relaxivity with respect to changes in water exchange time, evaluated for the case of MS-325 bound to HSA. This plot shows that there is a band of mid field strengths, from about 4 MHz (0.1 T) to about 85 MHz (2 T), over which water exchange time has an appreciable influence on longitudinal relaxivity, with this influence peaking at 25 MHz with a relative influence of approximately 50 %. These results show that water exchange is a relatively minor contributor to total relaxivity, but that over a narrow range of mid field strengths, this influence is significant. Secondly, this sensitivity analysis shows that longitudinal relaxivity is negatively correlated with water exchange time, such that decreases in τ_m cause increases in relaxivity.

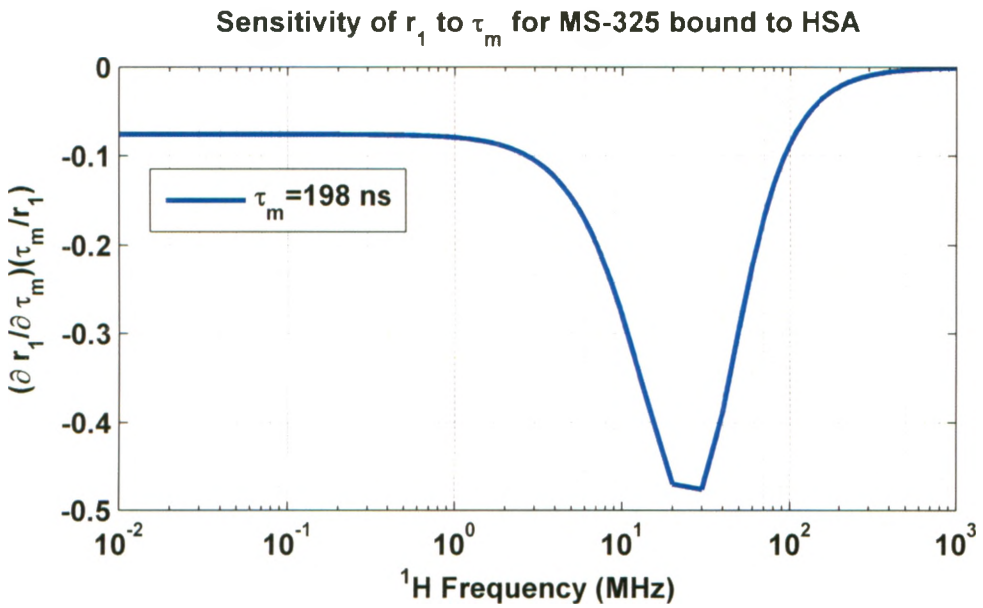

Fig. 3.8: Influence of τ_m on relaxivity for MS-325 bound to HSA

3.2.3 Magnitude of Transient Zero Field Splitting Δ_t

Fig. 3.9 plots the relative sensitivity of longitudinal relaxivity to changes in the magnitude of transient zero field splitting, using parameters for MS-325 bound to HSA. In the low field range between 0 and 4 MHz, the relative sensitivity of relaxivity to changes in the magnitude of transient zero field splitting is approximately 90 % and, like τ_m, changes in this variable are negatively correlated with changes in relaxivity. This relative sensitivity drops to 15 % at 63.87 MHz (1.5 T), and 10 % at 127.7 MHz (3 T). At very high field strengths such as 7 T and above, the magnitude of transient zero field splitting's influence on relaxivity is negligible. This analysis would indicate that the magnitude of transient zero field splitting is not a significant contributor to relaxivity at clinical field strengths.

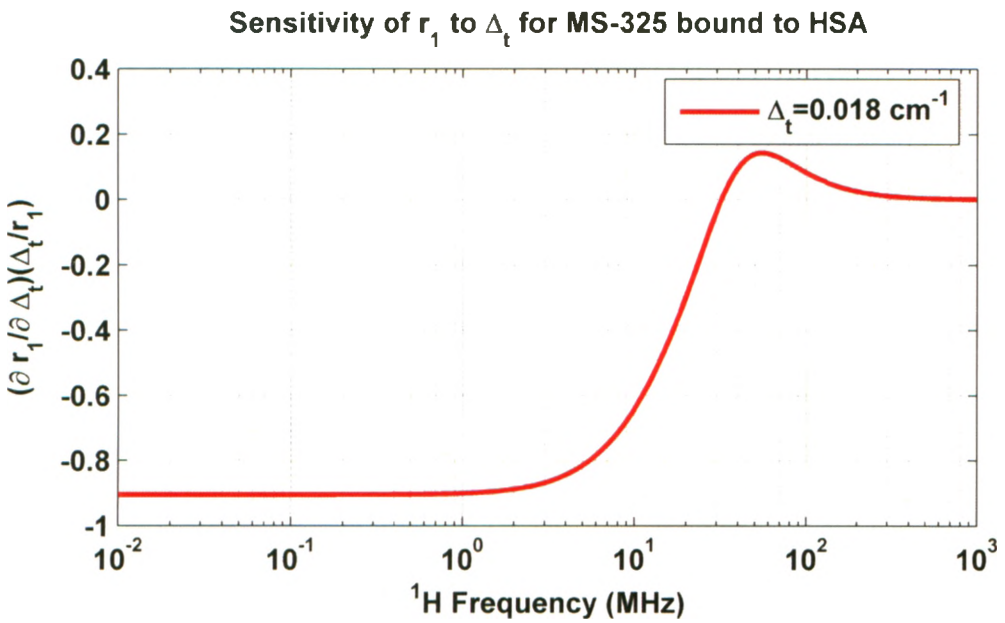

Fig. 3.9: Influence of Δ_t on relaxivity for MS-325 bound to HSA

3.2.4 Comparison of Unbound Contrast Agents

Fig. 3.10 compares the NMRD profiles of the eight clinically approved contrast agents as well as Primovist which is the most recent contrast agent to be approved by the FDA. The parameters used for these simulations, derived using a combination of ^{17}O NMR measurements and NMRD fitting, were extracted from references [19], [22] and [23] and are listed in Table 3.1. Gadofluorine was omitted from this analysis due to the lack of published parameters for this contrast agent. In Fig. 3.10, contrast agent

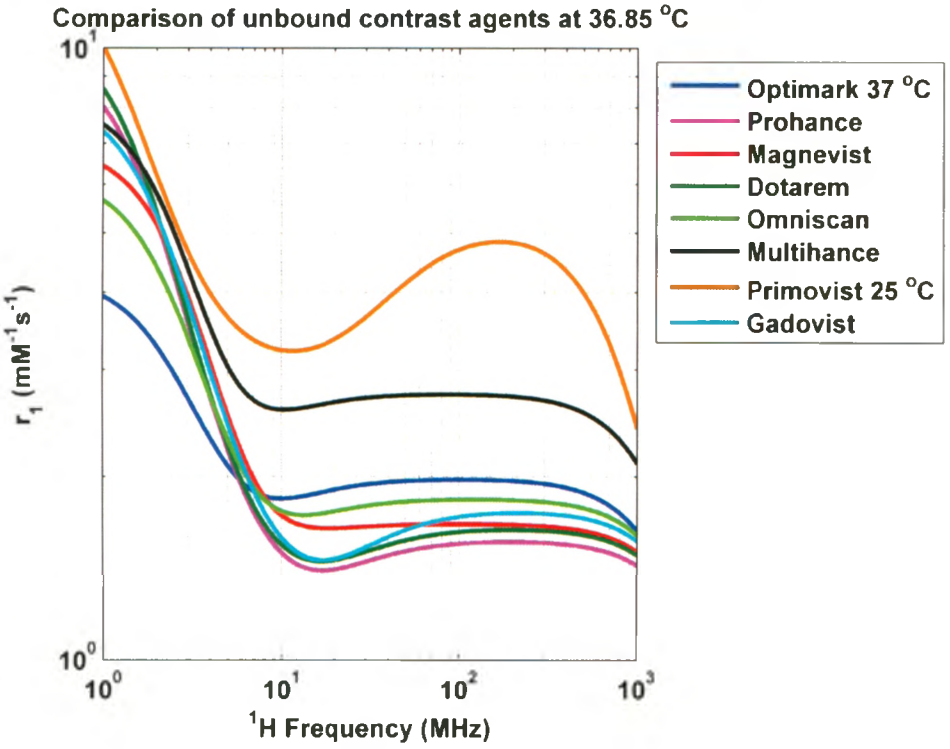

Fig. 3.10: Comparison of unbound clinically approved contrast agents

relaxivity in the higher frequency range of 1 to 1000 MHz increases with increasing rotational diffusion τ_R of the contrast agents. Primovist has the highest relaxivity with τ_R of 178 ps followed by Multihance with τ_R of 89 ps, OptiMARK with τ_R of 88 ps, Omniscan with τ_R of 65 ps, Gadovist with τ_R of 57 ps; relaxivities are approximately

Table 3.1: Parameters describing relaxivity for a selection of Gd(III) complexes

Complex	temp (°C)	τ_m(ns)	τ_R (ps)	τ_{S0}(ps)	τ_v(ps)	$\Delta_t(cm^{-1})$	r(nm)	method	ref
Magnevist	36.85	143 ± 25	54 ± 1.4	87 ± 3	25 ± 3		0.31	NMRD/O-17	[19]
Dotarem	36.85	122 ± 10	53 ± 1.3	404 ± 24	7 ± 1		0.31	NMRD/O-17	[19]
Omniscan	36.85	967 ± 36	65 ± 2	95 ± 3	18 ± 3		0.31	NMRD/O-17	[19]
Prohance	36.85	217 ± 13	51 ± 2	142 ± 10	7.5 ± 2		0.31	NMRD/O-17	[19]
Multihance	36.85	140 ± 11	89 ± 1.5	102 ± 2	30 ± 1		0.31	NMRD/O-17	[19]
Multihance	36.85	140 ± 11	72 ± 1.3	88 ± 2	25 ± 1		0.30	NMRD/O-17	[19]
Gadovist	36.85	176 ± 21	57 ± 2	111 ± 6	6.5 ± 2		0.31	NMRD/O-17	[19]
Primovist	25	278	178	91	4	0.081	0.31	O-17	[22]
Optimark	37	2564	88	53	21	0.046	0.31	NMRD	[23]
Multihance + HSA	36.85	450 ± 14	11800 ± 900	207 ± 12	38.8 ± 1		0.30	NMRD	[19]

equal for Magnevist with τ_R of 54 ps, Dotarem with τ_R of 53 ps and ProHance of 51 ps [9], [22], [23]. In other words, the order of contrast agents in terms of relaxivity is the same as the order in terms of τ_R. Here it must be noted that the parameters used to calculate relaxivity for Primovist correspond to a temperature of 25 ^oC which may account for the slower rotational rate and higher relaxivity of Primovist in comparison to the other contrast agents, all of which which were measured at a temperature of 37 ^oC [22].

For larger macromolecular contrast agents there is a direct correlation between the rate of rotational correlation time τ_R and molecular weight. In lower molecular weight contrast agents there isn't a direct correlation but there is a rough correlation of rotational diffusion increasing with increasing molecular weight [20]. Excluding Primovist, the contrast agents ordered in terms of decreasing relaxivity, along with their molecular weights are: Multihance 667.73 Da, OptiMARK 661.77 Da, Omniscan 573.66 Da, Gadovist 604.72 Da and relaxivity is about equal for Magnevist 547.58 Da, Dotarem 558.65 Da and ProHance 558.7 Da [9], [22], [23].

There is no visible pattern correlating τ_m, τ_v or Δ_t with relaxivity in these unbound contrast agents, indicating that τ_R is the most important factor in determining relaxivity, even for these unbound agents.

3.2.5 Comparison of MS-325 and Multihance

Fig. 3.11 compares the NMRD profiles of MS-325 and Multihance in their HSA-bound states. There is a drastic increase in relaxivity for MS-325 and Multihance when bound to HSA in the frequency range of 2 to 100 MHz. The rotational correlation times of HSA-bound Multihance, 11.8 ns, and MS-325, 10 ns are very similar. The remaining difference in NMRD profiles of HSA-bound Multihance and MS-325 is the result of significantly different water residency times: 198 ns for MS-325 versus 450 ns for Multihance.

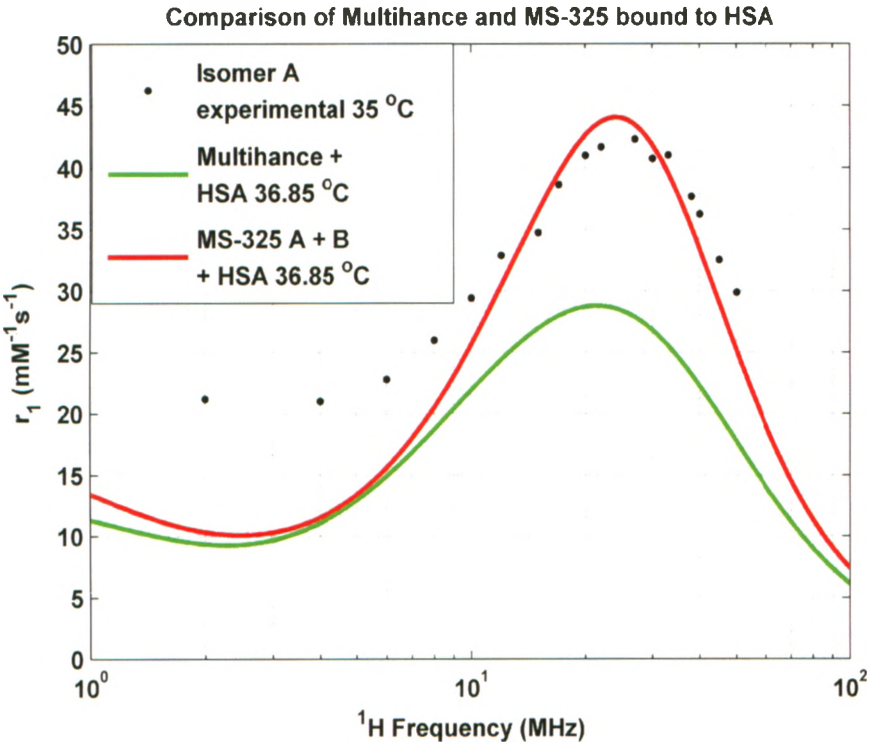

Fig. 3.11: Comparison of Multihance and MS-325 bound to HSA

3.3 NMRD Fitting to Experimental Results for MS-325 Bound to HSA

A collaborator of our group, Dr. John Chen, has written a set of multi-dimensional fitting programs called NMRD, based on the inner-sphere Lauffer variation of the SBM model (section 2.2.1). The model used in these fitting routines did not include the scalar contribution to relaxivity but did include the Hwang and Freed equations for translational outer-sphere relaxivity (section 2.3). Working with Dr. Chen, I modified this code to include Caravan's model (section 2.2.2) and the anisotropic Szabo & Lipari model (section 2.2.4) for inner-sphere relaxivity. The simulation program is tailored to allow an arbitrary number of underlying parameters to be either fixed or allowed to vary. The Caravan module within the NMRD program is isotropic and the Szabo & Lipari module includes anisotropic motion. The optimization (fitting) methodology used in this NMRD program is a genetic algorithm allowing for user defined population size of gene, number of generations and number of iterations. The fitting program seeks to minimize the residual, defined as the squared sum of the differences between the simulated profile and the actual experimental data. The accuracy of the fit is described using the R^2 value which is the Pearson's coefficient squared [24].

NMRD fitting was performed on experimental results from Caravan *et al.* on Isomer A of MS-325 bound to HSA at temperatures of 5, 15, 25 and 35 ^oC simultaneously. These experimental results were acquired under the condition of significant excess of HSA (0.67 mM) compared to the metal complex (0.085 mM); under these conditions, a large fraction (88 %) of Isomer A is bound to HSA [17]. Two sets of fits were done for each case of the isotropic Caravan model (section 2.2.2), and the anisotropic Szabo & Lipari model (section 2.2.4), these results were compared to Caravan's results using the same models. The experimental NMRD profiles for MS-325 bound to HSA were acquired in such a way that only inner-sphere relaxivity was

measured, therefore only inner-sphere theories were used in these fittings. The best four fits were used to compute the mean and standard deviation of each paramater for the ansiotropic and isotropic cases.

The objective of this fitting study was to assess the ability of the Caravan (section 2.2.2) and Szabo & Lipari (section 2.2.4) models to extract underlying parameters accurately and precisely, using a limited number of fixed parameters and broad initial ranges for the free parameters. We were interested in asking the question: could these two models accurately predict underlying parameters of novel contrast agents using experimental NMRD profiles alone?

3.3.1 Isotropic Fit for MS-325 Bound to HSA

Preliminary runs were done to determine the optimal algorithm parameters that provided adequate accuracy and acceptable computation time. These parameters were: population size of the gene 128, number of generations 100,000 and number of iterations 1,000,000. The mutation rate used was 0.1 and the crossover rate used was 0.8. Several parameters were fixed because their values are known to be relatively invariant from other experimental measurements. These were: gadolinium-water distance of 3.113 Å and hydration number q equal to one.

Simultaneous multi-temperature fits were used to increase accuracy of the extracted structural parameters. The following equations correlate change in temperature with each of the structural parameters from Caravan *et. al.*

$$\tau_R = \tau_R^{308} exp\left[\frac{\Delta E_R}{R}\left(\frac{1}{T} - \frac{1}{308.15}\right)\right] \tag{3.6}$$

$$\frac{1}{\tau_m} = \frac{T}{298.15\ \tau_m^{298}} exp\left[\frac{\Delta H^{\ddagger}}{R}\left(\frac{1}{298.15} - \frac{1}{T}\right)\right] \tag{3.7}$$

$$\tau_v = \tau_v^{308} exp\left[\frac{\Delta E_v}{R}\left(\frac{1}{T} - \frac{1}{308.15}\right)\right] \tag{3.8}$$

where T is temperature in Kelvin and R is the gas constant 8.314 (J/K mol). The parameters fit to the experimental results were τ_R^{308} the rotational correlation time of the molecule at temperature 308 K, ΔE_R the change in energy with rotation of the molecule, τ_m^{298} the water exchange time, $\Delta H^{\ddagger}$ the enthalpy of activation, τ_v^{308} the correlation time of transient zero-field splitting modulation at 308 K, ΔE_v the change in energy with transient zero-field splitting modulation.

A total of 56 isotropic runs were completed with the two best sets of four fits were averaged and compared. For both isotropic sets τ_m, τ_v, Δ_t and $\Delta H^{\ddagger}$ were within the fit result ranges published by Caravan *et. al.* τ_R, ΔE_R and ΔE_v were within the fit result ranges by Caravan for set one but not set two. The accuracy of the fit is quantified via the residual difference: the square difference between the experimental data and the simulated fit and R^2, the squared Pearson coefficient for which 1 indicates a perfect correlation between experimental and simulated data. The residual difference and

Table 3.2: Isotropic Fit Results

Parameter	Set 1 Mean ± Std. Dev.	Set 2 Mean ± Std. Dev.	Caravan results [17]
τ_R^{308} (ns)	7 ± 1	7.8 ± 0.3	5 ± 1
τ_m^{308} (ps)	190 ± 4	190.8 ± 0.1	198 ± 39.6
τ_v^{308} (ps)	18 ± 2	17.3 ± 0.2	20 ± 4
Δ_t (cm^{-1})	0.015 ± 0.008	0.0155 ± 0.0005	0.0147 ± 0.0029
ΔE_R (kJ/mol)	19 ± 10	11 ± 2	26 ± 5
ΔE_v (kJ/mol)	3 ± 3	5.4 ± 0.5	1.1 ± 0.2
$\Delta H^{\ddagger}$ (kJ/mol)	31.94 ± 0.05	31.8 ± 0.0	31 ± 6.2
Res. Diff	98 ± 2	95.93 ± 0.06	
R^2	0.9798 ± 0.0004	0.9801 ± 0	

Pearson's coefficient squared for set two are respectively 95.93 and 0.9801 indicating that set two is more accurate then set one with residual difference of 98 and R^2 equal to 0.9798. A comparison of both sets of fits indicate good overall correlation with Caravan's results. The difference in rotational correlation τ_R and the change in energy with rotational correlation ΔE_R between the two sets of fits and between Caravan's results is troubling. As discussed earlier the key factor in determining relaxivity is the

rotational rate of the molecule. Ideally a very good R^2 value of 0.99 or higher would be obtained using this program, indicating a high level of accuracy and confidence in the resulting parameters. A large number of simulations were completed but correlations this high could not be achived. This indicates that the isotropic rotational model does not accurately depict relaxivity for MS-325 bound to HSA using the chosen fitting scope with a large number of unbound structural parameters.

3.3.2 Anisotropic Fit for MS-325 Bound to HSA

In calculating anisotropic results the same simulation parameters were used as those for the isotropic analysis, size of gene equal to 128, the number of generations equal to 100,000 and the number of iterations equal to 1,000,000. The mutation rate used was 0.1 and the crossover rate used was 0.8. Several parameters were fixed because their values are known to be relatively invariant from other experimental measurements. These were: gadolinium-water distance of 3.113 Å and hydration number q equal to one. The anisotropy order parameter F^2 was left to be varied between zero and one.

Table 3.3: Anisotropic Fit Results

Parameter	Set 1 Mean ± Std. Dev.	Set 2 Mean ± Std. Dev.	Caravan results [17]
τ_R^{308} (ns)	8 ± 2	5.1 ± 0.6	4.9 ± 0.98
τ_m^{308} (ps)	163 ± 57	70.6 ± 0.2	67 ± 13
τ_v^{308} (ps)	20 ± 2	16.9 ± 0.3	16 ± 3.2
Δ_t (cm^{-1})	0.0146 ± 0.0005	0.0131 ± 0.0004	0.0128 ± 0.0026
ΔE_R (kJ/mol)	5e1 ± 4e1	12.4 ± 0.3	8.5 ± 1.7
ΔE_v (kJ/mol)	0.9 ± 0.8	0.5 ± 0.6	1.5 ± 0.3
$\Delta H^{\ddagger}$ (kJ/mol)	36 ± 9	53.7 ± 0.1	55 ± 11
F^2	0.5 ± 0.3	0.79 ± 0.04	0.63 ± 0.13
τ_f (ns)	7 ± 4	2e2 ± 2e2	< 0.3
Res. Diff	8e1 ± 3e1	19 ± 2	
R^2	0.984 ± 0.007	0.9961 ± 0.0004	

A total of 48 anisotropic runs were completed with and the two best sets of four

results were averaged and compared. In the case of anisotropic fitting the two sets of results substantially differed from each other. Most notable are the significant differences in τ_R and τ_m 8 $\pm$ 2 ns and 163 $\pm$ 57 for the first set and 5.1 $\pm$ 0.6 ns and 70.2 $\pm$ 0.2 for the second set. The first set of results show a large margin of error in the key parameters of τ_R and τ_m at an R^2 value of 0.984. In set 1 a wide range of different sets of structural parameter results produce a correlation of 0.984. This would indicate that this correlation is not high enough. The R^2 correlation should be high enough such that the algorithm consistently comes up with one solution within a small margin of error. The second set of results consistently produced results within a small margin of error. The R^2 value for this set of results is also very high 0.996 and is above the desired 0.99 boundary. Indeed the second set of results produce anisotropic parameters τ_R, τ_m, τ_v, Δ_t, τ_{s0}, ΔE_v, $\Delta H^{\ddagger}$ and F^2 that are well within the fitted parameter ranges shown by Caravan *et. al.* ΔE_v was the only parameter outside the fitted parameter ranges shown by Caravan. Overall these results are very good. This comparison would indicate that the ansiotropic model is more representative of the HSA-bound MS-325 system. The better fit to the anisotropic model is an anticipated result, since HSA-bound MS-325 is a large molecule and anisotropic motion of its molecular side chains is expected.

3.4 NMRD Fitting for Novel Gadolinium Contrast Agents

Dr. Weissleder's group has synthesized a library of novel activatable gadolinium contrast agents. These contrast agents in their native form are similar in size to Magnevist. In the presence of active myeloperoxidase (MPO) enzyme these contrast agents form small oligomers (dimers, trimers etc). Once these contrast agents oligomerize, they have an affinity for certain peptides. I investigated two variants of these contrast agents: Mono-C and Mono-C-TYR. The "mono" indicates that a single

serotonin moiety exists in each molecule. The serotonin moiety makes the contrast agents responsive to MPO, the serotonin is oxidized and the contrast agents form oligomers. The Mono-C contrast agent represented the control agent, which had no added peptides. The Mono-C-TYR contrast agent had the peptide tyrosine added to the solution but was still a form of control, since there was not MPO enzyme added to the solution.

NMRD fitting was performed on experimental NMRD profiles generated by Dr. Yuanxin Chen in Dr. Rutt's group. These profiles were acquired over the frequency range of 0 to 40 MHz at four temperatures 5, 15, 25 and 35 ^oC. As in the case of the HSA-bound MS-325 analysis, each contrast agent was fit using both the isotropic Caravan model and the anisotropic Szabo & Lipari models. Due to the larger size of both of these contrast agents we would expect that the anisotropic model would correlate better to the experimental results, but nonetheless, both isotropic and anisotropic fits were performed for comparison.

The HSA-bound MS-325 fitting was performed on experimental inner-sphere relaxivity results only, therefore only inner-sphere theories were needed in the analysis. The Mono-C and Mono-C-TYR results include both inner and outer sphere relaxivity, therefore the Hwang and Freed equations were used to fit translational outer-sphere relaxivity.

3.4.1 Mono-C Isotropic and Anisotropic Fits

The following fit parameters were used in the isotropic and anisotropic analysis: population size of the gene 128, number of generations 100,000 and number of iterations 1,000,000. The mutation rate used was 0.1 and the crossover rate used was 0.8. For the anisotropic analysis the anisotropy order parameter F^2 was left to be varied between zero and one.

Forty-eight simulations for the isotropic case and twenty one simulations were completed for the anisotropic case. These simulations were completed by gradually

changing the input parameters ranges until consistent parameter values were extracted with a high correlation to experimental data ($R^2 > 0.99$). The four fits with the highest R^2 for each case; anisotropic and isotropic were used to calculate mean and standard deviation for each of the underlying parameters. Both the anisotropic

Table 3.4: Mono-C Fit Results

Parameter	Isotropic Fit Mean ± Std. Dev.	Anisotropic Fit Mean ± Std. Dev.
τ_R^{308} (ns)	0.076998 ± 0.000005	0.222 ± 0.008
τ_m^{308} (us)	2.5 ± 0.01	1.76 ± 0.05
τ_v^{308} (ps)	3.409 ± 0.003	3.15 ± 0.08
Δ_t (cm^{-1})	0.4817 ± 0.00134	2.32 ± 0.023
ΔE_R (kJ/mol)	63.63 ± 0.08	70.6 ± 0.4
ΔE_v (kJ/mol)	11.5 ± 0.3	2.9 ± 0.2
$\Delta H^{\ddagger}$ (kJ/mol)	0.0006 ± 0.0006	0.152± 0.003
q	0.346 ± 0.002	0.36 ± 0.1
$r(nm)$	0.2461 ± 0.0002	0.307 ± 0.003
$a(nm)$	0.4709 ± 0.0007	0.421 ± 0.002
$D * 10^{-9}(cm^2/s)$	4.404 ± 0.006	4.80 ± 0.02
F^2		0.05 ± 0.02
τ_f (ns)		0.905 ± 0.004
Res. Diff	0.06895 ± 0.00002	0.0623 ± 0.0004
R^2	0.996224 ± 0.000001	0.99659 ± 0.00003

and isotropic fits for Mono-C showed high correlation to experimental data 0.996224 and 0.99659 respectively and low residual difference between simulated data and experimental data (0.06895 and 0.0623 respectively).

3.4.2 Mono-C-TYR

The same algorithm parameters were used in the isotropic and anisotropic fitting of Mono-C-TYR as Mono-C. Similarly the best four fits with the highest R^2 for each case (anisotropic and isotropic) were used to calculate the mean and standard deviation for each of the structural parameters. Both the anisotropic and isotropic fits showed a high correlation to experimental data with R^2 of 0.997369 and 0.998095

respectively and low residual differences of 0.04122 and 0.02985 respectively.

Table 3.5: Mono-C-TYR Fit Results

Parameter	Isotropic Fit Mean ± Std. Dev.	Anisotropic Fit Mean ± Std. Dev.
τ_R^{308} (ns)	0.0450 ± 0.002	0.0742 ± 0.0002
τ_m^{308} (us)	1.54 ± 0.04	1.93 ± 0.01
τ_v^{308} (ps)	128 ± 6	3.902 ± 0.001
Δ_t (cm^{-1})	0.0468 ± 0.0002	0.3891 ± 0.0001
ΔE_R (kJ/mol)	33.4 ± 0.2	40.69 ± 0.17
ΔE_v (kJ/mol)	0.607 ± 0.005	0.15 ± 0.02
$\Delta H^{\ddagger}$ (kJ/mol)	5.7 ± 0.2	4.2 ± 0.1
q	0.33 ± 0.01	0.379 ± 0.001
$r(nm)$	0.233 ± 0.002	0.2604 ± 0.0003
$a(nm)$	0.62 ± 0.002	0.4885 ± 0.0007
$D * 10^{-9}(cm^2/s)$	4.31 ± 0.07	5.005 ± 0.003
F^2		0.77 ± 0.03
τ_f (ns)		13 ± 1
Res. Diff	0.04122 ± 0.00008	0.02985 ± 0.00006
R^2	0.997369 ± 0.000005	0.998095 ± 0.000006

3.4.3 Conclusions

In these fittings a high number of unbound parameters were used with broad initial ranges for each parameter. This was done due to the lack of experimentally determined structural parameters and the novelty of these contrast agents. Usually some combination of q, r, τ_R and τ_m are determined experimentally and held constant when calculating other underlying parameters. Underlying parameter ranges can also be limited, based on knowledge of parameters of similarly structured contrast agents. These contrast MPO(Gd) agents are very different from the clinically approved contrast agents with known parameters. Multihance and MS-325 both bind to HSA, but these novel contrast agents oligomerize in the presence of MPO and in the case of Mono-C-TYR subsequently bind to tyrosine. Upon oligomerization these compounds will substantially increase in size, increasing τ_R we would expect the τ_R of

these contrast agents to be substantially slower than that of MS-325 bound to HSA. Once these contrast agents oligomerize access to the inner coordination sphere will be limited due to competing side chains of each contrast agent unit, intuitively water exchange time τ_m should also slow down in comparison to that of MS-325 bound to HSA. There is really no intuition as to changes in other structural parameters. It is likely that zero field splitting effects will be affected by close proximity between gadolinium ions. Oligomerization will affect q the number of water molecules bound to the gadolinium ion and may affect r the gadolinium water binding distance. Further experiments are needed to calculate structural parameters to validate or increase the accuracy of fitted results. Relaxivity measurements at clinical field strengths 1.5 and 3 T should be completed to assess the potential of these compounds as clincal contrast agents.

3.5 Conclusions

Comparison of the three theoretical models of relaxivity of paramagnetic contrast agents indicated that GSBM theory was most accurate in describing high field relaxivity. Unfortunately GSBM theory is significantly more complex than other theories and requires additional input parameters not readily available in literature or based on experimental analysis. The Caravan and second SL variations which characterise isotropic and anisotropic relaxivity, respectively, were found to be reasonably accurate, simple to use and reliant on structural parameters available in literature and experimental analysis.

Rotational diffusion (τ_R) is the most dominant parameter in determining relaxivity of bound and unbound contrast agents at both 1.5 and 3 T. Water residency time (τ_m) is insignificant for unbound contrast agents but significant for bound contrast agents at 1.5 T but not 3 T. Relaxivity increases with decreasing gadolinium water distance but is unlikely to be significant due to the difficulty in changing gadolinium

water distance due to the surrounding chelate structure. Correlation time of transient zero field splitting (τ_v), magnitude of static zero field splitting (Δ_s) and magnitude of transient zero field splitting (Δ_t) are only significant in the low field.

A comparison of unbound clinically approved contrast agents indicated that rotational rate and molecular weight were biggest indicators of relaxivity.

Using Dr. Chen's multi-dimensional fitting programs anisotropic (second SL variation) fits of MS-325 bound to HSA were most accurate and closest to Caravan's results.

Underlying parameters for novel activatable gadolinium MPO contrast agents Mono-C and Mono-C-TYR were calculated using a modified version of Dr. Chen's multi-dimensional fitting programs. Further experimental analysis is needed to validate or add accuracy to these results.

Chapter 4

Relaxivity of Iron Based Contrast Agents

The vast majority of clinically approved MRI contrast agents are either gadolinium or iron based. Although gadolinium and iron based contrast agents differ significantly, the major theories of iron relaxivity are modeled on gadolinium SBM and outer-sphere relaxivity theories. As discussed in the previous chapter, the major contribution to relaxivity of a paramagnetic gadolinium based contrast agent is inner-sphere, while for a superparamagnetic iron oxide based agent, relaxivity is dominated by outer-sphere effects. Knowledge of iron relaxivity theory informs gadolinium relaxivity and vice versa.

One of the key motivations behind this thesis is a novel class of both gadolinium and iron based contrast agents that increase in size and change their relaxometric properties upon reaction with a specific enzyme. The novel gadolinium contrast agents bind to macromolecules or polymerize after sensing certain enzymatic species. Similarly a new class of iron contrast agents has been developed which form tight clusters upon sensing certain enzymatic species and change their relaxometric properties [36]. In this chapter, I present the development of a new theory describing the relaxation properties of these "smart" clusterable iron oxide nanoparticles. A very

preliminary experiment is used in validating this theory .

4.1 Relaxation Components of Iron Nanoparticles

The variation in magnetic energy of a nanoparticle crystal with precessional frequency is called anisotropy energy and is a strong influence on the magnetic relaxation of iron nanoparticles. Iron magnetic relaxation occurs via two components: Néel and Brownian relaxation. Néel relaxation is primarily dependent on anisotropy energy while Brownian relaxation is dependent on the rotational motion of the particle [25].

4.1.1 Magnetization

Magnetization is the measure of magnetic moment per unit volume. Magnetic moments are the result of microscopic electric currents resulting from the motion of electrons and/or spins in atoms. Net magnetization results from the response of a material to an external magnetic field, together with any unbalanced magnetic dipole moments that may be inherent in the material itself such as ferromagnets like iron [25].

4.1.2 Anisotropy Energy

The magnetic energy of a nanomagnet depends upon the direction of its magnetization vector. The directions that minimize this magnetic energy are called anisotropy directions or easy axes. The magnetic energy increases with the tilt angle between the magnetization vector and the easy directions. The variation in magnetic energy due to the tilt angle is called the anisotropy energy E_a and is given by the product of the crystal volume, V, and a constant, called the anisotropy constant, K_a and R is the radius of the nanomagnet [25].

$$E_a = K_a V = K_a * \frac{4\pi R^3}{3} \tag{4.1}$$

There are four contributions to the anisotropy field, which may be influenced by nanoparticle clustering and would be of interest in analyzing relaxometric properties of clusterable iron contrast agents. The first one is the bulk magnetocrystalline anisotropy field, which depends upon the chemical composition and the crystallographic structure of the material. The second one is the demagnetising field, which is determined by the shape of the crystal. For a sphere this component of the anisotropy energy is zero and increases with elongation of the shape. The third component is the anisotropy constant which depends on the surface structure of the crystal. The final contribution to anisotropy energy for clustered nanoparticles is the dipolar interaction between two neighboring crystals, which increases with decreasing inter-crystal distance [25].

4.1.3 Néel and Brownian Relaxation

In the case of iron oxide based nanoparticles the return of magnetization to equilibrium is determined by two different processes Néel and Brownian relaxation. The anisotropy energy determines the Néel relaxation time, which is characterized by the time constant of the return to equilibrium of the magnetization after a perturbation. In the case of superparamagnetism the Néel relaxation time is much faster than the physical measurement time. Brownian relaxation characterizes the viscous rotation of the particle. For large particles Brownian relaxation time is shorter than Néel relaxation time and the viscous rotation of the particle becomes the dominant process determining the global relaxation. In these conditions, the fast magnetic relaxation allows the system to be always at thermodynamic equilibrium and the magnetization evolution with the external magnetic field is proportional to the Langevin function. The Langevin function takes into account a Boltzmann distribution of energy levels corresponding to all of the possible orientations of the particle magnetization moment,

$$m_a(B_0) = m_a(\infty)L(x) \tag{4.2}$$

where $m_a(B_0)$ is the magnetization at field B_0, $m_a(\infty)$ is the magnetization at saturation, N_c is the number of nanoparticles in a cluster, μ_{sp} is the magnetic moment of the nanocrystal and L(x) is the Langevin function

$$L(x) = \left[coth(x) - \frac{1}{x}\right] \quad where \quad x = \frac{\mu_{sp} N_c V B_0}{kT} \tag{4.3}$$

[25].

4.2 Theories of Iron Relaxivity

Superparamagnetic relaxation physics is based on the original SBM theory developed for paramagnetic systems. As in paramagnetic systems there are two contributions to proton relaxation, inner- and outer-sphere relaxation. For superparamagnetic particles, the inner-sphere contribution to the relaxation is minor and often completely negligible in comparison to the dominant outer-sphere contribution. Outer-sphere relaxation occurs due to the movement of water protons through local magnetic field gradients generated by the superparamagnetic ion oxide particle [25].

There are two models describing superparamagnetic relaxation by Muller *et al.*, the high anisotropy model and the low anisotropy model [25].

4.2.1 High Anisotropy Model

For large superparamagnetic crystals or crystals which have a very high anisotropy constant, the anisotropy energy is larger than the thermal energy. In this model the direction of the crystal magnetic moment is very close to that of the anisotropy axes, in which case the precession of the electron magnetization is forbidden. Magnetic fluctuations then arise from the jumps of the moment between different easy directions, quantified by τ_N, the Néel relaxation time. At low field, the proton longitudinal relaxation rate is characterized by the Freed spectral density function J_F dependent on τ_N and τ_D. The translational correlation time τ_D, is $\tau_D = \frac{R^2}{D}$, where R is the

distance of closest approach of a water molecule to the paramagnetic center while D is the diffusion coefficient of water. Freed's spectral density function, J_F is defined according to

$$J_F(\omega_I, \tau_D, \tau_N) = Re\left(\frac{1+\frac{1}{4}\Omega^{\frac{1}{2}}}{1+\Omega^{\frac{1}{2}}+\frac{4}{9}\Omega+\frac{1}{9}\Omega^{\frac{3}{2}}}\right) \tag{4.4}$$

where $\Omega = i\omega_I\tau_D + \frac{\tau_D}{\tau_N}$. At high field, the magnetic vector is locked along the B_0 direction and the so-called Curie relaxation dominates. Curie relaxation is caused by water molecules diffusing through the inhomogeneous nonfluctuating magnetic field created by the mean crystal moment, aligned along B_0. The corresponding relaxation rates are given by Ayant's model assuming a stationary magnetization component in the B_0 direction where J_A, Ayant's density spectral function is

$$J_A(z) = \frac{1+\frac{5z}{8}+\frac{z^2}{8}}{1+z+\frac{z^2}{2}+\frac{z^3}{6}+\frac{4z^4}{81}+\frac{z^5}{81}+\frac{z^6}{648}} \tag{4.5}$$

where $z = \sqrt{2\omega_I\tau_D}$. The proton relaxation rates (R_1 and R_2) are combinations of the high and low-field contributions, weighed by factors depending upon the Langevin function L(x)

$$\begin{aligned}\frac{1}{T_1} &= \frac{32\pi}{405000}\left(\frac{\mu_{sp}\mu_0\gamma}{4\pi}\right)^2\left(\frac{N_A C}{RD}\right) \\ &\quad *\left[\frac{L(x)}{x}21J_F(\omega_I,\tau_D,\tau_N)+9\left(1-L^2(x)-2\frac{L(x)}{x}\right)J_F(\omega_I,\tau_D,\tau_N)\right. \\ &\quad \left.+9L^2(x)J_A(\sqrt{2\omega_I,\tau_D})\right]\end{aligned} \tag{4.6}$$

$$\begin{aligned}\frac{1}{T_2} &= \frac{32\pi}{405000}\left(\frac{\mu_{sp}\mu_0\gamma}{4\pi}\right)^2\left(\frac{N_A C}{RD}\right) \\ &\quad *\left[\frac{L(x)}{x}19.5J_F(\omega_I,\tau_D,\tau_N)+4.5\left(1-L^2(x)-2\frac{L(x)}{x}\right)(J_F(\omega_I,\tau_D,\tau_N)\right. \\ &\quad \left.+6J_F(0,\tau_D,\tau_N))+L^2(x)(4.5J_A(\sqrt{2\omega_I,\tau_D})+6J_A(0))\right]\end{aligned} \tag{4.7}$$

[25].

4.2.2 Small Crystal and Low Anisotropy Energy Limit

For small crystals, the anisotropy energy is comparable to thermal energy such that the magnetic moment direction is more random, and can vary farther away from the easy axis. Equations 4.6 and 4.7 assume an infinite anisotropy energy, this assumption becomes less valid with decreasing particle size and thereby decreasing anisotropy energy. To model this more accurately, $\frac{1}{T_1}$ and $\frac{1}{T_2}$ are expressed as weighted sums of rates for infinite anisotropy $E_A \to \infty$ and for anisotropy equal to zero $E_A = 0$. The variable P is introduced as a weighing factor in this weighted sum, and adjusted to provide a better fit to the experimental relaxivity curve.

$$\begin{aligned}\frac{1}{T_1} &= \frac{32\pi}{405000}\left(\frac{\mu_{sp}\mu_0\gamma}{4\pi}\right)^2\left(\frac{N_A C}{RD}\right) \\ &\quad *\left[\frac{L(x)}{x}21PJ_F(\omega_S,\tau_D,\tau_N)+\frac{L(x)}{x}21(1-P)J_F(\omega_I,\tau_D,\tau_N)\right. \\ &\quad \left.+9\left(1-L^2(x)-2\frac{L(x)}{x}\right)J_F(\omega_I,\tau_D,\tau_N)+9L^2(x)J_A(\sqrt{2\omega_I,\tau_D})\right] \quad (4.8)\end{aligned}$$

$$\begin{aligned}\frac{1}{T_2} &= \frac{32\pi}{405000}\left(\frac{\mu_{sp}\mu_0\gamma}{4\pi}\right)^2\left(\frac{N_A C}{RD}\right) \\ &\quad *\left[\frac{L(x)}{x}10.5PJ_F(\omega_S,\tau_D,\tau_N)+\frac{L(x)}{x}9PJ_F(\omega_I,\tau_D,\tau_N)\right. \\ &\quad +\frac{L(x)}{x}19.5(1-P)J_F(\omega_I,\tau_D,\tau_N)+\left(1-L^2(x)-2\frac{L(x)}{x}\right)(4.5J_F(\omega_I,\tau_D,\tau_N) \\ &\quad \left.+6J_F(0,\tau_D,\tau_N))+L^2(x)(4.5J_A(\sqrt{2\omega_I,\tau_D})+6J_A(0))\right] \quad (4.9)\end{aligned}$$

[25].

4.3 Theories of Nanoparticle Clustering

The aggregation of nanomagnets affects relaxation properties related to the global structure of the cluster and properties related to the inner part of the aggregate. The global effect mainly affects the outer-sphere and R_2, the inner one influences less R_2 and affects mainly the inner-sphere and R_1 [25].

There is one theory describing the spin-lattice relaxivity ratio between clustered and dispersed states as described by Billotey *et al.* The original Billotey model was created for iron oxide nanoparticles compartmentalized within endosomes where "clustering" was defined as compartmentalization or non-uniform distribution of these nanoparticles. Billotey's model was used in the derivation of a transverse relaxivity ratio for clustering nanoparticles by Bowen [26], [27].

There are two theories of transverse relaxivity which apply to iron nanoparticles clustering; diffusion theory and chemical exchange theory. Both of these theories were used in this thesis to form the basis for a new clustering theory for superparamagnetic iron oxide nanoparticles.

4.3.1 Longitudinal Relaxivity Model

The longitudinal relaxivity ratio between clustered and dispersed superparamagnetic iron oxide nanoparticle states is described by Billotey *et al.* The original Billotey model was created for cells with iron oxide nanoparticles internalized within endosomes. The relaxation mechanism is based on the diffusion of water molecules in and out of the endosomal compartment [26].

The model consists of two phases, the first representing water molecules within the endosomes occupied by iron oxide nanoparticles, characterized by a high relaxation rate R_1^{end} and low-volume fraction f_{end} compared to the second phase. The second phase consists of the environment outside the endosomes, which includes the rest of the cell interior as well as all the extracellular space and has a relaxation rate R_1^{solv}

and volume fraction $f_{solv} = 1 - f_{end} \approx 1$. The relaxation rate within the endosomes R_1^{end} is given by

$$R_1^{end} = \frac{1}{T_1^{end}} = R_1^{solv} + r_1^{dispersed} C_{end} \tag{4.10}$$

where C_{end} is the local iron concentration within the endosomes and $r_1^{dispersed}$ is the relaxivity of the dispersed nanoparticles. This dispersed relaxivity is used for the endosomal compartment because the nanoparticles are well separated. There is also an assumption that there are no iron oxide particles outside of the endosomes. The two phases in this model are dispersed nanoparticles compartmentalized within endosomes and an area without nanoparticles. The diphasic system has a global iron concentration of $C = f_{end} C_{end}$ and a relaxation rate of

$$R_1 = R_1^{solv} + r_1^{confined} C \tag{4.11}$$

where $r_1^{confined}$ is the relaxivity of the diphasic system containing confined particles. In this case R_1 is the relaxation rate of the whole system as influenced by the particles confined within the endosomes. The relaxation rate R_1 of the diphasic system has a term which is weighted by the mean residency time of a diffusing water molecule within the endosome, $\tau_D = d_{end}^2/D$ where d_{end} is the endosome diameter. T_1^{end} can be calculated using the appropriate theory of iron relaxivity equations (4.6) or (4.8). Therefore

$$R_1 = R_1^{solv} + R_1^{end} \frac{f_{end}}{1 + \tau_D/T_1^{end}} \tag{4.12}$$

where $R_1 - R_1^{solv} = r_1^{confined} C$ then

$$r_1^{confined} C = R_1^{end} \frac{f_{end}}{1 + \tau_D/T_1^{end}} \tag{4.13}$$

If the residence time τ_D is much smaller than the relaxation time T_1^{end} in the endosome ($\tau_D \ll T_1^{end}$), the relaxation of the diphasic system is equal to that of a dispersed solution of particles, taking care to use the effective iron concentration C:

$$\Delta R_1 = R_1 - R_1^{solv} = R_1^{end} f_{end} = r_1^{dispersed} C \tag{4.14}$$

If T_1^{end} becomes smaller than τ_D residence time of waters in the endosomes, the relaxing effect of the particles confined in the endosome saturates and the longitudinal relaxivity is reduced for compartmentalized particles compared to dispersed particles. The ratio of relaxivity for dispersed isolated particles $r_1^{dispersed}$ over the relaxivity of cell-internalized particles $r_1^{confined}$ is given by:

$$\frac{r_1^{confined}}{r_1^{dispersed}} = \frac{1}{1 + \tau_D R_1^{end}}. \tag{4.15}$$

The key feature in the Billotey theory is the characterization of relaxivity under conditions of fast water exchange and slow water exchange. If the water residency time τ_D is much less then longitudinal relaxation time in the endosome, the relaxivity of the whole system is equal to that of the nanoparticles within the endosomes. Conversely if the relaxation time within the endosomes is less than water residency time τ_D in the endosomes, the longitudinal relaxivity of the whole endosomal system will be less than that of a system of freely dispersed nanoparticles.

Bowen applied this theory directly to represent the behavior of clusterable iron nanoparticles. The fundamental assumption here is that nanoparticles in a clustered state can be well represented by the Billotey endosomal compartmentalized state. The big difference in these two cases is that the clusterable iron nanparticles are chemically bound, and therefore much more tightly clustered compared to the endosomally compartmentalized iron nanoparticles which are just in close physical proximity to each other. In both cases two phases exist: one of greater relaxivity (nanoparticle clusters or endosomally compartmentalized nanoparticles) and a phase of lower relaxivity (dispersed iron nanoparticles or iron free solvent). Bowen relabled the equation as

$$\frac{r_1^{clustered}}{r_1^{dispersed}} = \frac{1}{1 + \tau_D R_1^{clustered}} \tag{4.16}$$

[26], [28]. The common feature of both situations is that the effects of slow vs fast water exchange should be the key determinant of longitudinal relaxivity.

4.4 Models of Transverse Relaxivity

There are two theories of transverse relaxivity which apply to iron nanoparticles; diffusion theory and chemical exchange theory. Diffusion theory predicts transverse relaxivity as affected by water protons diffusing past the magnetic particles. The transverse relaxivity of an iron cluster in diffusion theory is composed of inner-sphere and outer-sphere contributions. In the case of superparamagnetic contrast agents, the magnetization is much stronger than in the case of paramagnetism and therefore the field perturbation has a much larger distance span. This means that the inner-sphere contribution is much smaller than outer-sphere contribution due to the much smaller number of water molecules affected. The inner-sphere contribution can therefore be neglected [25].

Chemical exchange theory is based on the effect of water protons exchanging in and out of the iron nanoparticle cluster [29].

4.4.1 Diffusion Theory, Outer-Sphere Contribution

The transverse relaxation rate is readily calculated by outer-sphere diffusion theory, provided the motional averaging condition is fulfilled: $\Delta\omega\tau_D << 1$, where $\Delta\omega$ is the difference in angular frequency experienced by a proton at the equatorial line of the cluster surface (assuming that the nanoparticle cluster can be treated as a sphere) and in the bulk. $\Delta\omega$ is calculated as the root mean square frequency shift at the radius of the cluster R_c,

$$\Delta\omega^2 = (4/5)N_c^2\gamma^2\mu_{sp}^2/R_c^6. \tag{4.17}$$

which is obtained by integrating the square of the z-component of the magnetic field

$$B_z(r,\theta) = (N_c\mu_{sp}/R_c^3)(1 - 2cos^2\theta) \tag{4.18}$$

over a spherical surface of radius R_c and dividing by the surface area and the gyromagnetic ratio. N_c is the number of nanoparticles within a cluster and μ_{sp} is the

magnetic moment of an elementary crystal of the nanoparticle. If we define τ_D as the mean water molecule residency time within the cluster

$$\tau_D = R_c^2/D \tag{4.19}$$

where D is the water molecule diffusion coefficient and f_c as the fractional cluster volume i.e., the volume of all clusters divided by total volume

$$f_c = \frac{4\pi R_c^3 N_A[M]}{3 * 1000 * N_c}. \tag{4.20}$$

where [M] is the molar concentration of the nanoparticle then transverse relaxivity is given by

$$\frac{1}{T_2} = (4/9) f_c \Delta\omega^2 \tau_D \tag{4.21}$$

and can be rewritten as,

$$\frac{1}{T_2} = (64\pi/135)[\mu_0 \gamma \mu_{sp} N_c/(4\pi)]^2 N_A M/(N_c R_c D) \tag{4.22}$$

[29].

4.4.2 Diffusion Theory, Outer-Sphere Contribution with Langevin Function

The diffusion theory outer sphere contribution described in section 4.4.1 is very simple, in fact a closer look at 4.22 will reveal the lack of direct magnetic field and temperature dependence on relaxation time. Due to these crucial oversights, *Muller et. al* introduced the Langevin function into diffusion theory. The nanoparticle cluster can be considered as a large magnetized sphere where the total magnetic moment in an external magnetic field is proportional to the Langevin function. The expression for outer-sphere relaxivity can be modified to include the Langevin function,

$$\frac{1}{T_2} = (64\pi/135)[\mu_0 \gamma \mu_{sp} N_c L(x)/(4\pi)]^2 N_A M/(N_c R_c D). \tag{4.23}$$

The Langevin function is $L(x) = coth(x) - 1/x$ where $x = \mu_{sp} N_c B_0/(kT)$, B_0 is the static field, k is Boltzmann constant, and T is the temperature [25].

4.4.3 Chemical Exchange Theory

Chemical exchange theory assumes a two compartment model in which water protons are exchanged between two compartments. In diffusion theory relaxivity is based on water diffusing near the contrast agent. Chemical exchange relaxivity is based on water protons exchanging in and out of two sites. In the case of clusterable iron nanoparticles, the two compartments are the nanoparticle cluster, site a and the bulk water, site b. The two-site chemical exchange model is described by: F_a, F_b = fraction of protons in each site ($F_a + F_b = 1$), τ_a, τ_b = mean water residency times in each site, $\Delta\omega_b$ = difference in angular Larmor frequency at site b relative to site a. An iron oxide nanoparticle will cause water protons in its vicinity to precess at a different frequency then water protons outside its range. If these nanoparticles are clustered the local magnetic field inhomogeneities will be greater and the difference in precession frequency will be larger. The mean water residency times are related to the population fractions by

$$\tau_a/\tau_b = F_a/F_b, \tag{4.24}$$

and the exchange time τ_{ex} is

$$1/\tau_{ex} = 1/\tau_a + 1/\tau_b. \tag{4.25}$$

Chemical exchange theory is depended on two pulse sequences most commonly used to measure transverse relaxivity, the Carr-Purcell-Meiboom-Gill (CPMG) multiple spin echo pulse sequence and the Hahn single spin echo sequence. The contribution of chemical exchange to $1/T_2$ is then given by:

$$[1/T_2]_{CE} = F_a F_b (\Delta\omega_b)^2 \tau_{ex}[1 - (\tau_{ex}/\tau_{CP}) tanh(\tau_{CP}/\tau_{ex})]. \tag{4.26}$$

The time parameter τ_{CP}, is defined as half the interval between successive 180^o pulses in a CPMG sequence, or half the echo time for a single (Hahn) spin-echo sequence ($\tau_{CP} = TE/2$). For spherical particles in both the long echo time limit and the short

echo time limit and with the assumption of a dilute solution of particles $F_b << 1$

$$\tau_{ex} = 0.26\tau_D \tag{4.27}$$

and

$$F_b(\Delta\omega_b)^2 = 1.73f(\Delta\omega)^2. \tag{4.28}$$

Equation 4.26 is valid if $\tau_{CP} < 1/\Delta\omega_b$, which coincides with a weak magnetization condition. The above equations are valid in both the long and short echo time limit. In the "long-echo" time limit ($\tau_{CP} \gg \tau_D$), the standard quantum-mechanical theory of relaxation applies and covers induced magnetization and the "Curie effect". In the "short-echo" time limit ($\tau_{CP} \ll \tau_D$), the classical theory of diffusion in magnetic gradients is commonly referred to as the mean gradient diffusion theory (MGDT). Outer-sphere theories (chemical exchange or diffusion theory) apply only in the "long-echo" time limit, therefore the following derivation is under "long-echo" time limit [29].

4.5 Derivations of Relaxivity Ratios of Nanoparticle Clustering

Perez *et. al.* completed experiments on clusterable iron nanoparticles measuring transverse and longitudinal relaxivity before and after enzyme activated nanoparticle clustering. For the case of clusterable nanoparticles, the $r_2^{clustered}/r_2^{dispersed}$ ratio was found to be substantially greater than one, whereas the r_1(clustered)/r_1(dispersed) ratio was found to be non-significantly different than one [36]. This was a novel and intriguing experimental observation. There are currently only three theories describing superparamagnetic nanoparticle clustering: Taktak *et. al.*, Muller *et. al.* both based on diffusion theory and Bowen *et. al.* based on chemical exchange theory [37], [31] and [27]. I found that none of the these theories accurately predicted the results observed by Perez *et. al.*, and this motived me to develop a better theory.

Clusterable iron oxide nanoparticles are of particular interest due to their potential use as clinical activatable contrast agents. Iron oxide particles are the most powerful MR probes developed to date, allowing the most sensitive detection of cells and molecules using MRI. The concept of iron oxide nanoparticle clustering could very well be the most effective mechanism to turn MRI into a true molecular imaging tool capable of sensing very small concentrations of specific molecular species such as enzymes.

Dr. Bowen derived a transverse relaxivity ratio based on chemical exchange processes alone [27]. I have derived an expression based on outer-sphere theory alone, which produces the same ratio as Bowen's model, and another expression based on outer-sphere theory modifed by the addition of the Langevin function, which is more accurate. Finally I have derived a model based on both chemical exchange and outer-sphere theories combined.

4.5.1 Bowen's Derivation, Chemical Exchange Only

Bowen's derivation is modeled on the two-compartment weak exchange model, where region a is within the cluster and region b is outside the cluster.

$$R_2^{clustered} = f_c R_2^{clustered} + (1 - f_c) R_{2\,CE}^{dispersed} \tag{4.29}$$

where

$$f_c = \frac{4\pi R_c^3 N_A M}{3 * 1000 * N_c} = C * R_c^3/(N_c R_d^3) f_d \quad and \quad f_d = \frac{4\pi R_d^3 N_A M}{3 * 1000} \tag{4.30}$$

in which case C is nanoparticle concentration within the solution.

$$\frac{R_2^{clustered}}{C} = r_2^{clustered} = \frac{f_c R_2^{clustered}}{C} + \frac{(1 - f_c) R_{2\,CE}^{dispersed}}{C} \tag{4.31}$$

From Billotey *et al.* if the residence time τ_D is much smaller than the relaxation time $T_1^{clustered}$ in the cluster ($\tau_D \ll T_1^{clustered}$), the relaxation of the diphasic system is equal to that of a dispersed solution of particles (with iron concentration C):

$R_1^{clustered} f^{clustered} \approx r_1^{dispersed} C$. Applying this to T_2

$$r_2^{clustered} = r_2^{dispersed} + \frac{(1-f_c)R_{2\ dispersed}^{Chemical\ exchange}}{C}. \tag{4.32}$$

The outer-sphere transverse relaxivity of dispersed crystals where the number of nanoparticles within the cluster $N_d = 1$ based on Equation 4.21 becomes

$$\begin{aligned} r_2^{dispersed} = \frac{R_{2\,OS}^{dispersed}}{C} &= (4/9) f_d \tau_D (\Delta\omega)^2 \\ &= (4/9) f_d R_d^2 / D((4/5)\gamma^2 \mu_{sp}^2 / R_d^6) \\ &= (4/9) f_d R_d^2 / D((4/5)\gamma^2 \mu_{sp}^2 / R_d^6) \\ &= \frac{16 f_d \gamma^2 \mu_{sp}^2}{45 D R_d^4}. \end{aligned} \tag{4.33}$$

The ratio of transverse relaxivity of clustered crystals divided by transverse relaxivity of dispersed crystals becomes

$$\begin{aligned} \frac{r_2^{clustered}}{r_2^{dispersed}} &\approx 1 + 0.4498 \frac{4 f_d N_c \gamma^2 \mu_{sp}^2}{5 D R_c R_d^3} * \frac{45 D R_d^4}{16 f_d \gamma^2 \mu_{sp}^2} \\ \frac{r_2^{clustered}}{r_2^{dispersed}} &\approx 1 + \frac{N_c R_d}{R_c}. \end{aligned} \tag{4.34}$$

4.5.2 Diffusion Theory Outer Sphere Only

The transverse relaxivity of a crystal cluster solution is composed of the relaxivity component within the cluster and the relaxivity component of the bulk solution outside the cluster. In this variation both are modeled by diffusion outer-sphere theory.

$$R_2^{clustered} = f_c R_{2\,OS}^{clustered} + (1-f_c) R_{2\,OS}^{dispersed} \tag{4.35}$$

where f_c is the fractional volume occupied by the cluster

$$f_c = \frac{4\pi R_c^3 N_A M}{3 * 1000 * N_c} = R_c^3 / (N_c R_d^3) f_d \quad where \quad f_d = \frac{4\pi R_d^3 N_A M}{3 * 1000} \tag{4.36}$$

and f_d is the fractional volume occupied by the disperse nanoparticles. Fractional volume of occupied by the cluster is much less than one, $f_c << 1$ therefore

$$R_2^{clustered} \approx f_c R_{2\,OS}^{clustered} + R_{2\,OS}^{dispersed} \tag{4.37}$$

and

$$\frac{r_2^{clustered}}{r_2^{dispersed}} \approx \frac{f_c R_{2\,OS}^{clustered}}{R_{2\,OS}^{dispersed}} + 1 \tag{4.38}$$

Transverse relaxivity of a crystal cluster is

$$f_c R_{2\,OS}^{clustered}/M = (64\pi/135)[\mu_0 \gamma \mu_{sp} N_c/(4\pi)]^2 N_A/(N_c R_c D). \tag{4.39}$$

Transverse relaxivity of dispersed crystals where $N_d = 1$ is

$$\begin{aligned} r_2^{dispersed} &= (64\pi/135)[\mu_0 \gamma \mu_{sp} N_d/(4\pi)]^2 N_A/(R_d D) \\ &= (64\pi/135)[\mu_0 \gamma \mu_{sp}/(4\pi)]^2 N_A/(R_d D). \end{aligned} \tag{4.40}$$

Transverse relaxivity of clustered crystals divided by transverse relaxivity of dispersed crystals becomes

$$\frac{r_2^{clustered}}{r_2^{dispersed}} = \frac{(64\pi/135)[\mu_0 \gamma \mu_{sp} N_c/(4\pi)]^2 N_A/(N_c R_c D)}{(64\pi/135)[\mu_0 \gamma \mu_{sp}/(4\pi)]^2 N_A/(R_d D)} + 1 \tag{4.41}$$

$$\frac{r_2^{clustered}}{r_2^{dispersed}} = \frac{N_c R_d}{R_c} + 1. \tag{4.42}$$

4.5.3 Diffusion Outer-Sphere Theory with Langevin Function

The transverse relaxivity of a crystal cluster solution is composed of the relaxivity component within the cluster and the relaxivity component of the bulk solution outside the cluster. In this variation both are modeled by outer-sphere theory but include the Langevin function.

$$R_2^{clustered} = f_c R_{2\,OS}^{clustered} + (1 - f_c) R_{2\,OS}^{dispersed} \tag{4.43}$$

where f_c is the fractional volume occupied by the cluster

$$f_c = \frac{4\pi R_c^3 N_A M}{3 * 1000 * N_c} = R_c^3/(N_c R_d^3) f_d \quad where \quad f_d = \frac{4\pi R_d^3 N_A M}{3 * 1000} \tag{4.44}$$

and f_d is the fractional volume occupied by the disperse nanoparticles. Fractional volume occupied by the cluster is much less than one, $f_c << 1$ therefore

$$R_2^{clustered} \approx f_c R_{2\,OS}^{clustered} + R_{2\,OS}^{dispersed} \tag{4.45}$$

and

$$\frac{r_2^{clustered}}{r_2^{dispersed}} \approx \frac{f_c R_{2\,OS}^{clustered}}{R_{2\,OS}^{dispersed}} + 1. \tag{4.46}$$

Transverse relaxivity of a crystal cluster is

$$f_c R_{2\,OS}^{clustered}/M = (64\pi/135)[\mu_0 \gamma \mu_{sp} N_c L(x)_c/(4\pi)]^2 N_A/(N_c R_c D). \tag{4.47}$$

Transverse relaxivity of dispersed crystals where $N_d = 1$ is

$$\begin{aligned} r_2^{dispersed} &= (64\pi/135)[\mu_0 \gamma \mu_{sp} N_d L(x)_d/(4\pi)]^2 N_A/(R_d D) \\ &= (64\pi/135)[\mu_0 \gamma \mu_{sp} L(x)_d/(4\pi)]^2 N_A/(R_d D). \end{aligned} \tag{4.48}$$

Transverse relaxivity of clustered crystals divided by transverse relaxivity of dispersed crystals becomes

$$\frac{r_2^{clustered}}{r_2^{dispersed}} = \frac{(64\pi/135)[\mu_0 \gamma \mu_{sp} N_c L(x)_c/(4\pi)]^2 N_A/(N_c R_c D)}{(64\pi/135)[\mu_0 \gamma \mu_{sp} L(x)_d/(4\pi)]^2 N_A/(R_d D)} + 1 \tag{4.49}$$

and

$$\frac{r_2^{clustered}}{r_2^{dispersed}} = \frac{N_c R_d [L(x)_c]^2}{R_c [L(x)_d]^2} + 1. \tag{4.50}$$

The Langevin function for a clustered crystal is

$$L(x)_c^2 = \left[coth\left(\frac{\mu_{sp} N_c B_0}{kT}\right) - \frac{kT}{\mu_{sp} N_c B_0} \right]^2. \tag{4.51}$$

The Langevin function for a dispersed crystal is

$$L(x)_d^2 = \left[coth\left(\frac{\mu_{sp} B_0}{kT}\right) - \frac{kT}{\mu_{sp} B_0} \right]^2. \tag{4.52}$$

Therefore the ratio becomes

$$\frac{r_2^{clustered}}{r_2^{dispersed}} = \frac{\left[coth\left(\frac{\mu_{sp} N_c B_0}{kT}\right) - \frac{N_c kT}{\mu_{sp} B_0} \right]^2 R_d}{\left[coth\left(\frac{\mu_{sp} B_0}{kT}\right) - \frac{kT}{\mu_{sp} B_0} \right]^2 R_c} + 1. \tag{4.53}$$

4.5.4 Chemical Exchange and Diffusion Outer-Sphere Combination

The relaxivity ratio of clustered to dispersed relaxivity assuming a constant concentration is

$$\frac{r_2^{clustered}}{r_2^{dispersed}} = \frac{T_2^{dispersed}}{T_2^{clustered}}. \tag{4.54}$$

Transverse relaxivity of a crystal cluster is composed of the relaxivity within the crystal cluster modeled using outer-sphere theory and relaxivity outside the crystal cluster modeled using chemical exchange theory. The two-site chemical exchange is the result of protons exchanging in and out of the crystal cluster. Fraction of protons with in the cluster is f_c and fraction of protons outside the cluster is $(1 - f_c)$.

$$R_2^{clustered} = \frac{f_c}{T_2^{OS}} + \frac{(1 - f_c)}{T_2^{CE}} \tag{4.55}$$

$$f_c = \frac{4\pi R_c^3 N_A M}{3 * 1000 * N_c} = R_c^3/(N_c R_d^3) f_d \quad where \quad f_d = \frac{4\pi R_d^3 N_A M}{3 * 1000} \tag{4.56}$$

Transverse relaxivity of a dispersed crystal is composed of the outer- sphere relaxivity only. The two-site chemical exchange is omitted as there is no cluster

$$R_2^{dispersed} = \frac{1}{T_2^{OS}}. \tag{4.57}$$

The outer-sphere transverse relaxivity of a crystal cluster is

$$\begin{aligned} R_{2\,OS}^{clustered} &= (4/9) f_c \tau_D (\Delta\omega)^2 \\ &= (4/9) f_c R_c^2 / D((4/5)\gamma^2 \mu_{sp}^2 N_c^2 / R_c^6) \\ &= (4/9) R_c^3 f_d / (N_c R_d^3) R_c^2 / D((4/5)\gamma^2 \mu_{sp}^2 N_c^2 / R_c^6) \\ &= \frac{16 f_d N_c \gamma^2 \mu_{sp}^2}{45 D R_c R_d^3}. \end{aligned} \tag{4.58}$$

The outer-sphere transverse relaxivity of dispersed crystals where $N_d = 1$ is

$$\begin{aligned} R_{2\,OS}^{dispersed} &= (4/9) f_d \tau_D (\Delta\omega)^2 \\ &= (4/9) f_d R_d^2 / D((4/5)\gamma^2 \mu_{sp}^2 / R_d^6) \\ &= (4/9) f_d R_d^2 / D((4/5)\gamma^2 \mu_{sp}^2 / R_d^6) \\ &= \frac{16 f_d \gamma^2 \mu_{sp}^2}{45 D R_d^4}. \end{aligned} \tag{4.59}$$

Using (4.28) and (4.27) the chemical exchange transverse relaxivity of a crystal cluster is

$$\begin{aligned} [1/T_2]_{CE} &= F_a F_b (\Delta\omega_b)^2 \tau_{ex} [1 - (\tau_{ex}/\tau_{CP}) tanh(\tau_{CP}/\tau_{ex})] \\ &= (1 - f_c) 1.73 f_c (\Delta\omega)^2 0.26 \tau_D [1 - (\tau_{ex}/\tau_{CP}) tanh(\tau_{CP}/\tau_{ex})] \\ &\approx (1 - f_c) 0.4498 f_c (\Delta\omega)^2 \tau_D \\ & \quad f_c << 1 \; therefore \; (1 - f_c) \approx 1 \\ &\approx 0.4498 \frac{4 f_d N_c \gamma^2 \mu_{sp}^2}{5 D R_c R_d^3} \end{aligned} \tag{4.60}$$

Transverse relaxivity of clustered crystals divided by transverse relaxivity of dispersed crystals becomes

$$\begin{aligned} \frac{r_2^{clustered}}{r_2^{dispersed}} &\approx \frac{16 f_d N_c \gamma^2 \mu_{sp}^2}{45 D R_c R_d^3} * \frac{45 D R_d^4}{16 f_d \gamma^2 \mu_{sp}^2} + 0.4498 \frac{4 f_d N_c \gamma^2 \mu_{sp}^2}{5 D R_c R_d^3} * \frac{45 D R_d^4}{16 f_d \gamma^2 \mu_{sp}^2} \\ \frac{r_2^{clustered}}{r_2^{dispersed}} &\approx \frac{2 * N_c R_d}{R_c}. \end{aligned} \tag{4.61}$$

4.6 Comparison of Relaxivity Ratios of Nanoparticle Clustering with Experimental Results

Magnetic relaxation switch agents are magnetic nanoparticles capable of sensing molecular interactions. In the presence of target analytes these nanoparticles switch from a dispersed to a clustered state. These dispersed and clustered states have different relaxometric properties. The clustered state in comparison to the dispersed

state has an enhanced spin-spin relaxivity r_2 while maintaining essentially the same longitudinal relaxivity r_1 [28].

Preliminary experimental results were conducted by Dr. Rutt's group on magnetic relaxation switch agents. These magnetic nanoparticles consisted of monocrystalline iron oxide cores with a dextran coating, producing a particle with an overall diameter of 22 nm. These nanoparticles were created by cross linking the dextran to form stable cross linked iorn oxide (CLIO) particles with conjugated synthetic oligonucleotides [36]. These oligonucleotides are hybridized and form a cluster with a total diameter of 140 $\pm$ 40 nm composed of 5 nanoparticles [28].

T_1 and T_2 were measured in solution-based assays using a relaxometer at 1.5 T before and after activation of the clustering mechanism. The experimentally measured rms field over the surface of the cluster ω_{rms} was determined as 1406 s^{-1}. There was no change in longitudinal relaxivity between clustered and dispersed states. The experimentally measured increase in transverse relaxivity upon clustering was 60% [28].

The three models of transverse relaxivity clustering ratios: Bowen's outer- sphere model, my outer-sphere with Langevin function model and my combined outer- sphere and chemical exchange model were compared to these preliminary experimental results

4.6.1 Bowen's Outer-Sphere Model

According to Bowen's outer-sphere model the transverse relaxivity ratio should be

$$\frac{r_2^{clustered}}{r_2^{dispersed}} = \frac{N_c R_d}{R_c} + 1 = 1 + \frac{5 * 11\ nm}{70\ nm} = 1.79 \tag{4.62}$$

resulting in a 79% increase in transverse relaxivity. Bowen's model predicts a 19% higher change in transverse relaxivity than the experimental results showed.

4.6.2 Outer-Sphere with Langevin Function

According to the outer-sphere with Langevin function model the transverse relaxivity ratio should be

$$\frac{r_2^{clustered}}{r_2^{dispersed}} = \frac{\left[coth\left(\frac{\mu_{sp}N_cB_0}{kT}\right) - \frac{N_ckT}{\mu_{sp}B_0}\right]^2 R_d}{\left[coth\left(\frac{\mu_{sp}B_0}{kT}\right) - \frac{kT}{\mu_{sp}B_0}\right]^2 R_c} + 1. \tag{4.63}$$

Using this theory, the clustered to dispersed ratio is calculated as 1.725. The outer-sphere with Langevin function model predicts a 13% higher change in transverse relaxivity than the experimental results showed.

4.6.3 Combined Chemical Exchange and Outer-Sphere Model

According to the combined chemical exchange and outer-sphere model the transverse relaxivity ratio should be

$$\frac{r_2^{clustered}}{r_2^{dispersed}} = \frac{2N_cR_d}{R_c} = \frac{2 * 5 * 11\ nm}{70\ nm} = 1.57 \tag{4.64}$$

resulting in a 57% increase in transverse relaxivity. The combined chemical exchange and outer-sphere model predicts 3% lower change in relaxivity than seen in experimental results.

These results indicate that the combined outer-sphere and chemical exchange model is most accurate in predicting the observed change in transverse relaxivity. This model should be validated further with additional experimental results.

4.7 Conclusions

The analysis in section 4.6 indicated that the combined outer-sphere and chemical exchange model predicts the change in transverse relaxivity upon nanoparticle clustering most accurately in comparison to peliminary experimental results. Further experimental trials should be completed at different field strengths and with

nanoparticles of various cluster sizes to validate the chemical outer-sphere diffusion and exchange exchange model.

Chapter 5

Summary and Future Work

5.1 Summary

In the first part of this thesis (Chapter 3), the three theoretical models of relaxivity of paramagnetic contrast agents were compared in terms of accuracy and ease of use. The dominant structural parameters dictating paramagnetic relaxivity were studied. GSBM theory was found to be the most accurate in describing high field relaxivity but was significantly more complex then other theories. The Caravan version of SBM theory characterizing anisotropic motion was also very accurate, very simple and reliant on structural parameters available in literature and experimental analysis.

Rotational diffusion (τ_R) is the most dominant parameter in determining relaxivity of bound and unbound contrast agents at both 1.5 and 3 T. Water residency time (τ_m) is insignificant for unbound contrast agents but significant for bound contrast agents at 1.5 T but not 3 T. Relaxivity increases with decreasing Gadolinium water distance but is unlikely to be significant due to the difficulty in changing Gadolinium water distance due to the surrounding chelate structure. Correlation time of transient zero field splitting (τ_v), magnitude of static zero field splitting (Δ_s) and magnitude of transient zero field splitting (Δ_t) are only significant in the low field.

Using Dr. Chen's multi-dimensional fitting programs anisotropic fits of MS-325

bound to HSA anisotropic fits were most accurate and closest to Caravan's results.

Underlying parameters for novel activatable gadolinium MPO contrast agents Mono-C and Mono-MPO were calculated using a modified version of Dr. Chen's multi-dimensional fitting program.

The second portion of the thesis (Chapter 4) was focused on ferromagnetic nanoparticle clustering and its effect on relaxivity. Nanoparticle clustering best predicted change in transverse relaxivity by the combined outer-sphere and chemical exchange model. Further experimental trials need to be completed to compare the combined outer-sphere and chemical exchange model to other experimental results.

5.2 Future Work

To validate the calculated structural parameters of activatable gadolinium MPO contrast agents Mono-C and Mono-MPO ^{17}O NMR measurements should be completed to experimentally determine τ_R and τ_m. ENDOR spectroscopy should be used to measure gadolinium water distance within these molecules. Additionally relaxivity should be measured for these compounds at clinical field strengths of 1.5 and 3 T to access their future viability as MR clinical contrast agents.

Further experimental results need to be obtained for iron clusterable contrast agents to validate the chemical exchange and outer sphere transverse relaxivity theory. The experiment should be conducted at multiple field strengths especially clinical field strengths of 1.5 and 3T. The nanoparticles studied should be of different cluster sizes if possible.

References

[1] Caravan, P., Strategies for increasing the sensitivity of gadolinium based MRI contrast agents [Review]. Chem Soc Rev, 2006. **35**: p. 512-523.

[2] Nishimura, D.G., Physics, in Principles of magnetic resonance imaging. 1995, Stanford University: Stanford, CA. p. 55-66.

[3] Nishimura, D.G., Overview, in Principles of magnetic resonance imaging. 1995, Stanford University: Stanford, CA. p. 33-54.

[4] Haacke, E.M., Magnetic Resonance Imaging: A preview, in Magnetic resonance imaging: physical principles and sequence design. 1999, J. Wiley-Liss: New York. p. 1-16.

[5] Nishimura, D.G., Excitation, in Principles of magnetic resonance imaging. 1995, Stanford University: Stanford, CA. p. 107-132.

[6] Haacke, E.M., Magnetic properties of tissues: theory and measurement, in Magnetic resonance imaging: physical principles and sequence design. 1999, J. Wiley-Liss: New York. p. 741-779.

[7] Smith, R.C. and R.C. Lange Relaxation times and mechanisms, in Understanding magnetic resonance imaging. 1998, CRC Press: Boca Raton, Fla. p. 45-57.

[8] Vejpravova, J.P., V. Sechovsky, D. Niznansky, J. Plocek, A. Hutlova and J-L. Rehspringer Superparamagnetism of co-ferrite nanoparticles. WDS'05 Proceedings of Contributed Papers, Part III. 2005: p. 519-523.

[9] Caravan, P., J.J. Ellison, T.J. McMurry and R.B. Lauffer Gadolinium(III) chelates as MRI contrast agents: structure, dynamics, and applications [Review]. Chem Rev, 1999. **99**: p. 2293-2352.

[10] Lauffer, R.B. Paramagnetic metal complex as water proton relaxation agents for NMR imaging: theory and design [Review]. Chem Rev, 1987. **87**: p. 901-927.

[11] Van Holde, K.E., Principles of Physical Biochemistry 1998, Prentice Hall: New Jersey.

[12] Rohrer, M., H. Bauer, J. Mintorovitch, M. Requardt and H-J Weinmann, Comparison of magnetic properties of MRI contrast media solutions at different magnetic field strengths. Inv Radiol, 1999. **40**(11): p. 715-714.

[13] Caravan, P. et. al., Structual, kinetic, and thermodynamic characterization of the interconverting isomers of MS-325, a gadolinium(III)-based magnetic resonance angiography contrast agent. Inorg Chem 2007. **46**: p. 6621-6631.

[14] Nicolle, G.M., L. Helm and A.E. Merbach ^{8}S paramagnetic centres in molecular assemblies: possible effect of their proximity on the water proton relaxivity. Mag Res Chem 2003. **41**: p. 794-799.

[15] McQuarrie, D.A. and J.D. Simon Multielectron atoms, in Physical Chemistry: a molecular approach. 1997, University Science Books: Sausalito, CA. p. 275-322.

[16] Kruk, D., T. Nilsson, and J. Kowalewski Nuclear spin relaxation in paramagnetic systems with zero-field splitting and arbitrary electron spin. Phys Chem Chem Phys, 2001. **3**: p. 4907-4917.

[17] Caravan, P. et. al., Albumin binding, relaxivity, and water exchange kinetics of the diastereoisomers of MS-325, a gadolinium(III)-based magnetic resonance angiography contarst agent. Inorg Chem 2007. **46**: p. 6632-6639.

[18] Nilsson T., and J. Kowalewski Low-field theory of nuclear spin relaxation in paramagnetic low symmetry complexes for electron spin systems of S=1, 3/2, 2, 5/2, 3 and 7/2. Mol Phys, 2001. **99**(4): p. 369-370.

[19] Zhou X., P. Caravan, R.B. Clarkson and P-O. Westlund On the philosophy of optimizing contrast agents. An analysis of ^{1}H NMRD profiles and ESR lineshapes of the Gd(III) complex MS-325 + HSA. J Mag Res, 2004. **167**: p. 147-160.

[20] Nicolle G.M., E. Toth, K-P. Eisenwiener, H.R. Macke and A.E. Merbach From monomers to micelles: investigation of the parameters influencing proton relaxivity. J Biol Inorg Chem, 2002. **7**: p. 757-769.

[21] Polnaszek, C.F. and R.G. Bryant Nitroxide radical induced solvent proton relaxation: Measurement of localized translational diffusion. J Chem Phys, 1984. **81**: p. 4038-4045.

[22] Toth E., L. Burai, E. Brucher and A.E. Merbach Tuning water exchange rates on (carboxymethyl)iminobis(ethylenenitrilo)tetraacetate (dtpa)-type gadolinium(III) complexes. J Chem Soc, Dalton Trans, 1997. p. 1587-1594.

[23] Muller R.N. et. al., Preparation, physico-chemical characterization, and relaxometry studies of various gadolinium(III)-DTPA-bis(amide) derivatives as potential magnetic resonance contrast agents. Magn Reson Imaging 1995. **13**: p. 401-420.

[24] Chen J., Rotatinal dynamics and proton relaxation of MRI paramagnetic contrast agents. Ph.D. thesis, Department of Chemistry, University of Illinois (1992).

[25] Muller R.N. et. al., Magnetic iron oxide nanoparticles. Chem Rev 2008. **108**: p. 2064-2110.

[26] Billotey C. et. al., Cell internalization of anionic maghemite nanopartilces: quantitative effect on magnetic resonance imaging. Magn Reson Med 2003. **49**: p. 646-654.

[27] Bowen C.V. et. al., Application of the static dephasing regime theory to superparamagnetic iron-oxide loaded cells. Magn Reson Med 2002. **48**: p. 52-61.

[28] Rutt B.K. and R. Weissleder, MR imaging of myeloperoxidase activity. Grant, Public Health Service (2005).

[29] Brooks R.A. et. al., On T_2-shortening by weakly magnetized particles: the chemical exchange model. Magn Reson Med 2001. **45**: p. 1014-1020.

[30] Morcos S.K. et. al., Extracellular gadolinium contrast agents: differences in stability. Eur J Radiol 2008. **66**: p. 175-179.

[31] Muller R.N. and P.A. Rinck, MRI contrast agents vary in stability, chelate power. Diagnostic Imaging May 1, 2009 http://www.diagnosticimaging.com/print/article/113619/1410686?printable=true.

[32] Hayat, M.A., Cancer imaging: Instrumentation and applications 2007, Academic Press: San Diego, CA. p. 82.

[33] Eldredge H.B et. al., Species dependence on plasma protein binding and relaxivity of the gadolinium-based MRI contrast agent MS-325. Investigative Radiology 2006. **41**: 229-243.

[34] Van Eldik R. and I. Bertini, Advances in Inorganic Chemisty, Volume 57: Relaxometry of Water-Metal Ion Interactions. Elsevier Academic Press: New York, NY p. 41-48.

[35] Powell D. H. et. al., Sturctural and Dynamic Parameters Obtained from ^{17}O NMR, EPR and NMRD Studies of Monomeric and Dimeric Gd^{3+} Complexes of Intrest in Magnetic Resonance Imaging: An Integrated and Theoretically Self-Consistent Approach. J. Am. Chem. Soc. 1996. **118**: 9333-9346.

[36] Perez J.M. et. al., Use of Magnetic Nanoparticles as Nanosensors to Probe for Molecular Interactions. Chem. Bio. Chem. 2004. **5**: 261-264.

[37] Taktak S. et. al., Multiparameter Magnetic Relaxation Switch Agents. Anal. Chem. 2007. **79**: 8863-8869.